Electrochemical Energy Reviews (2019) 2:332–371
https://doi.org/10.1007/s41918-019-00033-7

REVIEW ARTICLE

3D Hierarchical Porous Graphene-Based Energy Materials: Synthesis, Functionalization, and Application in Energy Storage and Conversion

Cheng Tang[1,2] · Hao-Fan Wang[1,3] · Jia-Qi Huang[4] · Weizhong Qian[1] · Fei Wei[1] · Shi-Zhang Qiao[2] · Qiang Zhang[1]

Received: 2 January 2019 / Revised: 24 January 2019 / Accepted: 27 February 2019 / Published online: 26 March 2019
© Shanghai University and Periodicals Agency of Shanghai University 2019

Abstract

The rational development of effective energy materials is crucial to the sustainable growth of society. Here, 3D hierarchical porous graphene (hpG)-based materials with micro-, meso-, and macroporous features have recently attracted extensive research efforts due to unique porosities, controllable synthesis, versatile functionalization, favorable mass/electron transport, and superior performances in which corresponding electrochemical performances are strongly dependent on the nature of the building blocks and structural hierarchy of the assemblies. In this review, recent achievements in the controllable synthesis, versatile functionalization, and device application of 3D hpG-based energy materials will be summarized, including controllable and facile synthesis through chemical vapor deposition on 3D porous templates, post-assembly/treatment of graphene oxide nanosheets, and templated polymerization. In addition, graphene material functionalization through heteroatom doping, spatially confined decoration of active nanoparticles, and surface hybridization of graphene-analogous components to enhance electrochemical properties will be discussed. Furthermore, applications of 3D hpG materials in various electrochemical energy storage and conversion systems will be summarized, including lithium-ion batteries, lithium-sulfur batteries, lithium metal anodes, oxygen reduction reaction, oxygen evolution reaction, hydrogen evolution reaction, and nitrogen reduction reaction. Overall, this review will comprehensively present the property advantages, design principles and synthesis strategies of 3D hpG-based energy materials and provide guidance in the development of various 2D graphene-analogous materials and nanomaterials for advanced electrochemical energy storage and conversion systems.

Keywords Graphene · Nanostructures · Hybrid · Li ion battery · Li sulfur batteries · Oxygen reduction reaction · Oxygen evolution reaction · Nitrogen reduction reaction

1 Introduction

Increasingly serious issues associated with the greenhouse effect, resource exhaustion, and enormous energy consumption have considerably affected and even threatened quality of life and economic and social development. To address this, current fossil fuel-based energy and chemical industries need to be revolutionized through the development of sustainable resources and highly green and efficient energy technologies. Here, rapid developments in renewable energy technologies such as solar, wind, geothermal, and nuclear have provided encouraging opportunities [1], and the direct and efficient utilization of these renewable energies depends on advanced electrochemical energy devices such as batteries and electrocatalysis cells for versatile storage, conversion, and transportation.

In general, advanced electrochemical energy devices involve complex multi-electron, multi-phase, and multi-stage

✉ Qiang Zhang
zhang-qiang@mails.tsinghua.edu.cn

1 Beijing Key Laboratory of Green Chemical Reaction Engineering and Technology, Department of Chemical Engineering, Tsinghua University, Beijing 100084, China

2 School of Chemical Engineering, The University of Adelaide, Adelaide, SA 5005, Australia

3 AIST-Kyoto University Chemical Energy Materials Open Innovation Laboratory (ChEM-OIL), National Institute of Advanced Industrial Science and Technology (AIST), Yoshida, Sakyo-ku, Kyoto 606-8501, Japan

4 Advanced Research Institute of Multidisciplinary Science, Beijing Institute of Technology, Beijing 100081, China

reactions, such as the rocking-chair process in lithium-ion batteries (LIBs) [2], solid–liquid–solid phase transitions of sulfur/lithium polysulfides/sulfides in lithium-sulfur (Li-S) batteries [3, 4], and proton-coupled electron transfer in electrocatalysis [5, 6]. And despite the significant progress in this field, the energy and power density, as well as the long-term stability of these devices, which is largely determined by the properties of the electrode materials, still does not meet commercialization requirements [7–18], in which the physicochemical properties of employed materials (e.g., conductivity, porosity, structure, density, composition, and surface) significantly influence the electrochemical behavior, kinetics, and ultimate performance of these advanced electrochemical energy devices. One promising electrode material is graphene and, since being discovered in 2004, has attracted great attention from researchers [19–30]. Graphene is a two-dimensional (2D) monolayer of carbon atoms arranged in a hexagonal lattice and possesses many appealing properties [8, 31–33] such as high carrier mobility (2×10^5 cm^2 V^{-1} s^{-1}) [34, 35], high thermal conductivity (5300 W m^{-1} K^{-1}) [36], high Young's modulus (~ 1 TPa) [37], high electrical conductivity (~ 10^6 S cm^{-1}), high specific surface area (2630 m^2 g^{-1}), and outstanding chemical and structural stability. More importantly, the uniqueness and superiority of graphene originates not only from these outstanding characteristics, but also from its overall advantages and its flexibility and versatility in regulating structural and compositional properties. And if coupled with favorable nanostructures, resulting three-dimensional hierarchical porous graphene (3D hpG) materials can demonstrate combined merits from both graphene and porous materials and serve as promising components in high-performance electrochemical energy storage and conversion devices [38–42]. Specifically, 3D hpG materials can exhibit multi-functionalities and provide opportunities to improve electrochemical performances as follows [3, 7, 9, 38, 39, 43–45]:

1. The outstanding electrical conductivity of sp^2 hybridized graphene scaffolds can provide interconnected and continuous electron transfer highways;
2. The high specific surface area can enhance interfacial transports and reactions as well as enable the uniform dispersion of active sites or guest functional nanomaterials;
3. The hierarchical porosity with shortened diffusion pathways can facilitate electrolyte infiltration or gas diffusion to enhance active material loading and preservation and improve active surface accessibility;
4. The high mechanical strength and flexibility of graphene nanosheets allows 3D porous frameworks to buffer the volume change of active non-carbon materials;
5. The ultrathin and hierarchical porous nanostructure can provide ideal scaffolds for diversified functionalization (e.g., functional groups, heteroatom doping, defects and edges) and incorporation (e.g., metals, metal oxides/hydroxides/sulfides and polymers) into 3D hpG materials with different functionalities and complexities.

Motivated by these advantages, intense research has been conducted to investigate the application of 3D hpG materials in different electrochemical energy devices, such as LIBs [46–48], Li-S batteries [49–52], supercapacitors [10, 53–64], metal-air batteries [65–70], fuel cells [71–75], water splitting devices [76–80], and flexible devices [42, 81–87]. Here, 3D hpG materials include pure-carbon graphene or hybrids of 3D hpG with guest components and are dominantly in the form of foams, aerogels, hydrogels, or sponges and can be facilely synthesized through direct chemical vapor deposition (CVD) on metal foam templates or through self-assembly of graphene oxide (GO) nanosheets [88–90]. Although many excellent reviews have already summarized the significant achievements in this area [7, 9, 11, 31, 38, 40, 72, 91–99], we want to emphasize that the electrochemical performance of 3D hpG materials is strongly dependent on the nature of the building blocks and structural hierarchy of the assemblies [100]. Overall, 3D porous graphene assemblies are always highly macroporous in nature, possess numerous micrometer-sized void spaces, and can severely limit the volumetric energy density and low packing density of porous graphene-based electrodes, greatly hindering commercialization [31]. In addition, macroporous voids strutted by ultrathin and flexible graphene nanosheets are mechanically unstable and tend to shrink or collapse during operation. Despite this, individual graphene nanosheets obtained in large-scale synthesis are always of low-to-medium quality with abundant intrinsic (e.g., edges, vacancies, holes, topological defects and deformations) and extrinsic defects (e.g., O, H and other foreign atom-containing groups) which can alter local electronic structures and serve as excellent active sites in various electrocatalysis applications, such as oxygen reduction reaction (ORR), oxygen evolution reaction (OER), hydrogen evolution reaction (HER), CO_2 reduction reaction (CRR), and nitrogen reduction reaction (NRR). However, these defects can also lead to serious issues in electrochemical energy storage devices such as high initial irreversible capacity with poor Coulombic efficiency for LIBs and reduced cycling stability and reversibility for supercapacitors [31]. In addition, despite improvements in electrical conductivity and power capability in many conditions, ion diffusion in porous graphene-based electrodes is considerably retarded by steric effects due to the large aspect ratio of planar graphene and difficult penetration through hexagonal carbon rings, thus worsening electrochemical performances depending on the thickness and tortuosity of electrode laminates and different active materials [31, 101, 102]. Therefore, the physical and chemical properties of

individual graphene nanosheets and the hierarchical porosity of assembled 3D frameworks need to be meticulously scrutinized and designed to achieve optimal 3D hpG-based energy materials.

To address these issues, a series of critical features for optimal 3D hpG-based energy materials have been proposed (Fig. 1) to fully demonstrate their advantage in advanced electrochemical energy applications, especially in batteries and electrocatalysis. This proposal includes the construction of strutted macropores (> 50 nm), wrinkled mesopores (2–50 nm), and in-plane micropores (< 2 nm) through in situ templated CVD growth, self-assembly of GO precursor, and post-treatment of 3D hpG scaffolds, as well as various functionalization strategies to enrich 3D hpG material properties and functionalities through heteroatom doping, confined decoration and surface hybridization with guest components, thus allowing as-obtained 3D hpG materials to act as ideal electrode materials in various electrochemical energy devices. Nevertheless, an overview of the progresses, principles, and perspectives in this specific field remains absent; therefore, in this review, recent achievements in the controllable synthesis, versatile functionalization, and device application of 3D hpG-based energy materials are summarized and corresponding nanostructure designs, synthesis mechanisms, structure–property relationships, and optimization principles are highlighted. Considering the dozens of excellent reviews on macroporous graphene assemblies and composites, this review will predominantly focus on hierarchical porous graphene materials with micro-, meso-, and macroporous features, and especially mesoporous nanostructures. In addition, because the most crucial challenge of 3D hpG materials lies in their fabrication with excellent controllability and reproducibility of their hierarchical porosity, this review will first discuss the controllable synthesis of 3D hpG frameworks with different precursors and strategies featuring excellent crystallinity and thickness. Following this, versatile functionalization strategies toward modified properties and higher application performances are summarized. Subsequently, applications of 3D hpG materials in various electrochemical energy devices are presented to demonstrate structure–property relationships and nanostructure design principles. Finally, discussions and perspectives on various challenges and opportunities for further research are provided. Overall, this review will not only demonstrate the advantages and principles of 3D hpG-based energy materials, but hopefully inspire future advancements in 2D graphene-analogous materials and other nanomaterials to provide breakthroughs in advanced electrochemical energy storage and conversion technologies.

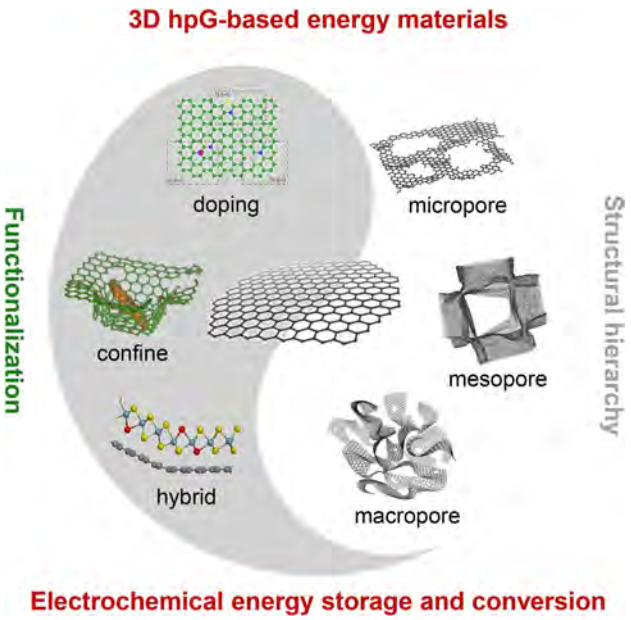

Fig. 1 Critical features of optimal 3D hpG-based energy materials, including structural hierarchy and various functionalization. Schematics are reprinted with permission from Ref. [103] (macropore), Ref. [104] (doping), Ref. [105] (confine), and Ref. [106] (hybrid)

2 Controllable Synthesis of 3D Hierarchical Porous Graphene

The controllable synthesis of 3D hpG materials greatly depends on the local growth of high-quality 2D graphene nanosheets, the construction of long-range 3D interconnected porous structures, and the seamless junction at the interfaces between adjacent nanosheets. And for the synthesis of 2D graphene nanosheets, there are two main synthetic routes including the wet chemical route involving the reduction of GO or liquid exfoliation of graphite and the CVD route involving the use of 2D metal foil substrates [107], in which CVD growth on 3D porous templates and post-assembly/treatment of GO nanosheets have been proposed to be the most efficient and promising synthetic strategies for 3D hpG materials. Furthermore, templated polymerization based on specific templates with pore-forming abilities and catalytic activities has also been widely reported. Therefore, to avoid the repetitive introduction of the traditional synthesis and assembly of macropore-dominant graphene materials which have been comprehensively reviewed [7, 9, 40, 88, 90, 94, 108], this review will mainly focus on the controllable design and fabrication of mesoporous nanostructures.

2.1 Direct Mesoporous Templated Chemical Vapor Deposition

2.1.1 Metal Templates

CVD is an efficient and promising method to synthesize high-quality, ultrathin, large surface area, and uniform graphene films [109–112], and the CVD growth of graphene

on substrates involves many elementary steps which can be divided into two processes including the mass transport of reactive species through the boundary layer and surface reactions to form graphene lattices at the catalyst surface (Fig. 2a) [113]. Here, CVD is mainly determined by the carbon precursors (types, flow rates, carrier gas, etc.), the growth substrates (catalytic ability, carbon solubility, surface morphology, defects, etc.) and the operation conditions (temperature, pressure, cooling rates, etc.). In the case of metal substrates, the growth mechanisms of graphene have been revealed to be through a bulk dissolution-surface segregation route for metals with high carbon solubility (e.g., Ni) and a surface decomposition–direct nucleation route for metals with poor carbon solubility (e.g., Cu) [114, 115]. And with advances in growth mechanisms, materials science, and process engineering, various strategies have been proposed to facilely regulate the thickness, grain boundaries, defects, and the doping of 2D graphene films grown on metal foil substrates in which high-quality porous 3D hpG materials can be obtained through the replacement of 2D metal foil substrates with 3D porous metal templates. For example, in 2011, Chen et al. [116] were the first to report the successful synthesis of 3D graphene macrostructures (graphene foam) using a template-directed CVD method. In their synthesis, commercial nickel foam instead of foil was employed as a porous metal template, and methane was introduced as a carbon precursor at 1000 °C under ambient pressure, resulting in a monolithic, continuous, and free-standing 3D porous graphene network with minimal shrinkage after the careful removal of the template and support layer. Here, the researchers reported that the as-obtained graphene foam replicated the 3D interconnected scaffold structure of the nickel foam template and that all the graphene nanosheets with an average thickness of ~ 3 layers were in direct contact with each other without breaks and were well separated (Fig. 3a). And as a result, this unique structure exhibited a high electrical conductivity with an extra-low density of ~ 5 mg cm^{-3}, a high porosity of ~ 99.7%, a high specific surface area of ~ 850 m^2 g^{-1}, and outstanding mechanical properties, transferring the excellent properties of the 2D graphene to the 3D macrostructure. In addition, the researchers reported that even with a graphene foam loading of ~ 0.5 wt%, the graphene foam/poly(dimethyl siloxane) composite delivered a high electrical conductivity of ~ 10 S cm^{-1} and excellent electromechanical stability under bending or stretching, showing great potential as flexible, foldable and stretchable electrode materials. Overall, this innovative pioneering study provided great insights into the smart design and fabrication of 3D porous graphene materials and has been extended to other templates as a general strategy.

Graphene foam possesses excellent electronic performances, structural porosity, and mechanical robustness and has been applied in many fields, including electrochemical energy storage [117–122], catalysis [123, 124], electrochemical sensors [125, 126], electromagnetic interference shielding [127], and so on. However, the pore size of as-obtained graphene foams is strictly determined by the structure of the metal foam templates, which can be as large as 200 μm, and these macropores are mechanically unstable, thus requiring the support of flexible polymers and careful operations. In addition, this macroporous structure also induces extra-low packing densities, which strongly limit performance in practical applications. Therefore, instead of the direct use of commercial metal foams, many studies have reported the in situ generation of porous templates through sintering and cross-linking metal particles or metal salts before graphene deposition [128–131], resulting in 3D porous graphene materials with significantly reduced pore sizes (several micrometers), but also with relatively uncontrollable and irregular nanostructures with more defective interfaces.

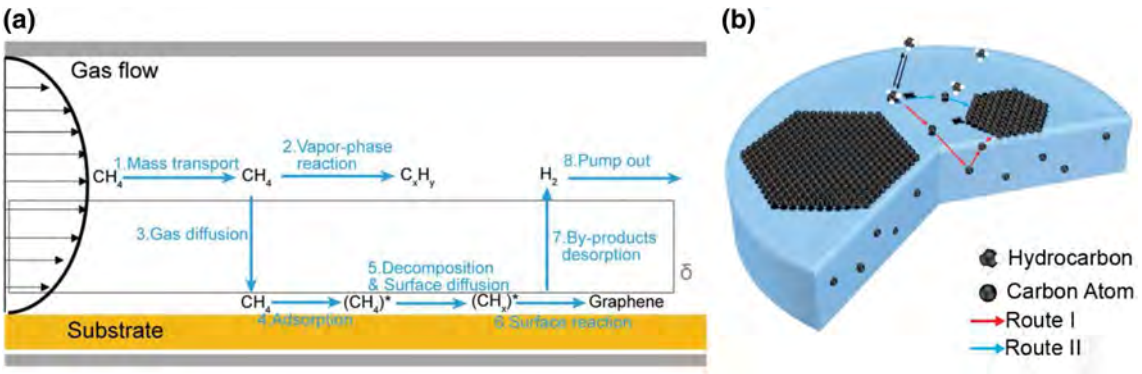

Fig. 2 CVD process. **a** Elementary steps in the CVD growth of graphene on a 2D catalytic substrate. Reprinted with permission from Ref. [113]. **b** Two different routes for substrates with high carbon solubility (route I) and low carbon solubility (route II). Reprinted with permission from Ref. [115]

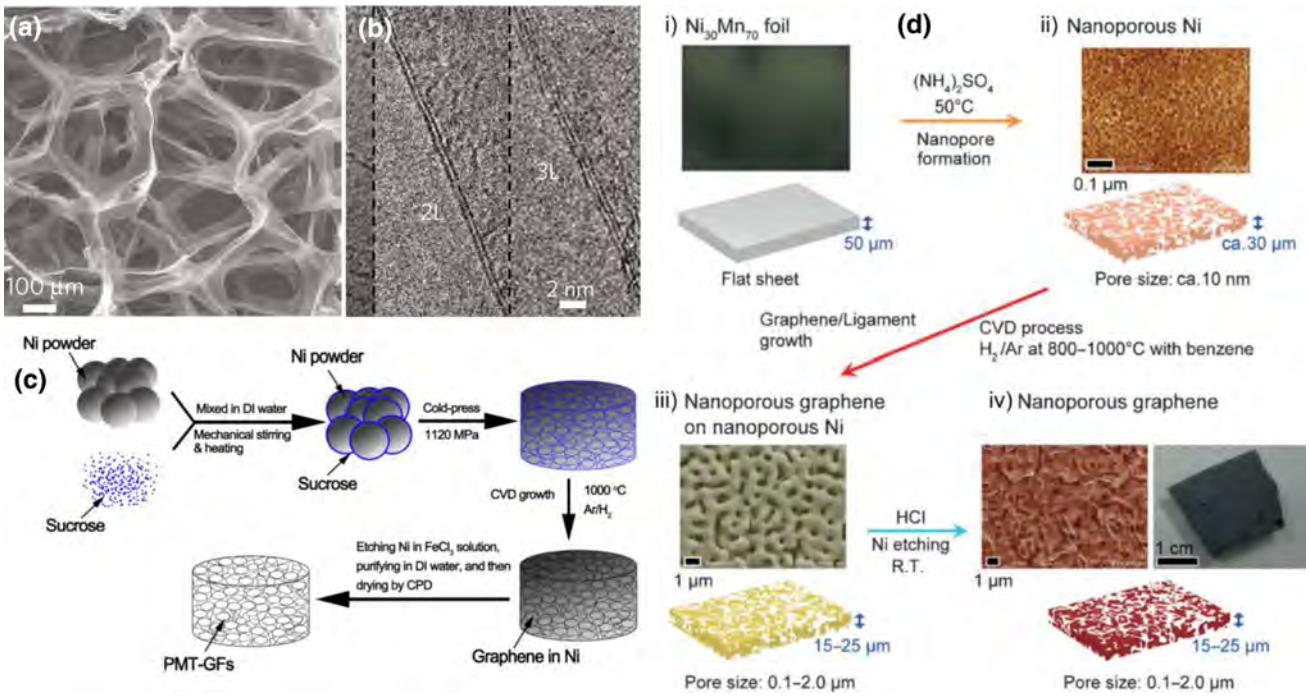

Fig. 3 Porous metal-templated CVD growth of 3D hpG. **a** Scanning electron microscopy (SEM) and **b** transmission electron microscopy (TEM) images of 3D graphene foam synthesized through nickel foam-templated CVD. Reprinted with permission from Ref. [116]. **c** Schematic of the preparation of 3D porous graphene foam using power metallurgy templates. Reprinted with permission from Ref. [132]. **d** Schematic of the synthesis of 3D bicontinuous mesoporous graphene materials using mesoporous Ni templates. Reprinted with permission from Ref. [137]

For example, Sha et al. [132] combined the merits of macroporous metal foam with metal nanoparticles through the simple synthesis of freestanding 3D porous graphene foam using powder metallurgy templates in which Ni powders (particle size: 2.2–3.0 μm) were mixed with sucrose in deionized water and subjected to heating, evaporation, and drying overnight. The resulting hybrid powder was subsequently pressed into pellets at a pressure of ~ 1120 MPa for 5 min by using a die and annealed at 1000 °C for 30 min to obtain in situ sintered Ni skeletons, which the researchers utilized as a template to grow graphene with an atmosphere of H_2/Ar (200 sccm (1 sccm = 6×10^{-5} m^3 h^{-1})/500 sccm) at a chamber pressure of ~ 9 Torr (1 Torr = 1/760 atm) (Fig. 3b). And as a result, the as-obtained 3D porous graphene network possessed particle-like carbon shells connected by multilayered graphene and exhibited a much smaller porosity, higher specific surface area (1080 m^2 g^{-1}), and good electrical conductivity (13.8 S cm^{-1}) as compared with graphene foam cast on Ni foam. In addition, the researchers reported that this porous structure can sustain direct flushing with water and is able to rapidly recover after being compressed with a loading weight of more than 150 times of the foam weight. Furthermore, researchers have reported that by varying metal powder compositions and size, pellet-pressing conditions, annealing temperatures, and pore-forming additives, the shape, density, and porosity of as-fabricated 3D porous graphene materials can be tuned on-demand [133, 134]. For example, Drieschner et al. [133] reported that the use of Cu powders (particle size 0.5–1.5 μm) as a precursor and $MgCO_3$ powders as a blowing agent with sintering at 800 °C for 45 min in a H_2/Ar atmosphere (100 sccm/400 sccm) can result in a freestanding, predominantly monolayer graphene 3D porous graphene foam with pore sizes smaller than 1 μm that can provide high volumetric and specific capacitances for electric double-layer capacitors (165 mF cm^{-3}, 100 F g^{-1}) and an electrochemically active area as high as 2500 m^2 g^{-1} [133].

To further optimize the structure and property of 3D porous graphene foams synthesized through metal-templated CVD growth, Ito et al. [135] developed a mesoporous metal substrate through the electrochemical leaching of bimetallic alloys to obtain graphene materials with a more regular framework, smaller porosity, and 3D interconnected networks in which Mn atoms were selectively leached from a 50-μm-thick $Ni_{30}Mn_{70}$ alloy sheet by using a weak acid solution to successfully obtain a 3D mesoporous Ni substrate with 10–20 nm open pores (Fig. 3d). Researchers have also reported that metal templates can exhibit not only nanosized porous scaffolds, but also thermally reconstruct very smooth surfaces and unique frameworks, such as a triply periodic minimal surface [136, 137]. For example,

Ito et al. [136–138] in a series of studies synthesized 3D bicontinuous mesoporous structures through the annealing of benzene, pyridine, and thiophene as carbon/heteroatom precursors at 800–1000 °C under a mixed atmosphere of Ar and H_2 to allow for the uniform growth of ultrathin graphene nanosheets on Ni ligament surfaces. Here, the researchers reported that the specific surface area of their resulting structures can reach ~ 1000 m^2 g^{-1} and that corresponding pore sizes can be altered ranging from 100 nm to 2 μm through the change of annealing temperatures and times. And in addition to the much smaller nanosized porosity as compared with graphene foam fabricated on commercial metal foams, this unique 3D graphene material is more impressive due to the preserved electronic and vibrational properties that are similar to those of the suspended 2D graphene layer [139–142]. Furthermore, Qin et al. [143, 144] also reported the successful synthesis of high-quality, flexible, robust, and freestanding 3D mesoporous duct-like hpG films through the use of $Cu_{40}Mn_{60}$ alloy as the precursor, 0.05 M HCl as the leaching solution and acetylene as the carbon source.

Due to the catalytic activity for high-quality graphene growth on metal surfaces, 3D porous graphene materials fabricated by using porous metal templates always exhibit high crystallinity, low defects, and high conductivity. In addition, graphene thickness can be finely tuned from several layers to monolayers through the optimization of growth conditions and metal compositions. Therefore, Raman spectra of obtained 3D porous graphene materials always exhibit low defect-related D bands and distinct 2D bands [116, 136]. Furthermore, the nanostructure and morphology of porous metal templates can be altered by using different precursors and fabrication methods, leading to adjustable nanostructures for the grown graphene materials. However, metal nanoparticles or ligaments tend to coarsen and aggregate under high temperatures and severely limit the templated growth of 3D porous graphene with porosities lower than 100 nm. In addition, this method also suffers from high costs and low yields and therefore cannot meet the requirements of scalable fabrication and practical application.

2.1.2 Metal Oxide Templates

Analogous to the catalytic growth of carbon nanotubes (CNTs), the prerequisite for the successful growth of graphene through CVD is the efficient adsorption and decomposition of carbon precursors. Therefore, metal catalysts had been considered to be essential substrates in the synthesis of high-quality CNTs and graphene. However, during their study into CNTs, Rümmeli et al. [145–148] reported "catalyst-free" substrates such as Al_2O_3 that can provide interfaces for ordered carbon formation and thus systematically explored the graphitization role of various oxides (e.g., SiO_2, Al_2O_3, MgO, Ga_2O_3, ZrO) under typical CVD synthesis conditions [145]. Here, the researchers revealed that graphene layers can be formed on oxide particle surfaces, especially MgO nanoparticles, at around 850 °C under a carbon flow of ethanol, methane, or cyclohexane, in which each graphene layer grew from the oxide substrates or even anchored to every second lattice plane, bending if necessary (Fig. 4a, b) [145, 147]. In addition, the researchers reported that the number of graphene layers was always limited regardless of the reaction time (10–90 min) and that the perfect honeycomb lattice of graphene can be observed after annealing in vacuum (Fig. 4c) [147]. The researchers also reported that the observation of the growth of any graphene or graphitic carbon materials on the surface of single-crystalline oxides was difficult, implying the potential to catalyze the decomposition of carbon precursors and growth of graphene on defective or step-edge sites of metal oxide nanoparticle surfaces, which was subsequently validated through theoretical investigations (Fig. 4d) [148]. Based on this, metal oxide nanoparticles can serve as promising templates for the CVD growth of 3D hpG materials with different nanostructures and properties as compared with those grown on porous metal templates.

MgO is the most widely used oxide template for the CVD growth of 3D hpG materials due to its simple synthesis, structure variability and moderate activity. In 2011, Ning et al. [149] demonstrated the gram-scale synthesis of nanomesh graphene materials using porous MgO nanosheets annealed from $Mg(OH)_2$ precursors as the template and methane as the carbon source at 900 °C for 10 min in a vertical fluidized reactor. Here, the researchers reported that the as-obtained graphene sheets possessed a polygonal morphology and porous framework with ~ 10 nm pores that were similar to the porous MgO template (Fig. 4e) in which the graphene layer thickness was predominantly less than two layers and their agglomeration was prevented by the mesoporous structure with large corrugations. And as a result, the nanomesh graphene material provided a high specific surface area of up to 1654 m^2 g^{-1} and a large total pore volume of 2.35 cm^3 g^{-1}. In addition, the researchers reported that the graphene yield normalized on the template reached 3–5 wt% after a 10-min reaction (Fig. 4f), which is promising for the large-scale production of 3D hpG materials if coupled with nano-agglomerate fluidized bed reactors [149, 150]. Furthermore, the Raman spectra of the nanomesh graphene material exhibited dominate D band, upshifted G band, and weak 2D band peaks (Fig. 4g) [149], which are common in oxide templates [147] but distinct from porous graphene grown on metal templates [116, 136], indicating more pores and edges on the mesoporous structure and possibly lower crystallinity due to the relatively lower catalytic activity.

Nonetheless, MgO is an excellent template for the synthesis of mesopore-rich 3D hpG graphene materials by using different carbon precursors [151–154]. In a series of studies, Hu et al. [95, 155, 156] developed an in situ MgO template

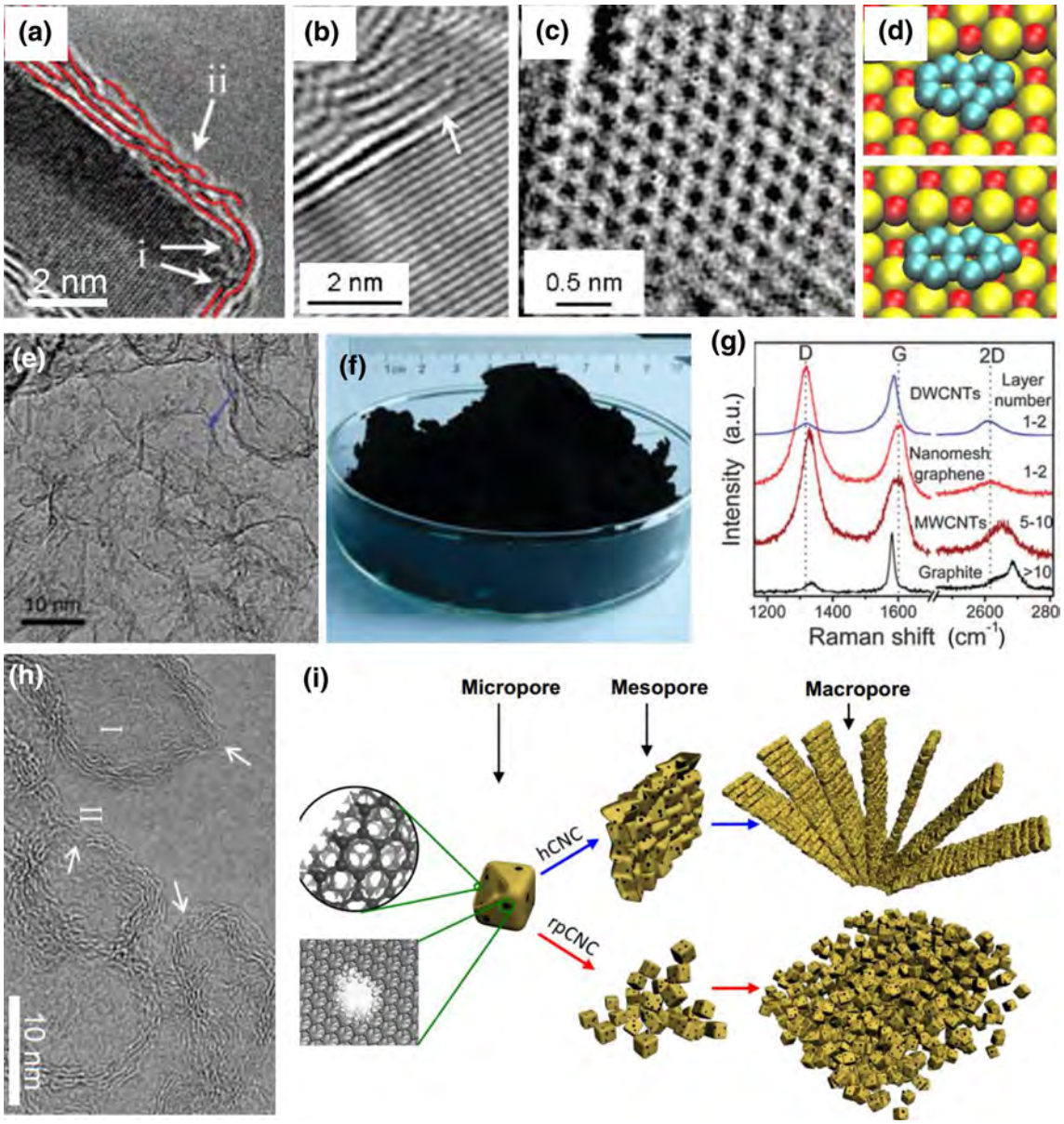

Fig. 4 Porous MgO-templated CVD growth of 3D hpG. **a** TEM image of MgO nanocrystals coated with graphene layers. Reprinted with permission from Ref. [145]. **b** TEM image showing the interface between graphene layers and MgO lattice fringes. **c** High-resolution TEM image highlighting the honeycomb lattice for graphene after annealing in vacuum. **b**, **c** are reprinted with permission from Ref. [147]. **d** Carbon adsorption on the step-edge of MgO surfaces by theoretical calculation. Reprinted with permission from Ref. [148]. **e** TEM image and **f** photograph of nanomesh graphene. **g** Raman spectra at 633 nm of the nanomesh graphene compared with calibration materials. **e**–**g** are reprinted with permission from Ref. [149]. **h** TEM image of graphene nanocages obtained using the in situ MgO template method. **i** Schematic structural characteristics of the hierarchical porous graphene nanocage at multi-scales. **h**, **i** are reprinted with permission from Ref. [156]

method to prepare graphene nanocages using basic magnesium carbonate [$4MgCO_3{\cdot}Mg(OH)_2{\cdot}5H_2O$] as the template precursor, benzene as the carbon source and Ar as the carrier gas and reported that nanosized MgO particles can be obtained upon basic magnesium carbonate decomposition at elevated temperatures and can serve as catalytic templates for the coating of graphene nanocages (Fig. 4h) [156]. The researchers also reported that varying annealing/CVD temperatures can lead to varying graphitic degrees and porosities in the resulting graphene in which the specific surface area decreased from 2053 to 1854, 1633 and 312 $m^2\ g^{-1}$ with corresponding pore sizes shifting from 5–7 to 7–15, 10–25, and 20–30 nm for growth temperatures of 670, 700, 800, and 900 °C, respectively [155]. Furthermore, the 3D

hierarchical porous characteristics of basic magnesium carbonate precursors can carry over to MgO templates and subsequently to the graphene nanocages, allowing for coexisting micro-, meso-, and macropores with remarkable pore volumes as high as 4.2 $cm^3\ g^{-1}$ (Fig. 4i) [156]. Moreover, the chemical composition and hierarchical framework of the graphene nanocages can also be facilely regulated by varying carbon/heteroatom precursors [151, 153, 157, 158] and template precursors/structures (e.g., MgO flakes [152], nanofibers [159–162], nanowires [153], rods [163]), suggesting the significant advantage of porous MgO templates in the controllable synthesis and structural regulation of 3D hpG materials.

Other metal oxides have also been reported as alternative templates for the CVD growth of 3D hpG materials, such as CaO [164–170], porous anodic alumina [171–173], ZnO [174, 175], MnO [176]. Here, in addition to the surface chemical characteristics, the nanostructural porosity of templates can significantly regulate the quality, thickness, and porosity of resulting porous graphene. For example, Tang et al. [164] revealed that porous CaO templates with smaller pore sizes can result in thinner graphene layers, higher specific surface areas, larger mesopore volumes, and slightly more collapsed and irregular cavities. Researchers have also reported that the effects of ZnO templates are specific due to possible carbothermal reductions and volatilization during high-temperature growth (> 800 °C) and that compared with MgO templates, graphene layers grown on these ZnO templates are always thicker with more defects and lower crystallinity [174, 175]. As for MgO, the strong interaction/charge transfer between top layer O atoms and coated graphene layers [177], as well as the interfacial reconstruction and therefore the lattice match on relatively unstable O-terminated MgO (111) surfaces [178], is the crucial factor for the self-limiting growth of high-quality graphene and requires deeper investigation.

Layered double hydroxides (LDHs) are a typical class of 2D lamellar inorganic materials with hydrotalcite-like structures and are composed of positively charged layers and charge-balancing interlayer anions [179]. LDHs usually exhibit anticipated compositions and morphology with uniform hexagonal flakes and atomic-level dispersions of various metals (e.g., Mg, Al, Fe, Co) in the positively charged layers and the calcination of LDHs at high temperatures can lead to the sequential removal of interlayer water, interlayer anions, and lattice hydroxyls, enabling the transformation to layered double oxides (LDOs) with mixed metal oxides and metal nanoparticles as the main components [180, 181]. And due to the dehydration of hydroxides to oxides and the Kirkendall diffusion effect in multi-metal systems, obtained LDOs possess abundant mesopores uniformly distributed in lamellar metal oxide flakes, which is favorable for the CVD growth of 3D hpG materials. For example, Zhao et al. [182, 183] first reported the synthesis of an intrinsically unstacked double-layer mesoporous graphene using MgAl LDO templated CVD (Fig. 5a) in which their MgAl LDO was obtained through the calcination of MgAl LDHs and the catalysis of methane decomposition for the uniform deposition of graphene at 950 °C for 10 min. Here, the researchers observed continuous and bent graphene layers on the surface and in the mesopores of the MgAl LDO flakes (Fig. 5b) [182] and reported that the as-obtained graphene possessed a hexagonal morphology similar to that of the original LDO flakes (Fig. 5c), which consisted of a lamellar box-like structure with two unstacked graphene layers separated by many mesosized graphene protuberances (Fig. 5d). These small graphene protuberances were replicated from the mesopores in the LDO template and can covalently bond with graphene layers to effectively prevent the stacking of the up/down graphene layers [184], which can be supported by the much larger thickness (~ 10 nm) with only a few layers (< 3) of graphene (Fig. 5e). And as a result, this unstacked mesoporous graphene can provide a high specific surface area of 1628 $m^2\ g^{-1}$, a large pore volume of 2.0 $cm^3\ g^{-1}$ with abundant mesopores (2–7 nm, Fig. 5f), and an outstanding electrical conductivity of 438 S cm^{-1}, suggesting significant advantages in rapid electron transport and smooth mass diffusion for electrochemical energy applications. Furthermore, the regulation of LDH flake size and morphology [185, 186] and the improvement in pore-forming mechanisms during LDH transformation (e.g., volatile Zn metal [187] and catalytically active Fe [188]) can allow for the controlled synthesis of desirable MgAl LDO nanostructures and optimal hierarchical porosity of 3D hpG frameworks.

2.1.3 Other Mesoporous Templates

In addition to mesoporous metal and metal oxide templates, many other materials have also been demonstrated to be promising templates for the CVD growth of 3D hpG materials with desirable qualities and unique nanostructures. And because of the excellent catalytic activity and template effect of metal/metal oxides, metal-promoted fabrication of porous graphene through phase interface reactions and self-generated template-guided growth (e.g., $2Mg + CO_2 \rightarrow 2MgO + C$ [189–191] and $Li_2O + 2CO \rightarrow C + Li_2CO_3$ [192]) has also been explored.

Given the possible growth of high-quality single-crystal graphene on dielectric substrates such as SiO_2 [193, 194], the successful fabrication of various mesoporous graphene materials by using mesoporous SiO_2 templates has been demonstrated [174, 195–197]. For example, Bi et al. [196] synthesized a unique graphene monolith through CVD using a 3D mesoporous silica template at 1100 °C and reported that the unique graphene monolith completely inherited the interconnected 3D scaffold and mesoporous structure of the

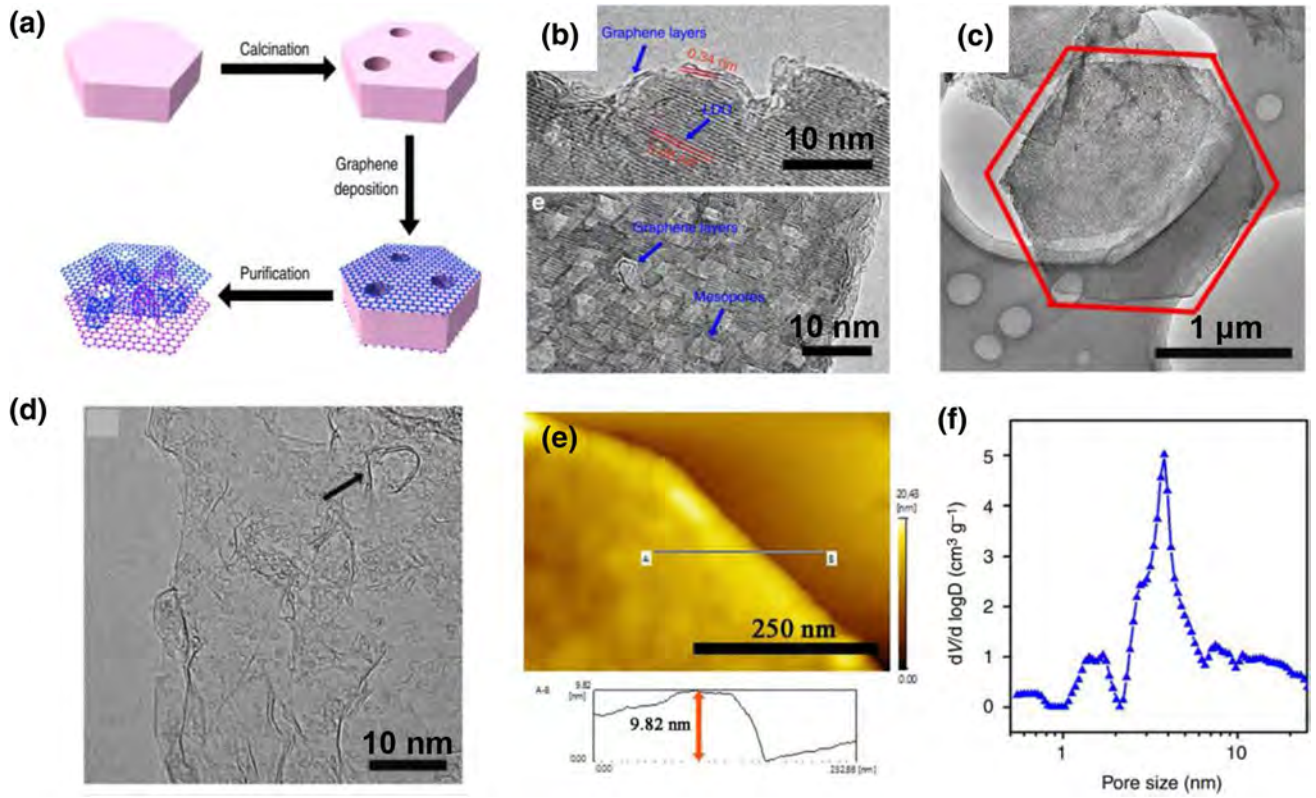

Fig. 5 MgAl LDO-templated CVD growth of unstacked double-layer mesoporous graphene. **a** Schematic for the synthesis of unstacked graphene. **b** TEM image of the graphene cast onto the mesoporous LDO flake. **c**, **d** TEM images and **e** atomic force microscopy (AFM) image of the purified unstacked graphene. **f** Pore size distribution of the unstacked graphene. Reprinted with permission from Ref. [182]

template (Fig. 6a). Here, the hierarchical porous graphene monolith was covalently constructed by using internally connected graphene microrods which were built up through the integration of many hollow graphene nanocages/nanorods (Fig. 6b, c), resulting in a high specific surface area of 1590 $m^2 g^{-1}$, a large pore volume of 2.62 $cm^3 g^{-1}$, an excellent electrical conductivity of 32.5 S cm^{-1}, and an outstanding mechanical stability to support over 10,000 times its own weight. Researchers have reported that other complex compounds and even natural materials containing active oxides can also serve as promising porous templates for the CVD synthesis of 3D hpG materials, such as molecular sieves [198, 199], vermiculites [200–203], diatomites [204], seashells [167], cuttlebones [168], and possess remarkable promise for the effective construction of biomineral and delicate hierarchical structures. In particular, NaCl powder is an attractive template for the green and scalable synthesis of 3D hpG materials, contributing to cost reductions, water-soluble nature, excellent graphitization activity and template effects [205–207]. For example, Li et al. [207] reported the fabrication of a freestanding flexible graphene paper composed of polyhedron graphene nanoboxes using NaCl as the template in a microwave plasma-enhanced CVD system (Fig. 6d–f). Here, the fabrication procedure consisted of the synthesis of a graphene base layer, the melting of NaCl to form a NaCl nanocrystal film and the growth of 3D prism-like graphene building blocks, during which the melting of NaCl by a direct current bias of 270 V was crucial for the formation of the unique film-type nanocrystal template.

Both metal and metal oxide templates are attractive for the CVD growth of 3D hpG materials due to the feasible tunability of the as-obtained hierarchical porosity and graphene quality, whereas other templates are less effective in the growth of high-quality ultrathin graphene layers. And compared with porous metal templates, metal oxide templates can provide more advantages and opportunities in the controllable regulation of the nanostructure and morphology of as-obtained porous graphene frameworks, especially in the mesoscale. In addition, the metal oxide route is free of active metal species and easy to purify, which is vital for advanced electrochemical energy storage devices. Moreover, effective scaled-up synthesis by using nano-agglomerate fluidized bed reactors [149, 150] and the low-cost and potential cycling of powdery metal oxide templates make it possible to fabricate 3D hpG materials in a large-scale, cost-effective, and green method. However, current understandings of the

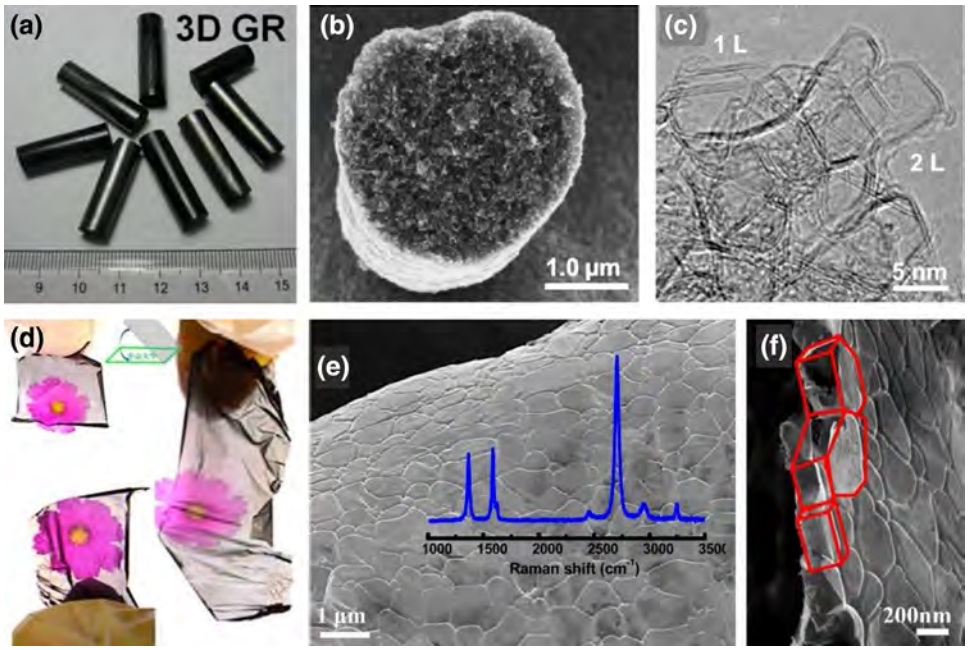

Fig. 6 Other mesoporous templates for CVD growth of 3D hpG materials. **a** Photograph, **b** SEM images and **c** TEM image of the hierarchical porous graphene monolith grown using SiO_2 templates. **a**–**c** are reprinted with permission from Ref. [196]. **d** Photograph and **e**, **f** SEM images of the freestanding flexible graphene paper grown using NaCl templates. **d**–**f** are reprinted with permission from Ref. [207]

growth mechanism and kinetics of 3D hpG materials on metal oxide substrates are limited, especially for the tuning of graphene layers and crystallinities, which significantly restrict the exploration and design of more effective templates and the rational construction of advanced 3D hpG materials. And as a result, further investigations are required.

2.2 Graphene Oxide-Based Post-treatment

2.2.1 Porosity Regulation in Graphene Oxide Assembly

In addition to CVD, wet chemical synthesis involving the exfoliation of graphite flakes into GO intermediates followed by reduction to recover the graphene structure (reduced graphene oxide, rGO) is currently an effective and mature method to fabricate graphene [107, 108, 208]. These as-obtained GO materials are ultrathin 2D nanosheets with abundant oxygen-containing functional groups and defects on the surface, resulting in excellent dispersity in water and versatile processability. Thus, GO and rGO nanosheets are the most commonly used building blocks to assemble 3D porous graphene scaffolds by using methods such as spin-coating, vacuum filtration, hydrothermal reaction, templated assembly, layer-by-layer assembly and activation [7, 89, 92–94, 209–211].

Due to the high hydrophilicity and surface functional groups of GO and the van der Waals (vdW) interactions between rGO, GO nanosheets can be self-assembled under hydrothermal reactions [212–215] or covalently interconnected with polymer monomers [216], resulting in GO hydrogels and 3D porous graphene macrostructures after drying and reduction. Xu et al. [213] were the first to demonstrate the self-assembly of 2D GO sheets into 3D hydrogel macrostructures using a convenient one-step hydrothermal process at 180 °C for 1–12 h (Fig. 7a) and reported that the as-fabricated graphene hydrogel was electrically conductive, mechanically strong, and thermally stable, even with 97.4 wt% water (Fig. 7b). Furthermore, the researchers reported that after freeze-drying, a well-defined, and interconnected 3D porous network can be obtained due to the physical cross-linking effect because of the partial overlapping or coalescing of the flexible graphene sheets (Fig. 7c) with pore sizes in the range of sub-micrometers to several micrometers and walls consisting of thin layers of stacked graphene sheets. Researchers have also reported that pore sizes and porosities can be tailored by changing the drying methods or GO precursor size. For example, Xie et al. [217] reported that increased freeze-drying temperatures can significantly tune the pore size and wall thickness of obtained 3D porous graphene by 80 times (from 10 to 800 μm) and 4000 times (from 20 nm to 80 mm), respectively, and that 3D porous graphene can change from hydrophilic to hydrophobic with Young's modulus varying by 15 times (from 13.7 to 204.4 kPa). In a further study, instead of using the widely accepted freeze-drying method, Tao et al. [218] used the evaporation-induced drying of graphene hydrogels (Fig. 7d) to obtain a compactly interlinked but porous graphene monolith with a density as high as 1.58 g cm^{-3} and a high surface area of 720 m^2 g^{-1} (Fig. 7e) and reported that although freeze-drying can retain the 3D porous network of the hydrogel due to the ice template and subsequent sublimation, the evaporation-induced drying of water can exert a "pulling force" due to the strong interaction between graphene and water to significantly shrink the 3D network.

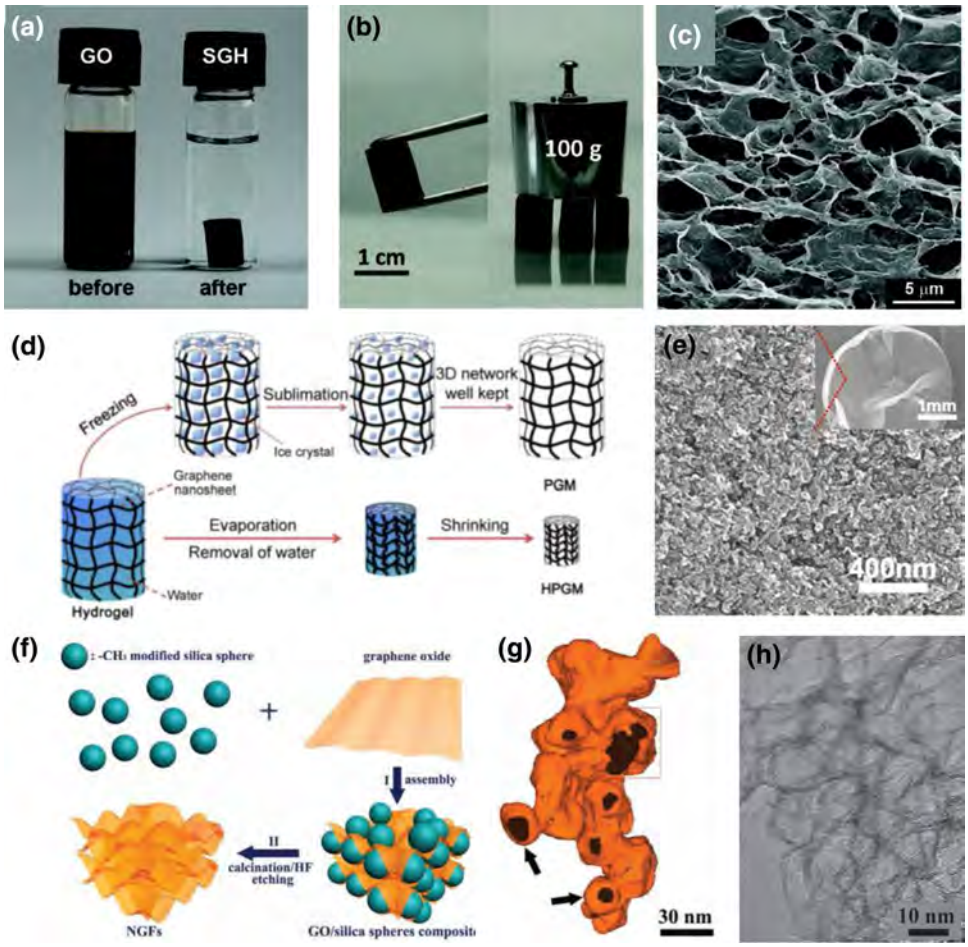

Fig. 7 Porosity regulation in GO assembly. **a** Photograph of GO dispersion before and after hydrothermal reduction. **b** Photographs of the self-assembled graphene hydrogel. **c** SEM image of the dried graphene hydrogel. **a**–**c** are reprinted with permission from Ref. [213]. **d** Comparison between the freeze-drying and evaporation-induced drying of graphene hydrogels. **e** SEM images of the compact but porous graphene monolith obtained through evaporation-induced drying. **d**, **e** are reprinted with permission from Ref. [218]. **f** Schematic of the synthesis of mesoporous graphene foam with silica spheres as the template. **g** 3D electron tomography reconstruction and **h** TEM image of the obtained mesoporous graphene foam. **f**–**h** are reprinted with permission from Ref. [223]

Despite simple processes and scalable production, the fabrication of hierarchical porous graphene frameworks through the liquid self-assembly of GO precursors is difficult due to the large size of GO sheets, limiting pore sizes to the micrometer scale. However, with the introduction of nano-sized or mesosized templates, the construction of graphene macrostructures with more delicate porosities and emerging properties becomes possible. Here, various hard and soft templates have been reported to be capable of directing the interfacial assembly of GO nanosheets with pore sizes varying from 20 nm to 2 μm, such as anodic aluminum oxide [219], cellulose fibers [220], polystyrene colloidal particles [221], silica spheres [222, 223], ice nanocrystal [224], hexane droplets [225], polyethylenimine droplets [226], microemulsion [227] and polystyrene spheres [228]. For example, Huang et al. [223] reported a hydrophobic interaction-driven hard templating approach using silica spheres to synthesize mesoporous graphene foam (Fig. 7f) in which the mixing of methyl group grafted silica spheres with GO nanosheets in a neutral aqueous solution can allow for GO nanosheets to wrap around silica spheres and form 3D continuous mesoporous networks due to the strong hydrophobic interaction between them. Here, the porous structure was fully confirmed by 3D electron tomography reconstruction and exhibited highly interconnected pores with a near spherical morphology and a diameter of ~ 30 nm, which originated from the silica spheres (Fig. 7g). And as a result of this template–direction assembly using mesosized silica spheres, this resulting mesoporous graphene foam exhibited thin pore walls (~ 1 nm, 2–3 layers), controllable pore sizes (30–120 nm), ultrahigh pore volumes (4.3 $cm^3\ g^{-1}$), and high specific areas (851 $m^2\ g^{-1}$) (Fig. 7h). In addition, a novel autoclaved leavening and steaming treatment of GO layered films was proposed to synthesize paper-like, lightweight, and highly conductive rGO foams by using the pore-forming effect of in situ generated gases. Here, the compact layered GO structure as the "dough" and the fast hydrazine vapor reduction of GO to rGO were key to the rapid evolution of gaseous species, mimicking the "leavening" process and forming porous graphene materials.

2.2.2 Surface Polymerization on Graphene Oxide Sheets

In addition to serving as pore walls for the synthesis of 3D macrostructures, GO nanosheets can also act as excellent substrates for surface polymerization with micro-/

mesoporous secondary structures in which the large surface area, ultrathin structure, and abundant surface functional groups make GO nanosheets favorable for the adsorption and decoration of nanosized templates such as SiO_2 nanoparticles [229], molecular sieves (e.g., SBA-15) [230], triblock copolymer (e.g., F127) [231], polymer monomers [222, 232, 233]. For example, Chen et al. [229] synthesized a sandwich-type hierarchical porous graphene material with abundant surface micro-/mesopores (0.8–6 nm) through a double-template method using GO as the shape-directing substrate, SiO_2 nanoparticles as the mesopore guide and in situ formed polypyrrole as the carbon precursor (Fig. 8a) and reported that the as-obtained sandwich-type graphene nanosheets with a thickness of 10–25 nm were highly interconnected to form a 3D hierarchical porous structure (Fig. 8b), delivering a high specific surface area of 1558 $m^2\ g^{-1}$ (a micropore area of 1058 $m^2\ g^{-1}$) and a total pore volume of 1.1 $cm^3\ g^{-1}$. In another example, Song et al. [231] synthesized nitrogen-doped ordered mesoporous carbon on GO nanosheets using an interfacial triblock copolymer assembly to obtain a 3D hpG material with a high specific surface area of 1569 $m^2\ g^{-1}$, a total pore volume of 1.38 $cm^3\ g^{-1}$, an interconnected micro-/mesoporous structure, a highly accessible nitrogen content (6.52 at%), and good electronic conductivity.

2.2.3 Activation to Generate In-Plane Micro-/Mesopores

Another important method to enrich the hierarchical porosity of GO-derived graphene materials involves the moderate chemical activation of GO nanosheets to generate in-plane micro-/mesopores, such as through the use of KOH [234–238], $KMnO_4$ [239], H_2O_2 [240, 241], Fe/$Fe_{3-x}O_4$ [242–244], etc. in which graphene lattices can be maintained as abundant in-plane holes due to the removal of functional groups or carbothermal reactions. For example, Zhu et al. [234] were the first to introduce a routine KOH activation method in 2011 for the synthesis of porous graphene materials with high specific surface areas involving the mixing

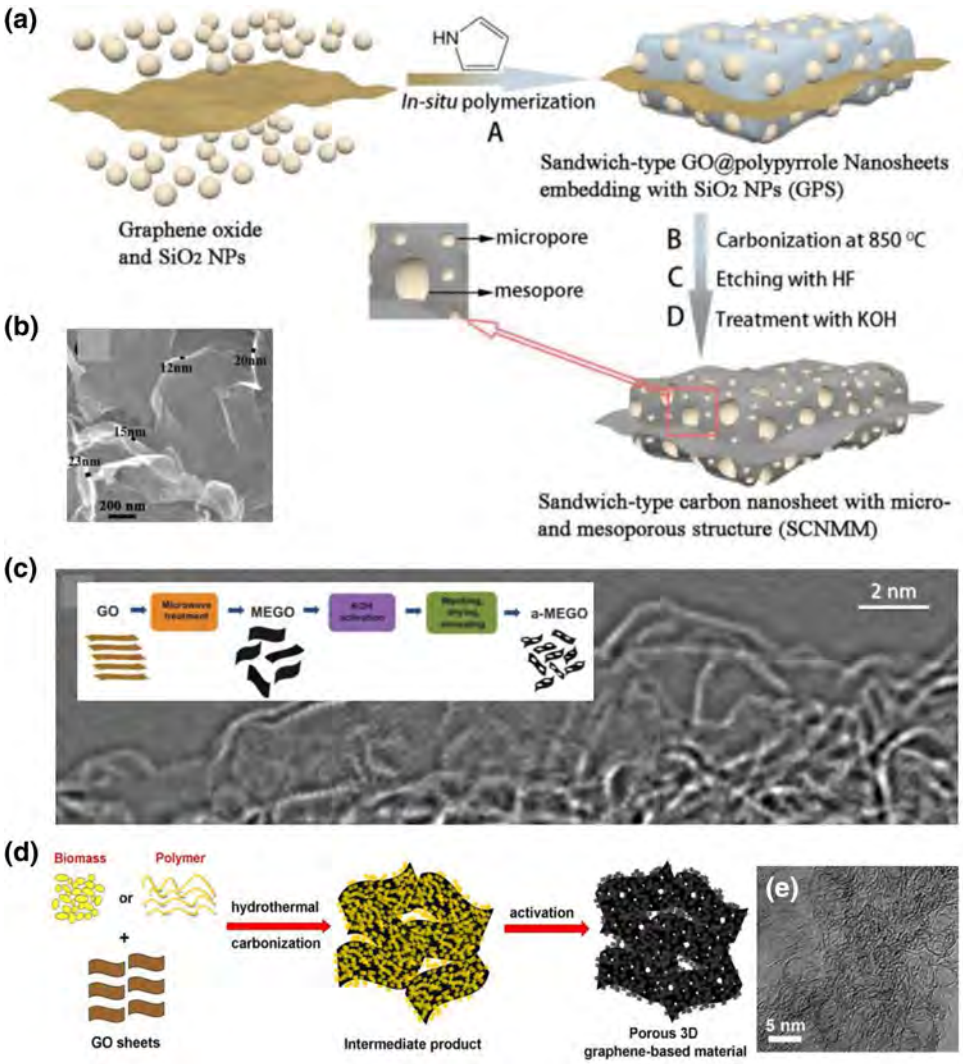

Fig. 8 Surface polymerization or activation of GO nanosheets. **a** Schematic of the preparation of sandwich-type hierarchical porous graphene materials through a double-template method. **b** SEM image of the obtained sandwich-type hierarchical porous graphene nanosheets. **a**, **b** are reprinted with permission from Ref. [229]. **c** HRTEM image of KOH activated GO and the schematic of the fabrication procedure (inset). Reprinted with permission from Ref. [234]. **d** Schematic of the two-step approach to synthesize high specific surface area hpG materials. **e** High-resolution TEM image of the obtained 3D hpG material. **d**, **e** are reprinted with permission from Ref. [103]

of microwave exfoliated GO with KOH solution to form a series of GO/KOH mixtures and subsequent chemical activation under flowing argon at 400 Torr and 800 °C for 1 h (Fig. 8c). Here, sp^2-bonded graphene can transform into a continuous 3D network of highly curved, atom-thick walls with primarily 0.6 to 5 nm pores, resulting in a high specific surface area of up to 3100 $m^2\ g^{-1}$ coupled with a total pore volume of 2.14 $cm^3\ g^{-1}$, which can also be readily tailored through the ratio of KOH and GO. The researchers in this study suggested that the activation of graphene with KOH proceeded as $6KOH + 2C \leftrightarrow 2K + 3H_2 + 2K_2CO_3$, followed by the decomposition of K_2CO_3 and/or reaction of $K/K_2CO_3/CO_2$ with carbon. And as a result, despite the abundant micropores and mesopores, the graphene lattice structure was well preserved with a very low H and O content (a C/O atomic ratio of up to ~ 35), a small fraction of edge atoms, and essentially the absence of dangling bonds, leading to a high electrical conductivity of ~ 500 S m^{-1} and outstanding performances in supercapacitors. Furthermore, Lacey et al. [245] combined controlled air oxidation with liquid-phase oxidation to synthesize holey graphene oxides with 4–25 nm through-holes and excellent hydrophilicity, which facilitated stable 3D printable ink dispersions in H_2O without any additive and the facile 3D printing of 3D hpG architectures.

Researchers have also reported that the coupling of templated self-assembly, surface polymerization, and chemical activation strategies can enable the efficient and versatile synthesis of 3D hpG materials using GO precursors with trimodal porosities in the nanoscale (in-plane vacancies and holes), microscale (surface mesopores and wrinkles) and macroscale (void spaces) [103, 241, 246]. For example, Zhang et al. [103] proposed a simple but efficient two-step approach to obtain 3D hpG materials in bulk (Fig. 8d) in which in situ hydrothermal polymerization/carbonization was first used to transform a mixture of cheap carbon sources with GO to 3D hybrid precursors, followed by chemical activation to generate desired micro-/mesoporosities. And as a result, the as-obtained 3D hpG material, consisting of mainly defected/wrinkled single-layer graphene sheets a few nanometers in size (Fig. 9e), exhibited an ultrahigh specific surface area of 3523 $m^2\ g^{-1}$ and an excellent bulk conductivity up to 303 S m^{-1} in which the ultrahigh specific surface area above theoretical upper limits was attributed to the nanosized graphene domains and abundant edge carbons.

In summary, the GO-based post-treatment is a facile, simple, and efficient method for the bulk fabrication of 3D hpG materials, allowing for heteroatom doping and hybridization with guest components. However, this method suffers significantly from poor structural controllability,

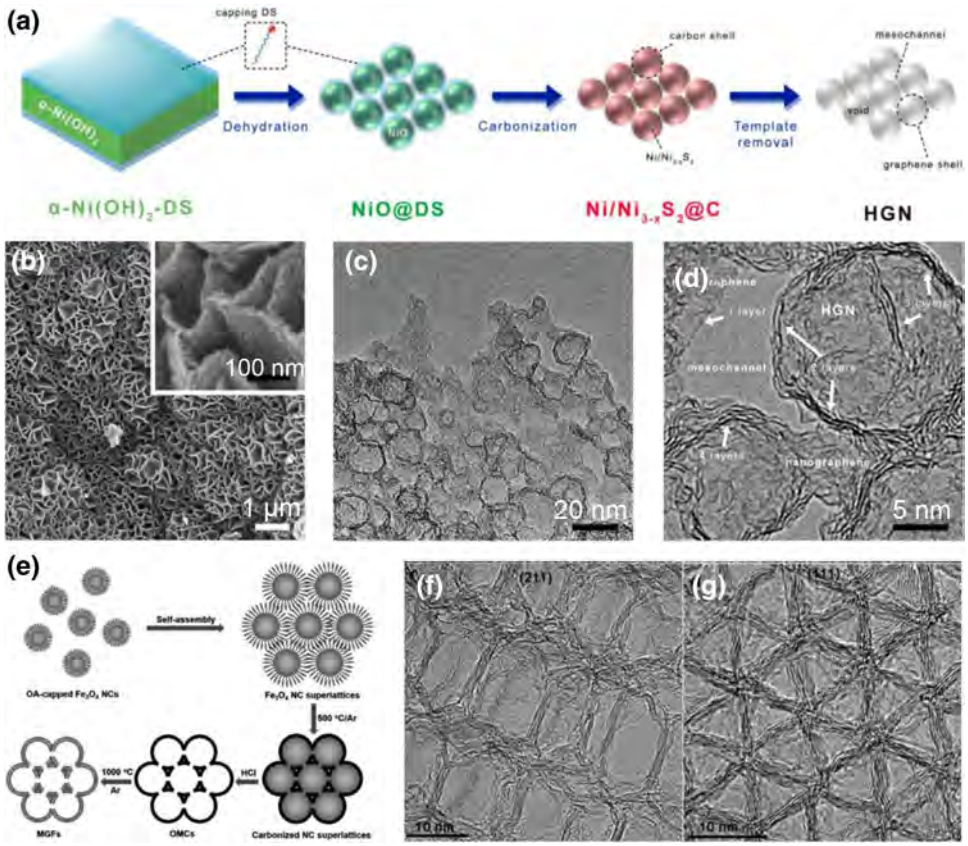

Fig. 9 Templated polymerization to fabricate 3D hpG materials. **a** Schematic of the self-limiting assembly of flower-like graphene materials from dodecyl sulfate-intercalated α-$Ni(OH)_2$. **b** SEM images and **c**, **d** TEM images of obtained hollow graphene. **a**–**d** are reprinted with permission from Ref. [254]. **e** Schematic of the fabrication of mesoporous graphene frameworks from colloidal Fe_3O_4 nanocrystals. **f**, **g** TEM images of the obtained graphene material. **e**–**g** are reprinted with permission from Ref. [256]

limited batch stability, and abundant defective sites, which cannot be fully recovered through subsequent reduction, resulting in limited properties.

2.3 Templated Polymerization

Although above-mentioned methods based on CVD or GO precursors are different, the utilization of appropriate porous templates is key to successfully fabricate 3D hpG materials. And in the case of GO-based post-treatments, templates mainly serve as pore-forming agents through physical effects and therefore should consist of uniform nanoparticles or nanospheres that are easily fabricated. Alternatively, templates during templated CVD growth, offering a delicately porous scaffold for graphene replication and necessary activity for carbon decomposition and graphene nucleation/growth, should consist of metal or metal oxides. These active templates can also catalyze the cracking and polymerization of complex solid carbon precursors and further promote the formation of highly graphitized graphene-like materials with thin layers, good conductivity, and hierarchical porosities, and include $Ni(OH)_2$/NiO nanoparticles for phenolic resin [247], FeO(OH) nanorods for poly(2-fluoroaniline) [248], NaCl for cysteine [249], $NaNO_3$ for gelatin [250], MgO nanosheets/nanowires for pitch [152], aromatic polyimides [153], sucrose [251], and starch [252, 253]. For example, Strubel et al. [175] were the first to report the synthesis of hierarchical porous graphene using ZnO nanoparticles as the template and sucrose as the carbon source at 950 °C for 2 h without the need for toxic/reactive gases or acid purification. And as a result, an outstanding specific surface area of 3060 $m^2\ g^{-1}$ coupled with a high total pore volume of 3.45 $cm^3\ g^{-1}$ was achieved, which was particularly suitable for application as sulfur host materials in Li-S batteries. In another example, Peng et al. [254] used a mesoscale catalytic self-limited assembly strategy to obtain a 3D hierarchical flower-like graphene material with single/few graphitic layers and interconnected hollow nanostructures. In their synthesis process, dodecyl sulfate-intercalated α-$Ni(OH)_2$ was first synthesized and dehydrated to form dodecyl sulfate-capped NiO nanosheets. Following this, the capping dodecyl sulfate was annealed at 800 °C and pyrolyzed into small carbon molecules and carbon segments, which subsequently catalytically recombined into highly graphitic shells on the surface of Ni-based hard templates (Fig. 9a) in which the obtained material was composed of hollow graphene spheres with a diameter of 10–30 nm, a pore volume of 1.98 $cm^3\ g^{-1}$ and a large specific surface area of 979 $m^2\ g^{-1}$ (Fig. 9b–d). Here, the researchers reported that the solid carbon precursors cannot fully permeate into the micro-/mesoporous scaffolds of the porous template, thus considerably limiting the precious replication of the inner hierarchical porous structure as compared with the CVD method. In addition, because the template and solid carbon precursors were mixed before pyrolysis, the cracking and polymerization of these carbon precursors can be simultaneously initiated from different sites and generate large numbers of gases in situ, resulting in the lack of control of the micro-/mesoporous structure and more defects in the graphene layers.

The self-assembly of colloidal nanoparticles can lead to 3D superlattices with controlled symmetry and periodicity, which are promising templates for the fabrication of 3D highly ordered hpG materials. For example, Yoon et al. [255] used the self-assembly of colloidal silica on various substrates (e.g., Al_2O_3, quartz, SiO_2/Si) as templates, infiltrated iron chloride hexahydrate as a Fe catalyst and polyvinyl alcohol as a solid carbon source for graphene growth in which after annealing under a hydrogen environment at 1000 °C, the carbon precursor transformed into few-layer graphene covering the surface of silica nanospheres. Here, the researchers reported that the 3D graphene network was composed of interconnected graphene nanoballs (220 nm in diameter) and mesopores (40 nm) on the surface and exhibited a high specific surface area of 1025 $m^2\ g^{-1}$ and an electrical conductivity of 52 S cm^{-1}. In further studies, Jiao et al. [256, 257] synthesized 3D highly ordered mesoporous graphene frameworks using self-assembled colloidal Fe_3O_4 nanocrystals as the template and capping oleic acid as precursors in which the precursors were first carbonized into partially graphitic frameworks at 500 °C under Ar, followed by template removal and further graphitization at 1000 °C under Ar (Fig. 9e). As a result, the obtained frameworks possessed a face-centered-cubic symmetry with interconnected mesoporosity, ultrathin pore walls with three-to-six graphene layers, tunable pore widths, high specific surface areas (~ 1000 $m^2\ g^{-1}$), and large pore volumes (~ 1.8 $cm^3\ g^{-1}$) [256]. Here, the researchers suggested that the ~ 10 nm large pores derived from the removed Fe_3O_4 nanoparticles, whereas the small ~ 3 nm pores corresponded to the interconnected windows (Fig. 9f, g). In addition, the researchers reported that the graphene wall thickness can be finely tuned from 2 to 6 layers through the adjustment of capped ligand chain lengths [258] and that different macroscale morphology can be obtained based on the type of super lattice assembly used, such as mesoporous films [259] and spheres [260].

In summary, great progress has been achieved in the fabrication of 3D hpG materials possessing hierarchical micro-/meso-/macroporous structures. And based on different synthetic strategies (templated CVD, GO-based post-treatment, and templated polymerization) and different types of templates (metal, metal oxide, soft templates, etc.), as-obtained 3D hpG materials can possess different qualities, morphology, properties, and applications. Here, although metal-templated CVD growth method is expensive and provides limited structural regulation, it can fabricate graphene with the

highest crystallinity and effectively construct uniform and high-quality graphene with delicate porosities. Therefore, more in-depth studies are needed to probe growth mechanisms. As for GO-based post-treatment, this is favorable for the large-scale production of porous graphene with rich porosities; however, more synthesis strategies need to be explored to recover defects. Furthermore, templated polymerization is a versatile and simple method to synthesize porous graphene with more opportunities to functionalize as-obtained materials in which 3D templates with tunable surface chemistry and nanostructures are highly expected.

3 Functionalization of 3D Hierarchical Porous Graphene

3D hpG materials with well-designed nanostructures and high electrical conductivities are believed to be excellent candidates for electrode materials in various electrochemical energy storage and conversion devices through the enhancement of electron transfer and mass transport in 3D interconnected pathways. However, perfect graphene lattices are chemically inert and require the rational functionalization of carbon-only graphene materials with active heteroatoms or guest components to imbue more appealing properties and practical applications [261–269]. Based on this, this section will highlight pivotal and unique functionalization strategies, including (1) heteroatom doping and single atomic metal coordination, (2) spatially confined decoration of active nanoparticles, and (3) surface hybridization of graphene-analogous components.

3.1 Heteroatom Doping and Single Atomic Metal Coordination

Heteroatom doping is among the most simple and effective approaches to regulate the electronic structure and chemical properties of graphene. And compared with the homogeneous nonpolar surface of pristine graphene, heteroatom-doped graphene can provide excellent active sites for various electrocatalysis applications [11, 104, 270] and can also enhance interactions between graphene and guest materials, such as polysulfides in Li-S batteries to prevent the shuttle effect [271]. In general, heteroatom doping can be divided into bulk doping and surface doping, which can be achieved by using different methods and exhibit different accessibilities. In addition, doping can involve single- or multi-non-carbon elements, including N, B, O, F, S, and P.

The bulk heteroatom doping of 3D hpG materials is mainly conducted through in situ CVD or templated polymerization with heteroatom-including precursors (e.g., NH_3, pyridine, thiophene, polyimide, polyaniline, phytic acid, urea, melamine, $(NH_4)_3PO_4$) [79, 136, 138, 151, 153, 155, 158, 253, 272–277] or through post-treatment of ultrathin GO with heteroatom-including chemicals (e.g., ionic liquid, polydopamine, thiourea, urea, NH_3) [232, 278–280]. For in situ CVD, the content of incorporated heteroatoms is always less than 5 wt% and can significantly decrease with increasing temperatures. For example, Chen et al. [158] used in situ CVD to controllably synthesize graphene nanocages with pyridine as the precursor and MgO as the template. Here, the researchers reported that nitrogen content remained at a high level of around 10 wt% at CVD temperatures of below 800 °C and decreased to 4.5 wt% as the temperature increased to 900 °C. In addition, researchers also reported that the predominant nitrogen configuration will transform from pyridine-N and pyrrolic-N below 650 °C to quaternary-N and pyridine-N above 700 °C and that annealing at 1150 °C for 2 h under N_2 atmosphere allowed for the complete removal of nitrogen atoms in the graphene (4 at%) and the reconstruction of the graphene lattice into multiple single-atom vacancies and defects [281]. In another example, Dai et al. [79] fabricated an N/S/O-doped hierarchical porous graphitic structure using KCl and Ni assisted polymerization in which a melamine–Ni_2SO_4–KCl mixture was used as the precursor with Ni_2SO_4 serving as the nickel and sulfur precursor, melamine as the carbon and nitrogen source, and KCl or KCl-coated Ni precursors as the catalytic template (Fig. 10a). Here, the precursor mixture was subjected to annealing at 700 °C for 2 h, followed by subsequent annealing at 800 °C for 2 h, metal removal and a final annealing at 900 °C for 2 h under Ar to obtain a unique hierarchical porous graphitic material with stereoscopic holes over the graphene surface (Fig. 10b). And as a result, this obtained material exhibited an excellent conductivity of 22 S cm^{-1}, a high specific surface area of 576 m^2 g^{-1}, a large pore volume of 1.40 cm^3 g^{-1} and abundant doping atoms, including nitrogen (2.1 at%), sulfur (0.8 at%), and oxygen (3.8 at%), resulting in effective trifunctional ORR/OER/HER electrocatalysis.

Given the ultrathin nature of graphene building units, the bulk doping of 3D hpG materials can be regarded as surface doping in most cases, which is important for the full exposure and utilization of active sites; however, it is difficult to achieve favorable hierarchical porosity and heteroatom doping simultaneously. In addition, the electrical conductivity of as-obtained materials can be harmed due to the destruction of graphene matrixes by lattice dopants. To address these issues, researchers have reported that two-step CVD or surface polymerization on GO nanosheets are effective in the synthesis of surface-doped 3D hpG materials without the influence of nanostructures constructed in advance [233, 282–285]. For example, Shi et al. [282] proposed the deposition of nitrogen-doped graphene skins on 3D porous graphene frameworks already grown on mesoporous MgO templates (Fig. 10c) and reported that as compared with

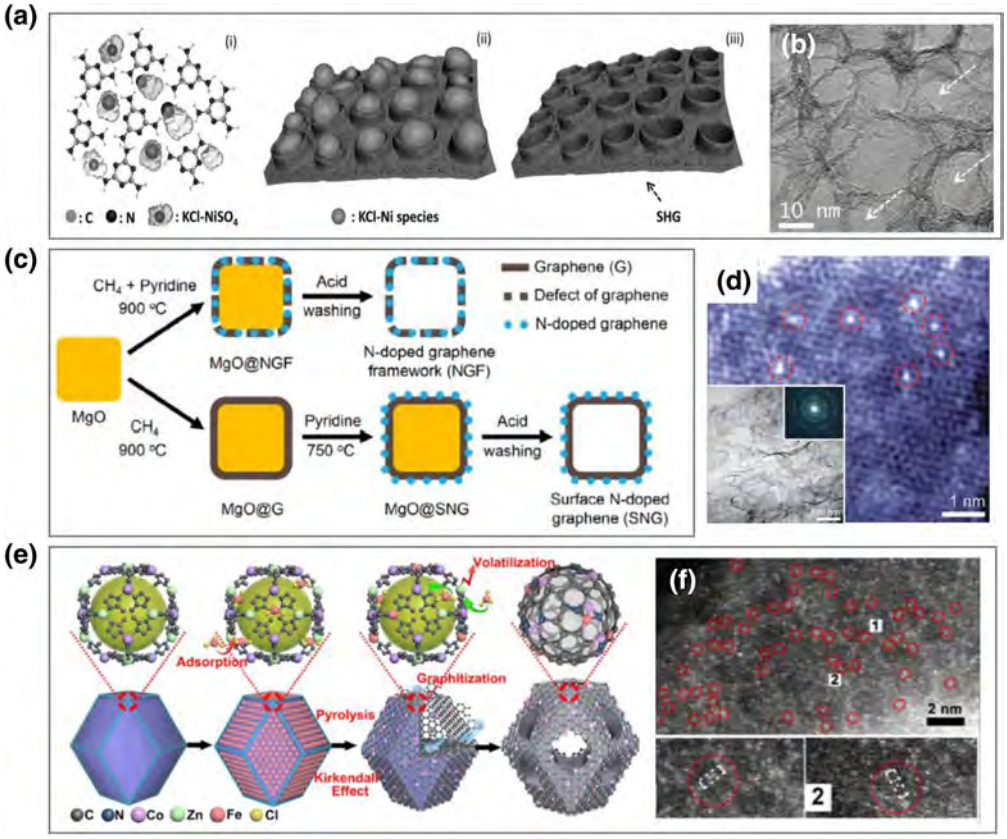

Fig. 10 Heteroatom doping and single atomic metal coordination in 3D hpG materials. **a** Schematic of the preparation of N/S/O-doped porous graphene with stereoscopic holes using KCl-Ni_2SO_4 as the template precursor. **b** TEM image of the obtained N/S/O-doped porous graphene. **a**, **b** are reprinted with permission from Ref. [79]. **c** Schematic of the preparation of surface N-doped mesoporous graphene frameworks through the two-step CVD process. Reprinted with permission from Ref. [282]. **d** High-angle annular dark-field scanning TEM (HAADF-STEM) image of the Ni-doped graphene. Reprinted with permission from Ref. [290]. **e** Schematic of the preparation of N-doped porous carbon with Fe-Co dual sites. **f** HAADF-STEM image showing the Fe-Co dual sites. **e**, **f** are reprinted with permission from Ref. [296]

routine N-doped graphene frameworks with bulk doping, the surface-doped graphene framework possessed a higher nitrogen content (1.81 vs. 1.18 at%) and enhanced electrical conductivity (31 vs. 23 S cm^{-1}) simultaneously. Furthermore, Li et al. [284] reported the synthesis of hierarchical porous sandwich-like N/P dual-doped graphene materials through the direct pyrolysis of a polymer gel composed of GO, polyaniline, and phytic acid in which the resulting N/P dual-doped mesoporous carbon layer generated during surface polymerization conformally coated both sides of the graphene nanosheet and thus preserved a large specific surface area of 900 m^2 g^{-1}, rendering a high doping level of N (4.71 at%) and P (1.72 at%).

Furthermore, atomically dispersed metal sites coordinated with/without nitrogen into graphene matrixes have recently been widely investigated as excellent candidates for various energy-related electrocatalytic reactions [286–289]. For example, Qiu et al. [290] in 2015 reported the fabrication of single atomic Ni-doped mesoporous graphene as superior HER catalysts in acidic solution. Here, the reported graphene was grown on a mesoporous Ni foam template by using benzene as the carbon precursor at 800 °C, followed by template removal using 2.0 M HCl solution. And after a 7-hour dissolution process, the residual Ni concentration reportedly remained nearly constant (4–8 at%), suggesting strong chemical affinity toward the mesoporous graphene in which the residual Ni atoms were confirmed to be individual atoms in the graphene lattice with a number density of ~ 10^{18}–10^{19} m^{-2} (Fig. 10d). More efficiently, researchers have also reported that atomically dispersed metal sites can be coordinated into porous graphene matrixes by using metal–organic framework (MOF)-assisted pyrolysis [291–293] or the defect trap effect [294, 295], and highly dispersed multi-metal sites can be achieved through delicate design and synthesis. For example, Wang et al. [296] investigated nitrogen-doped porous carbon with porphyrin-like Fe-Co dual sites as highly active and stable ORR electrocatalysts in acidic media and reported that the controllable

formation of Fe-Co dual sites can be achieved through the bonding between Co nodes (the host) and confined Fe ions (the guest) in the void space of MOFs (Fig. 10e) in which single Fe and Co atoms are homogeneously distributed in a porous carbon matrix with dual-site configurations originating from the strong bonding between Fe and neighboring Co atoms, which can provide two anchoring sites for dissociated O atoms for accelerated ORR (Fig. 10f).

3.2 Spatially Confined Decoration of Active Nanoparticles

In addition to the incorporation of atomically dispersed heteroatoms or metal sites into graphene matrixes, 3D hpG material functionalities can be further improved through hybridization with guest active materials, including metallic/metalloid materials or metal compounds with different dimensionalities (e.g., 0D nanoparticles, 1D nanotubes/nanoparticles, 2D nanoplates/nanosheets), in which hybridization can be achieved through in situ growth or ex situ assembly (Fig. 11a) [94]. Graphene-based composite nanostructures can generally be classified into six different models, including encapsulated, mixed, wrapped, anchored, sandwich-like and layered structures (Fig. 11b) [31], and in this review, spatially confined decoration and surface hybridization composites which fully utilize the unique nanostructure features of 3D hpG materials will be reviewed.

Owing to the hierarchical porous scaffold and the presence of abundant mesopores, guest active materials can be spatially confined in mesoporous areas with uniform decoration, controllable size, strongly coupled interfaces and enhanced accessibility. For example, Jiao et al. [257] reported the fabrication of 3D interconnected nanoparticle superlattices confined in mesoporous carbon frameworks

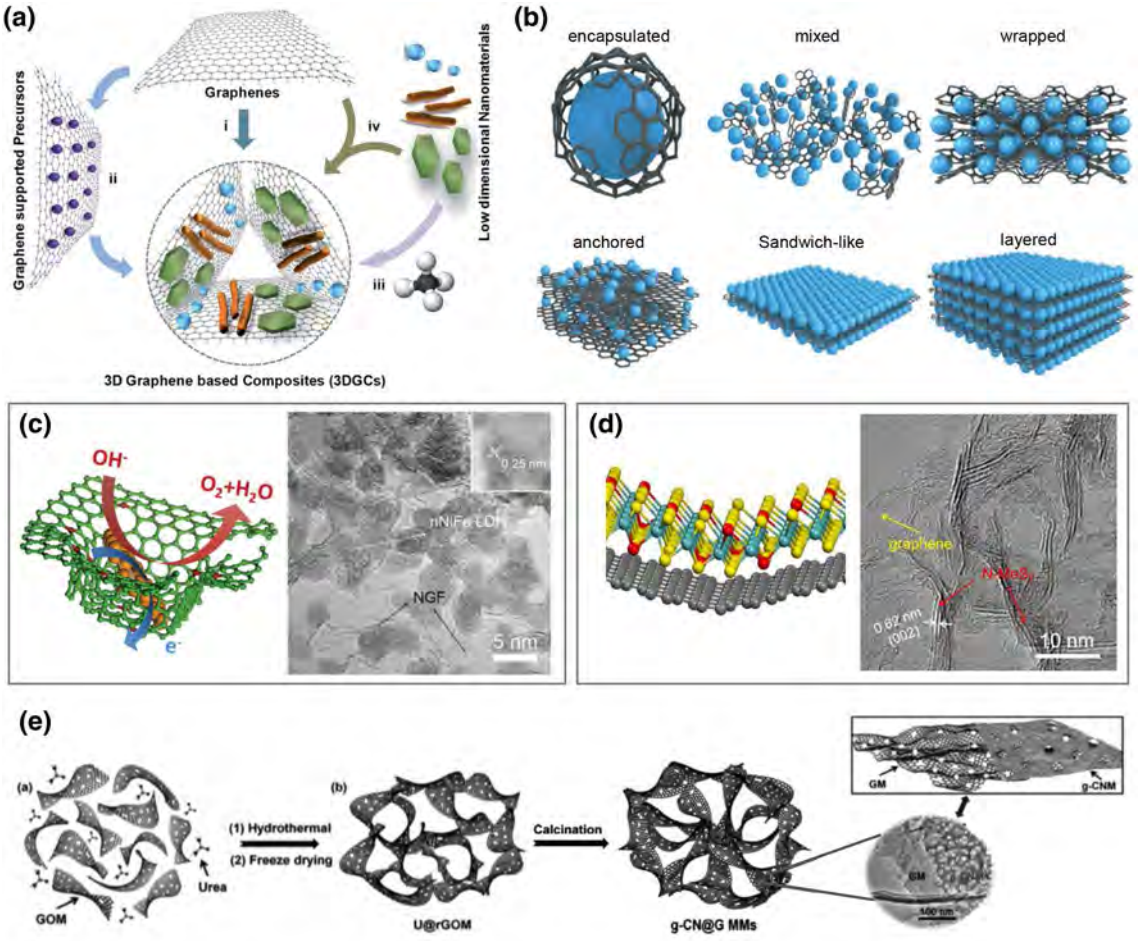

Fig. 11 Spatially confined decoration or surface hybridization of guest active components in 3D hpG materials. **a** Schematic of different types of 3D graphene-based composites. Reprinted with permission from Ref. [94]. **b** Different types of graphene composite electrode materials. Reprinted with permission from Ref. [31]. **c** Schematic and TEM image of spatially confined nanosized NiFe LDH in nitrogen-doped mesoporous graphene frameworks. Reprinted with permission from Ref. [105]. **d** Schematic and TEM image of the 3D mesoporous graphene@MoS_2 vdW heterostructure. Reprinted with permission from Ref. [106]. **e** Schematic of the preparation of mesh-on-mesh C_3N_4@graphene materials. Reprinted with permission from Ref. [309]

in which the 3D continuous porosity and high surface area of the employed carbon framework facilitated the diffusion of precursors and confined the growth of monodispersed nanoparticles. As a result, the researchers reported that their approach was an effective and general method to incorporate guest materials such as SiO_2, SnO_2, TiO_2, and $Ti_{0.3}Sn_{0.7}O_2$ nanoparticles. In another example, Chen et al. [297] used a facile two-step procedure involving the infiltration of metal precursors and spatially confined growth to fabricate N-doped graphene film-confined nickel nanoparticles as efficient OER electrocatalysts and reported that the graphene sheets and nickel nanoparticles can co-assemble into a well-organized hybrid film, resulting in a lamellar structure, well-developed porosity, nanosized nickel particles (~ 66 nm), high catalyst loading (0.91 mg cm^{-2} for Ni), and optimal electrode contact. Furthermore, Zhang et al. [105, 298–301] synthesized a series of nanoparticles spatially confined in N-doped mesoporous graphene frameworks for electrocatalysis and Li-S batteries in which the researchers reported that the nitrogen dopants and topological defects in graphene can contribute to the effective adsorption and the anchoring of metal precursors and that the in-plane mesopores can spatially confine the nucleation and growth of metal compounds, resulting in a strongly coupled and uniformly decorated hybrid (Fig. 11c) [105]. In addition, these researchers reported that the size of the hybridized components was strictly determined by the size of the graphene mesopores, which can be finely altered by the porous templates for graphene deposition and that the spatial confinement effect of 3D hpG materials can not only offer effective opportunities for composite synthesis, but also benefit the controllable transformation of the nanosized materials, in which with the assistance of mesoporous graphene frameworks, nanosized transition metal hydroxides (< 20 nm) can be facilely converted into hydroxysulfides with excellent morphology preservation and without any aggregation through simple immersion into solutions with high S^{2-} concentration [299].

3.3 Surface Hybridization of 2D Graphene-Analogous Components

Inspired by the unique structure and outstanding properties of 2D graphene monolayers, many 2D graphene-analogous materials such as MoS_2, LDH, graphitic carbon nitride ($g\text{-}C_3N_4$), have been investigated for application in electrochemical energy storage and conversion devices. And as a result of these investigations, an important family of nanomaterials called vdW heterostructures has emerged which can achieve the full potential of 2D materials through the combination of components with distinct properties and functionalities [302, 303]. Here, the replacement of 2D graphene materials with 3D hpG materials can result in 3D hierarchical porous vdW heterostructures that possess both enriched properties and delicate nanostructures beneficial for mass transfer in multi-phase electrochemical processes.

In general, 3D hierarchical porous vdW heterostructures of graphene and graphene-analogous components can be fabricated through layer-by-layer assembly or interfacial growth. For example, exfoliated cationic LDH nanosheets and anionic GO nanosheets can be heteroassembled into superlattice-like hybrids by taking advantage of the electrostatic interaction between them [304–307]. In another example Duan et al. [308] synthesized a 3D hybrid film of $g\text{-}C_3N_4$ and graphene through the integration of 2D porous $g\text{-}C_3N_4$ nanolayers with N-doped GO nanosheets using a simple vacuum filtration method in which the resulting freeze-dried hybrid was reported to be highly flexible and self-supported and contain abundant hierarchical pores ranging from nanometers to micrometers in the intra- and inter-layers as a result of the cross-linking between porous $g\text{-}C_3N_4$ nanolayers and graphene sheets. 3D hpG materials can also serve as interconnected and porous substrates for the subsequent growth of additional 2D graphene-analogous materials on the surface, leading to the formation of 3D vdW heterostructures with a similar scaffold as the graphene substrate. For example, Tang et al. [106] devised a two-step sequential CVD method using mesoporous MgO templates to fabricate a 3D mesoporous graphene/nitrogen-doped MoS_2 vdW heterostructure (Fig. 11d) in which ultrathin MoS_2 nanosheets were locally curved and intimately merged with the previously deposited graphene framework (Fig. 12d). Here, the researchers reported that this 3D mesoporous vdW heterostructure can allow for the engineering of optimal 2D materials with desirable properties such as morphology, interfaces, edges, defects, and electronic structure and therefore lead to superior electrochemical activities. In a further example, Han et al. [309] used a straightforward template-free method to in situ form a mesh-on-mesh hybrid of mesoporous $g\text{-}C_3N_4$ on mesoporous graphene (Fig. 11e) in which during the hydrothermal treatment of GO with urea, a 3D rGO mesh can form and merge with urea foam to convert into a $g\text{-}C_3N_4$ mesh on the surface of graphene. And as a result, this continuous interconnected mesh network can exhibit abundant edges, rich defects, strongly coupled binary structures, fast electron transport, and multi-pathways for charge/mass transport, and thereby demonstrate efficient HER performances.

In summary, heteroatom doping is the most important, effective, and feasible functionalization strategy for 3D hpG materials in which appropriate heteroatom doping can not only favorably regulate the electronic structure of graphene layers, but also enhance the hybridization and performance of guest materials. Here, spatially confined decoration can fully exhibit the properties of guest active materials with nanosized structures and strongly coupled interfaces, but is

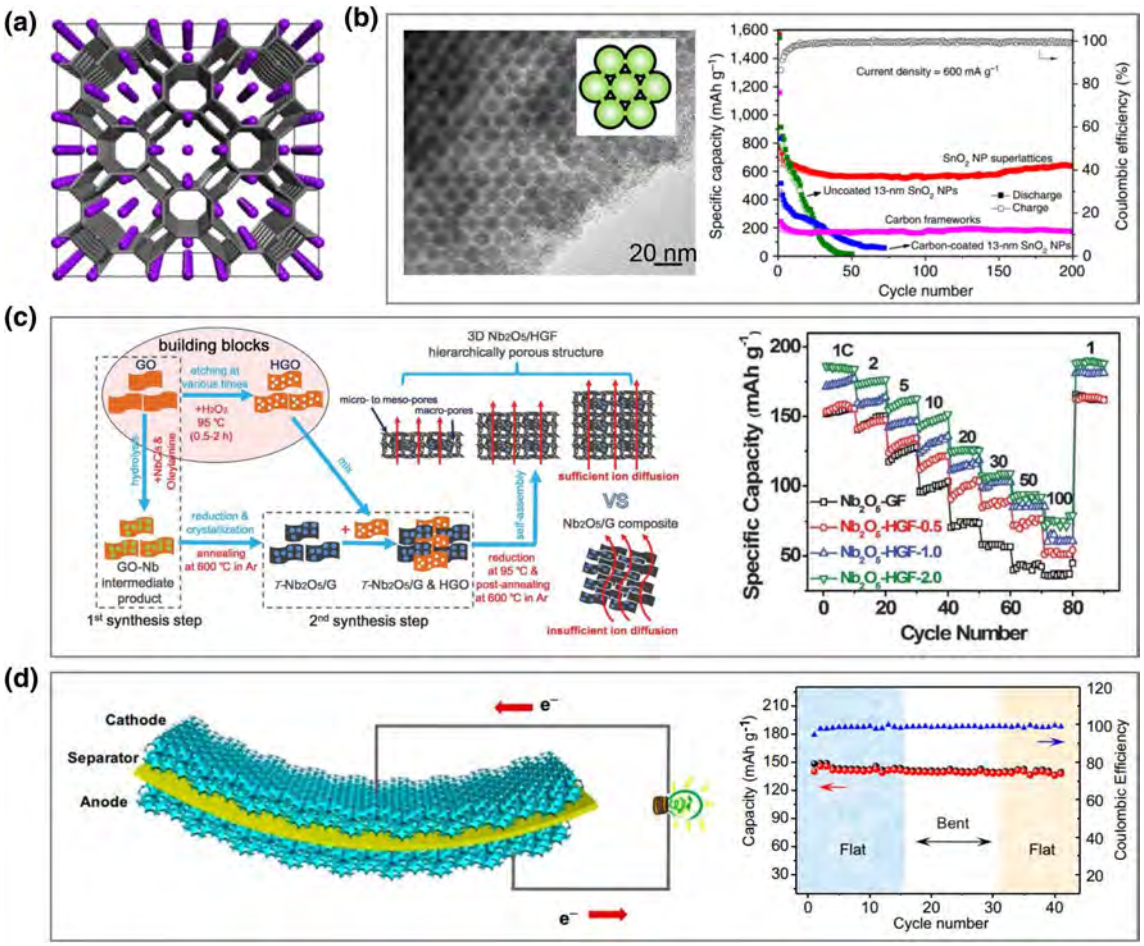

Fig. 12 Application in LIBs. **a** Atomic structure of Li intercalated 688P schwarzite at $Li_{1.5}C_6$. Reprinted with permission from Ref. [323]. **b** TEM image and cycling performance of SnO_2 nanoparticles embedded in mesoporous carbon frameworks. Reprinted with permission from Ref. [257]. **c** Schematic of the preparation and rate performance of 3D holey graphene/Nb_2O_5 composites. Reprinted with permission from Ref. [241]. **d** Schematic of a flexible battery made from 3D graphene foam and cycling performances under flat and bent states. Reprinted with permission from Ref. [121]

limited by the nanostructure of the 3D hpG substrates. Alternatively, surface hybridization is an efficient approach to construct advanced energy materials by using a large family of 2D components, especially vdW heterostructures; however, the fabrication of 3D vdW heterostructures in a facile method with controllable nanostructures is difficult, with little being reported. Despite this, these heterostructures are believed to be promising energy materials.

4 Application in Advanced Batteries and Electrocatalysis

3D hpG materials can be controllably fabricated and versatilely functionalized through many different methods. And although the seamless assembly of 2D graphene building units can preserve the unique properties of graphene layers such as high electrical conductivity, large specific surface areas, and mechanical robustness, 3D hierarchical porous nanostructures can achieve more functionalization and desirable properties such as 3D interconnected porosity, spatial confinement effect and macroscale flexibility. As a result, these unique structural features can enhance electron and mass transfer in 3D scaffolds and provide stable and flexible frameworks during electrochemical processes and large surface areas with accessible active sites. Because of this, 3D hpG materials can demonstrate outstanding performances in various electrochemical energy applications, such as LIBs, Li-S batteries, lithium metal anodes and electrocatalysis (ORR, OER, HER, NRR, etc.) [7, 8, 32, 38, 43, 77, 94, 208, 310].

4.1 Batteries

4.1.1 Lithium-Ion Batteries

LIBs are currently the dominant electrochemical energy storage device in portable devices, electric vehicles, grid energy storage, etc.; however, energy and power densities need to be significantly increased to meet increasing demands [311]. And because battery performance is mainly determined by cathode and anode materials, 3D hpG materials, possessing high conductivity, hierarchical porosity, and excellent flexibility, have been widely used as conducting additives, electrode scaffolds, or electrode materials to improve LIB energy and power densities. Here, conductive graphene is an ideal additive in cathodes to guarantee fast electron transfer to active materials such as $LiFePO_4$, $LiCoO_2$, $LiMnO_4$, through the "plane-to-point" contact mode [312–314] and 3D hpG materials can serve as both the active material and the scaffold in anodes to uniformly support and confine active nanoparticles [315–321].

Compared with conventional graphite anodes, 3D hpG materials can provide higher Li intercalation capabilities [322]. For example, Park et al. [323] examined the effects of the surface topology of negatively curved carbon on the storage and mobility of Li ions through an investigation into 688P schwarzite, a particular negatively curved nonplanar structure, and reported that the presence of pores in the schwarzite can lead to 3D Li ion diffusion pathways with relatively lower energy barriers. Here the researchers reported that the graphite anode possessed a maximum gravimetric density of 372 mAh g^{-1} due to lithiation limitations (LiC_6) and that the Li intercalated schwarzite was calculated to be stable for stoichiometry $Li_{1.5}C_6$ (Fig. 12a). In addition, the researchers reported that the volume change of the schwarzite at $Li_{1.5}C_6$ was half that of graphite in LiC_6 and that the open porous structure and atom-thick walls of the schwarzite made it a potential anode material in LIBs, in which the material is expected to provide extremely fast charging and discharging rates, higher specific gravimetric and volumetric capacities and perhaps improved durability. As for the synthesis of these negatively curved carbon structures, researcher have reported that fabrication is possible through mesoporous templated CVD processes using mesoporous Ni foam or porous MgO nanosheets/nanofibers [137, 149, 153, 200, 324]. For example, Zheng et al. [324] studied hierarchical porous carbon microrods (HPCMs) as high-performance anode electrode materials in which the HPCMs composed of vertically aligned graphene-like nanosheets were synthesized using $Mg(OH)_2$ microrods as the template and dopamine as the carbon precursor. Here, the researchers reported that the sample obtained at 900 °C exhibited a high specific surface area of 1511 m^2 g^{-1} and large pore volume of 2.82 m^3 g^{-1}. And if used as the anode material for LIBs, this HPCM electrode exhibited an excellent capability of 1150 mAh g^{-1} at 0.1 A g^{-1}, improved rate performances of 246 mAh g^{-1} at 10 A g^{-1}, and outstanding cycling stability with 833 mAh g^{-1} retained after 700 cycles at 1 A g^{-1}. As for GO-assembled 3D hpG materials, researchers have reported that the larger nanosheets and lower mesoporosity of the materials can lead to significant stacking and the hindering of ion transport and lower surface areas and that the introduction of sacrificial spacers between graphene layers can expand Li ion transport channels and enhance rate performances [325].

3D hpG frameworks have also been widely employed as electrode scaffolds for various active materials [94]. For example, Qin et al. [205] used a 3D porous graphene network anchored with Sn nanoparticles as a LIB anode and reported superior performances in which the graphene framework was obtained through a NaCl templated CVD process with Sn nanoparticles being encapsulated with 1 nm graphene shells. Here, the researchers reported that the graphene shells not only improved stability by preventing the direct exposure of Sn to electrolytes, but also suppressed Sn nanoparticle aggregation and buffered volume expansion, leading to high rate performances and long cycling stability even at high rates (682 mAh g^{-1} achieved at 2 A g^{-1} and maintained ~ 96% after 1000 cycles). The uniform, mesoporous, and interconnected pores of 3D hpG substrates can also serve as nanoreactors to spatially confine in situ growth and hybridization of active nanoparticles [160, 326]. For example, Jiao et al. [257] used a mesoporous carbon framework as a robust matrix for the confined growth and support of nanoparticle superlattices in which through repeated precursor infiltration and hydrolysis, allowed for the connection of obtained crystalline SnO_2 nanoparticles to each other through interconnected windows within the mesoporous carbon framework, resulting in greatly improved capacity and stability as compared with uncoated SnO_2 nanoparticles or carbon frameworks (Fig. 12b). Here, the researchers suggested that the unique graphene substrate allowed for the fabrication of micrometer-sized secondary particles with the original SnO_2 supercrystals, thus providing a continuous electron pathway and buffered embedded SnO_2 nanoparticle volume expansions. In another example, Sun et al. [241] combined self-assembly, chemical activation, and hybridization to synthesize a 3D holey graphene/Nb_2O_5 composite for ultrahigh-rate energy storage at practical mass loading levels (> 10 mg cm^{-2}). Here, the researchers reported that the highly interconnected graphene network in the obtained 3D framework can provide excellent electron transport properties and its hierarchical porous structure can facilitate rapid ion transport (Fig. 12c). And as a result, a high specific capacity of 75 mAh g^{-1} can be achieved at an ultrahigh current density (100 C) even with a high loading

of 11 mg cm^{-2}, suggesting significant potential in practical electrochemical energy storage devices.

Another advantage of 3D hpG materials is the possibility for application in flexible lithium batteries and great attention has been attracted recently to develop flexible electrochemical energy storage materials for flexible and wearable electronic devices [83, 327]. For example, Li et al. [121] in 2012 presented a flexible graphene-based LIB with ultrafast charge and discharge rates (Fig. 12d) in which 3D porous graphene foam fabricated through nickel foam-templated CVD was used as both the current collector and the electrode scaffold for the anode loading of $Li_4Ti_5O_{12}$ and the cathode loading of $LiFePO_4$ with no metal current collectors, conducting additives or binders being used. Here, the researchers reported that the excellent conductivity and porous structure of the graphene foam-based composite promoted rapid electron and ion transport and the outstanding mechanical flexibility enabled flexible full batteries with good performance even under repeated bending to a small radius of 5 mm.

4.1.2 Lithium-Sulfur Batteries

Recently, Li-S batteries have attracted enormous interest as promising substitutes for current LIBs due to a high specific energy of 2600 Wh kg^{-1}, the natural abundance and low cost of sulfur and environmental benignity [328–332]. However, practical applications still face several obstacles related to the insulating nature of sulfur compounds, the shuttle effect of soluble polysulfide intermediates and considerable volume change during charging/discharging. Here, different types of hierarchical porous carbon materials have been demonstrated to be favorable host materials for sulfur cathode to circumvent the obstacles [3, 328, 333], and among these, 3D hpG materials are particularly promising due to high surface areas and electrical conductivities, tunable porosity and versatile surface chemistry [334–338].

In the case of the physical host scaffold of sulfur, performance has been shown to be closely tied to the porous nanostructure of the employed graphene materials. For example, Li et al. [339] reported that the dense integration of sulfur and rGO gel (through oven drying instead of freeze-drying) can better increase bonding between sulfur and graphene to immobilize sulfur and restrain polysulfide diffusion within more compact pores, and thus achieve higher performances. In addition, the micro-/mesopores or functional groups on graphene surfaces can help to strongly absorb sulfur/polysulfides and effectively reduce polysulfide dissolution to improve cycling performances [246, 340]. For example, Zheng et al. [341] synthesized micro-/mesoporous graphitic carbon spheres with ordered mesoporous graphene cores and uniform microporous carbon shells through Fe_3O_4 templated polymerization and suggested that the 9.0-nm core spherical mesopores can provide sufficient space for S_8 molecule loading (70.4 wt%, 3.2 mg cm^{-2}) and that the 0.6 nm shell micropores can entrap only small S_{2-4} molecules to minimize the outward diffusion of polysulfides. Researchers have also reported that higher specific surface areas, more abundant micro-/mesopores and larger pore volumes of 3D hpG materials can lead to higher sulfur loadings with excellent capacity, rate, and cycling performances [156, 163, 175, 254, 342]. For example, Zheng et al. [163] fabricated hierarchical porous carbon rods (HPCR) through CVD using hierarchical $Mg(OH)_2$ microrod templates (Fig. 13a). Here, the HPCR was constructed by using vertically oriented porous graphene nanosheets with a high specific surface area (2226 m^2 g^{-1}), ultralarge pore volume (4.9 cm^3 g^{-1}), hierarchical porous structure, and a 3D interconnected conductive network, and is an excellent host for high sulfur loading. As a result, the HPCR-S composite with 78.9 wt% sulfur delivered an excellent rate performance (646 mAh g_{sulfur}^{-1} at 5 C) and cycling stability (700 mAh g_{sulfur}^{-1} after 300 cycles at 1 C). And even with a high sulfur loading of 88.8 wt%, the composite still exhibited a good rate performance (545 mAh g_{sulfur}^{-1} at 3 C), high energy density (880 mAh $cm_{cathode}^{-3}$), and cycling stability (632 mAh g_{sulfur}^{-1} after 200 cycles at 1 C). Besides these examples, graphene, due to its intrinsic conductivity, rich functionality, and high flexibility, is also an ideal substrate for flexible graphene/sulfur composite cathodes and can be obtained through vacuum filtration, solvent evaporation or cutting from graphene/sulfur gels [3].

In addition to physical confinement, the surface functionalization and appropriate hybridization of 3D hpG materials to adopt "sulfiphilic" surface chemistry to host lithium polysulfides is attractive in the development of high-performance sulfur cathodes [343–353]. Here, the hybridization of conductive graphene substrates with sulfiphilic guest materials can give rise to enhanced interactions with polysulfide adsorbates, leading to subsequent rapid surface redox chemistry and homogeneous nucleation/growth of Li_2S. And as a result, redox kinetics can be accelerated and the shuttle effect can be effectively suppressed. For example, Yuan et al. [354] employed CoS_2 as a conductive sulfiphilic host to enhance polysulfide redox in an aprotic electrolyte (Fig. 13b) in which the incorporation of 15 wt% CoS_2 was found to be able to substantially mitigate polarization, raising cathodic peaks and reducing the anodic peak by ~ 0.2 V. Here, the high polysulfide reactivity not only guaranteed effective polarization mitigation with an energy efficiency enhancement of 10%, but also ensured high discharge capacities and stable cycling performances for 2000 cycles in which a high initial capacity of 1368 mAh g^{-1} at 0.5 C and a slow capacity decay rate of 0.034% per cycle at 2.0 C can be achieved.

3D hpG materials with high specific surface areas and tunable surface chemistry can also serve as promising separators to effectively suppress the crossover of

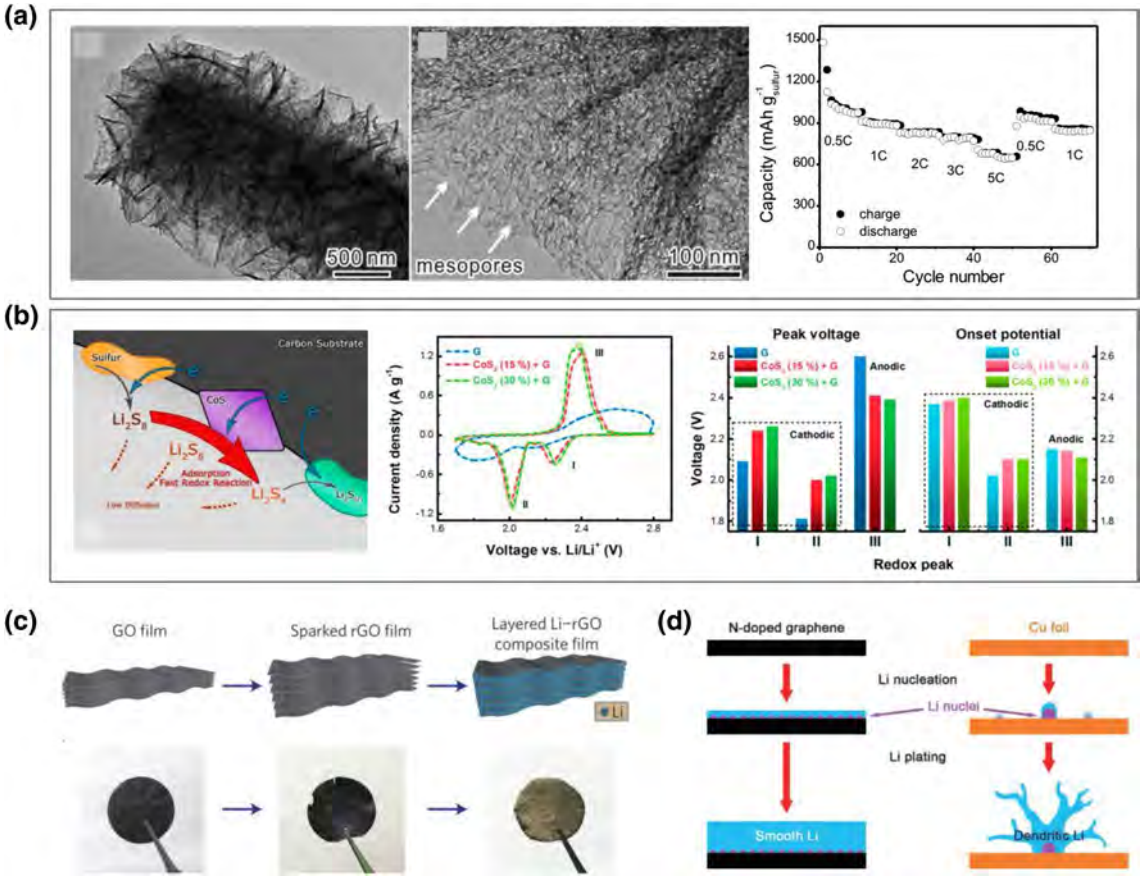

Fig. 13 Application in Li-S batteries and Li metal anodes. **a** TEM images of hierarchical porous carbon rods and corresponding Li-S battery rate performances. Reprinted with permission from Ref. [163]. **b** Schematic of the discharge process in CoS_2-graphene cathodes and corresponding redox kinetics of polysulfides. Reprinted with permission from Ref. [354]. **c** Schematic of the fabrication of layered Li-rGO composite films. Reprinted with permission from Ref. [373]. **d** Schematic of the Li nucleation and plating process on nitrogen-doped graphene electrodes or Cu foil. Reprinted with permission from Ref. [374]

sulfur-containing species and enhance the formation of Li_2S [338, 355, 356]. For example, researchers reported that an ultrathin layer of GO (0.0032 mg cm^{-2}) can help to block macropores of polymer matrixes [357] and that a mesoporous graphene framework with a high specific surface area of 2120 m^2 g^{-1} and a large mesopore volume of 3.1 cm^3 g^{-1} can be fabricated by using MgO-templated CVD and can adhere onto the cathode side of a porous polypropylene membrane to reactivate shuttling-back polysulfides and preserve ion channels [358]. Here, the researchers reported that such Janus separators can lead to significant improvements in capacity, cycling stability and electrochemical kinetics in which a high areal capacity of 5.5 mAh cm^{-2} can be achieved at a sulfur loading of 80 wt% and a areal loading of 5.3 mg cm^{-2} [358]. The suppression of the shuttle effect and improvement in reaction kinetics can further be enhanced through the incorporation of "sulfiphilic" multimetallic layered hydroxides and "lithiophilic" nitrogen-doped graphene frameworks [298]. Overall, this separator engineering strategy has been demonstrated to be facile and effective to scale up in which Li-S punch cells with a porous graphene-modified separator can provide a high initial discharge capacity of 1135 mAh g^{-1} at 0.1 C at a large areal sulfur loading of 7.8 mg cm^{-2} [359].

4.1.3 Lithium Metal Anodes

The lithium metal anode is regarded as the "Holy Grail" of the electrode due to its ultrahigh capacity (3860 mAh g^{-1}) in Li-S or Li-air batteries [360]. However, practical applications of rechargeable lithium metal anodes are greatly hindered by Li dendrites, leading to significant safety concerns and low cycling efficiencies [361–365]. Here, nanostructured carbon materials are emerging as important candidates to protect lithium metal anodes through the stabilization of the solid electrolyte interface (SEI), lowering of the local current density, the configuring of the ion flux and acting as stable hosts for Li deposition. This is a result of advantages

such as a 3D hierarchical porous structure with high specific surface areas, high strength, and flexibility to retain structural integrity and easy decoration of functional groups or lithiophilic materials [366–369].

In 2015, Cheng et al. [370] proposed a distinctive graphene framework (fabricated by GO self-assembly) coated by in situ formed SEI layers with Li plating in the pores as the anode for Li-S batteries in which the 3D hpG framework with unblocked ionic pathways and high electrical conductivity can allow for rapid Li ion transfer through the SEI layer and an ion conductivity of 0.078 mS cm^{-1}. And as a result, this graphene-modified Li anode demonstrated superior dendrite-inhibition behaviors in 70 h of lithiation at 0.5 mA cm^{-2} and improved Coulombic efficiencies of ~ 97% for more than 100 cycles. In another study, Zhang et al. [371] reported that their unstacked graphene framework-based Li anode, with a high specific surface area of 1666 m^2 g^{-1}, a large pore volume of 1.65 cm^3 g^{-1} and a high electrical conductivity of 435 S cm^{-1}, can exhibit an ultralow areal current density of 4.0×10^{-5} mA cm^{-2}, thus leading to the effective inhibition of Li dendrite growth. The researchers also reported that if coupled with a LiTFSI-LiFSI dual-salt electrolyte, a high Coulombic efficiency of 93% can be achieved at a high lithiation capacity of 5.0 mAh cm^{-2} and a high current density of 2.0 mA cm^{-2}, as well as stable depositing/stripping morphology for 800 cycles. Furthermore, Deng et al. [372] fabricated a novel porous graphene scaffold using zinc acetate-templated GO self-assembly with cellular chambers for incorporating Li metal and reported that the ultrathin 3-μm Li layer anchored onto the graphene nanosheets in the porous scaffold can provide more reaction sites to enhance the electrochemical reversibility of Li and inhibit lithium dendrite growth.

In addition to serving as a conductive substrate for Li deposition, the surface functionalization of 3D hpG materials can endow higher lithiophilicity and modify the incorporated morphology of Li. Lin et al. [373] verified this concept by synthesizing a uniform layered nanostructured Li-rGO electrode through molten Li infusion into the rGO film with uniform nanogaps (Fig. 13c). Here, rGO surface functional groups such as carbonyl and alkoxy groups can exhibit much stronger binding energies to lithium than bare graphene, thus guaranteeing uniform Li infusion and deposition during synthesis and subsequent cycling. In addition, layered porous rGO can provide a flexible and stable scaffold for Li stripping/plating, leading to small electrode dimensional changes (~ 20%) during cycling with stable SEIs. For example, Zhang et al. [374] utilized nitrogen-doped graphene as a Li plating matrix to regulate Li metal nucleation and suppress dendrite growth (Fig. 13d) and the subsequent theoretical investigation revealed that nitrogen-containing functional groups such as pyrrolic and pyridinic nitrogen can exhibit relatively larger binding energies than graphene and Cu, which can guide Li nucleation with uniform distribution on anode surfaces. And as a result, their nitrogen-doped graphene-based Li anode exhibited dendrite-free morphology during repeated Li plating and a high Coulombic efficiency of 98% for near 200 cycles at a current density of 1.0 mA cm^{-2} and a cycle capacity of 1.0 mAh cm^{-2}. Other lithiophilic sites and guest materials have also been reported in literature such as in situ formed ZnO in rGO foam [372] and atomically dispersed CoN_x sites in graphene [375]. In addition, this strategy of using 3D hpG materials as Li metal deposition scaffolds can also be attractive in the synthesis of other metal anodes such as Na, Mg, and Zn, as well as addressing overcharging issues of Li-ion batteries.

4.2 Electrocatalysis

4.2.1 Oxygen Reduction Reaction

Fuel cells and metal-air batteries have been intensely studied over the past decades due to their high energy densities and open cell designs [376, 377], and in both cases, electrocatalysts with highly efficient ORR activities ($O_2 + 4H^+ + 4e^- \rightarrow 2H_2O$, in acid) are required. Here, 3D hpG materials, especially heteroatom-doped (N, O, B, P, S, Si, etc.) graphene materials, have been demonstrated to be excellent alternatives to replace platinum group metals and possess outstanding ORR catalytic activities in alkaline conditions due to the altered charge [378] or spin distribution [379, 380] in sp^2 graphene matrixes.

3D hpG materials can provide more intrinsic active sites than other nanocarbon materials through abundant surface doping and topological defects [75, 264, 310, 381–383]. For example, Liang et al. [384] reported a N/S dual-doped mesoporous graphene as a metal-free ORR catalyst with a highly positive onset potential and a high kinetic limiting current that were comparable to Pt/C. In addition, theoretical calculations have revealed that the outstanding activities of 3D hpG materials can result from the redistribution of spin and charge densities through dual doping with S and N atoms. For example, Li et al. [284] reported a sandwich-like N/P dual-doped graphene material as an excellent ORR catalyst (Fig. 14a) that was even superior to commercial Pt/C with a 20 mV higher half-wave potential, larger cathodic current density and a smaller Tafel slope (51 mV dec^{-1}). In addition, the researchers also reported an outstanding ORR/OER bifunctional catalytic activity with a potential gap as low as 0.71 V between the ORR half-wave potential and the OER potential for 10 mA cm^{-2}. Here, the researchers attributed these impressive performances to the unique nanostructure of the 3D hpG material, including its multi-doping with

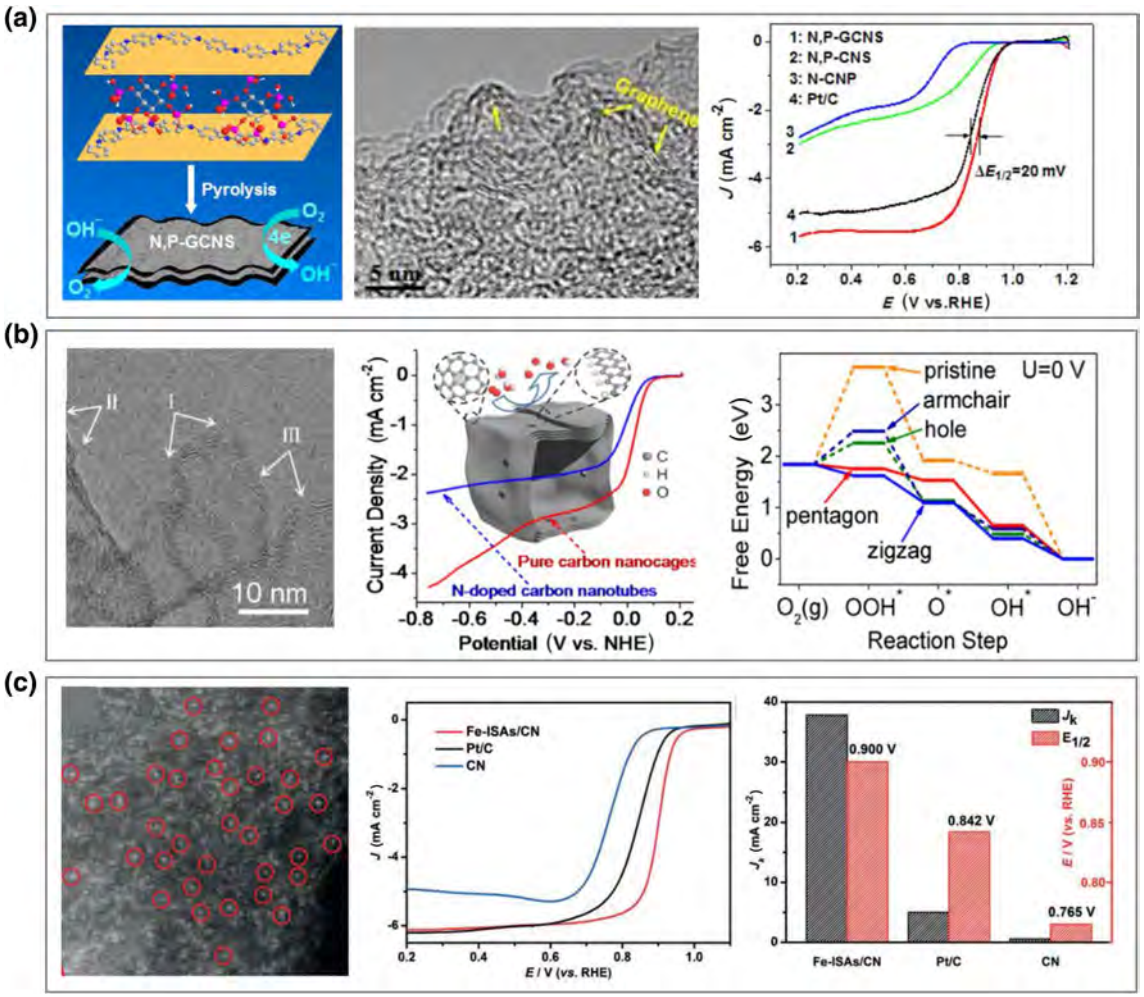

Fig. 14 Application in ORR electrocatalysis. **a** Schematic and TEM image of sandwich-like N/P dual-doped graphene materials and corresponding ORR performances. Reprinted with permission from Ref. [284]. **b** TEM image of dopant-free carbon nanocages, corresponding ORR performances and reaction pathways. Reprinted with permission from Ref. [387]. **c** HAADF-STEM image and ORR performance of the isolated single-atom Fe/N-doped porous carbon. Reprinted with permission from Ref. [291]

synergetic effects, more active sites on the surface exposed to reactants, large active surface areas, hierarchical pores for rapid mass transportation and integrated crystalline graphene for enhanced charge transfer. Researchers have also reported that due to the abundant micro-/mesopores in 3D hpG materials, a certain number of topological defects such as vacancies and non-hexagonal topologies are unavoidable in the edges, corners, holes, and that these topological defects can not only afford more efficient doping locations with higher activity [270], but also afford considerable intrinsic activities themselves [281, 310, 385, 386]. For example, Jiang et al. [387] synthesized dopant-free carbon nanocages using an in situ MgO template method with benzene as the precursor (Fig. 14b) and reported that due to the cuboidal hollow structure (10–20 nm), abundant defects were generated such as pentagons at the corners for positive curvature, edge defects at the broken fringes and hole defects in the microporous shells. And as compared with nitrogen-doped CNTs, this material reportedly delivered better ORR performances with a higher onset potential and much larger current density in which the pentagon and zigzag edge defects were revealed to be the main active sites due to the favorable electronic structures and facilitated electron transfer for OOH* formation. Overall, the combination of heteroatom doping and topological defects can enhance ORR activity [253, 388].

Recently, porous graphene with atomically dispersed metal sites has attracted great interest due to excellent ORR activities comparable to Pt/C catalysts even in acidic electrolytes [286–289, 389, 390]. Here, atomic metal sites can be incorporated into graphene matrixes during in situ fabrication, especially through MOF-assisted pyrolysis or post-treatment such as ball milling [288, 391]. For example, Chen et al. [291] reported a highly ORR reactive and stable

isolated single-atom Fe/N-doped porous carbon catalyst with a Fe loading up to 2.16 wt%(Fig. 14c) fabricated through the pyrolysis of zeolitic imidazolate frameworks (ZIF-8) at 900 °C under Ar atmosphere using $Fe(acac)_3$ trapped in ZIF cages as the metal precursor. Here, the as-obtained catalyst exhibited an unexpectedly efficient ORR activity with a high kinetic current density of 37.83 mA cm^{-2} at 0.85 V and a half-wave potential of 0.900 V, which was 58 mV more positive than Pt/C in 0.10 M KOH. Researchers have also reported that electrocatalytic performances can be regulated by tailoring the composition and property of atomic metal sites in graphene, such as different metal atoms [292, 295, 392–395], dual metal sites [296, 396], dual coordination atoms [397]. For example, Tang et al. [295] reported a defect engineering strategy to construct atomically dispersed Co-N_x-C active sites in a nitrogen-doped graphene mesh in which due to the highly active sites and hierarchical porous scaffold, the as-obtained catalyst exhibited excellent ORR activities comparable to Pt/C with a high limiting current density and a low Tafel slope (58 mV dec^{-1}). Here, the researchers integrated this material into a flexible solid Zn-air battery and obtained a high open-circuit voltage of 1.44 V, a stable discharge voltage of 1.19 V and a high energy efficiency of 63% at 1.0 mA cm^{-2} even under bending.

Single Fe atoms in graphene can provide desirable performances; however, they can also induce possible Fenton reactions and serious degradation of membranes in working fuel cells. To address this, Wu et al. in their studies synthesized atomically dispersed Co [395] and Mn [292] sites in a porous carbon matrix and reported respectable activities and stability in challenging acidic media for proton exchange membrane fuel cells. In addition, these 3D hpG materials with atomic metal sites can also serve as promising catalysts for other energy electrocatalysis applications, such as OER [398], HER [290], CRR [399–402] and multifunctional catalysis [403].

4.2.2 Oxygen Evolution Reaction and Hydrogen Evolution Reaction

Analogous to application in ORR, 3D hpG materials can also serve as active electrocatalysts for OER and HER, in which the activity mainly originates from heteroatom doping, oxygen-containing functional groups and defective sites. For example, Hashimoto et al. [404] synthesized a nitrogen-doped porous nanocarbon as an efficient OER electrocatalyst in alkaline media and reported comparable performances to iridium and cobalt oxide catalysts. Here, the catalyst was fabricated through the pyrolysis of melamine formaldehyde polymers with nickel nitrate and carbon particles as templates followed by acid leaching in which the nitrogen content of the obtained material was determined to be 4.1 at% with negligible nickel species (0.002 at%). And as a result, a low OER overpotential of 0.38 V was achieved at a current density of 10 mA cm^{-2}, demonstrating significant activities. In another example, Zheng et al. [405] synthesized a metal-free HER catalyst through the coupling of g-C_3N_4 with nitrogen-doped graphene in which g-C_3N_4 was directly grown onto the surface of GO nanosheets followed by thermal treatment for GO reduction and nitrogen doping. Here, the as-obtained material reportedly possessed a multilayered structure formed by stacking multilayered g-C_3N_4 onto N-doped graphene sheets with g-C_3N_4 providing highly active hydrogen adsorption sites and N-doped graphene facilitating the electron transfer process for proton reduction. As a result, the overpotential required for 10 mA cm^{-2} HER current density was ~ 240 mV with a Tafel slope of 51.5 mV dec^{-1}. Based on these results, extensive efforts have been made to develop metal-free heteroatom-doped porous graphene materials as highly efficient OER, HER, and even multifunctional electrocatalysts [276, 277, 281, 284, 406].

Current catalytic performances of metal-free nanocarbon catalysts cannot fully meet the demands of working fuel cells; therefore, dual- or multi-element doping has been proposed and well demonstrated to be a promising strategy to improve OER and HER activity. As an example, Zhao et al. [407] conducted theoretical studies into the ORR and OER activity of single-doped and dual-doped carbon nanomaterials (Fig. 15a) and reported that the overpotential for ORR and OER of dual-doped carbon materials can be significantly reduced by 10%–40% as compared with single-doped counterparts and is also much lower than precious-metal catalysts. The researchers rationalized this enhancement using the synergistic interactions of p-electrons between co-dopants within a certain distance, which can reduce overpotentials and stabilize adsorbates. Similarly, Jiao et al. [104] also reported the significance of dual doping in nanocarbon-based HER electrocatalysts. In their study, the researchers introduced secondary elements into nitrogen-doped graphene matrixes to further modify electron acceptor–donor properties and reported that HER activities can be significantly enhanced due to the lowered adsorption energy of H*. In addition, these researchers also reported that extrinsic physicochemical properties such as surface area/porosity/doping concentrations can also considerably govern HER overpotentials in which a combination of higher dopant concentrations and higher surface areas of up to 1000 m^2 g^{-1} can allow for resultant dual-doped graphene to possess superior HER performances as compared with MoS_2 materials (Fig. 15b). Based on these reports, 3D hpG materials are promising metal-free OER or HER electrocatalysts due to high surface areas, abundant micro-/mesopores, high conductivities, and the feasibility to obtain highly concentrated dual doping and even surface doping, with many graphene catalysts such as N, S co-doped nanoporous graphene

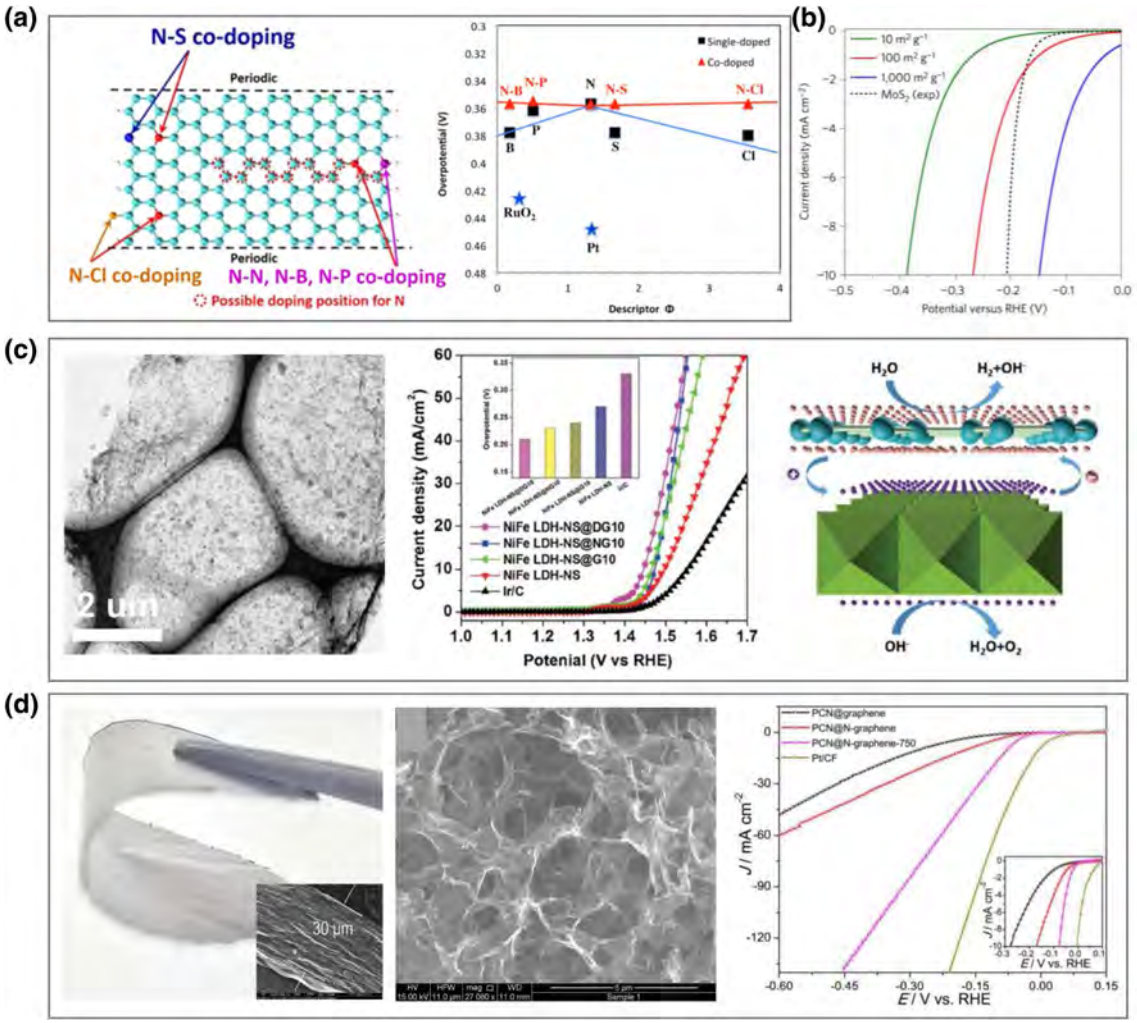

Fig. 15 Application in OER and HER electrocatalysis. **a** Schematic of the dual-doped graphene nanoribbon and calculated OER overpotentials. Reprinted with permission from Ref. [407]. **b** Calculated HER polarization curves of graphene-based materials with a doping level of 5%. Reprinted with permission from Ref. [104]. **c** TEM image, OER polarization curves, and mechanism schematic of the heterostructure of NiFe LDH/defective graphene. Reprinted with permission from Ref. [307]. **d** Photograph, SEM image, and HER polarization curves of a flexible 3D C_3N_4/N-graphene film. Reprinted with permission from Ref. [308]

[138] and N, P co-doped graphene [408] for HER, and N, S co-doped graphene [409], N, O co-doped graphene/CNT hydrogel films [278], and N, P co-doped graphene/carbon nanosheets [284] for OER being reported.

In addition to serving as active sites, 3D hpG materials can also serve as multifunctional substrates to hybridize with more efficient active materials such as LDH for OER and MoS_2 for HER [11, 78, 410–413] in which highly conductive and hierarchical porous graphene can accelerate electron and mass transport, regulate active component incorporation and provide strongly coupled interfaces in composite electrocatalysts [414–416]. For example, Li et al. [300] reported that spatially confined nanosized NiFe LDHs in nitrogen-doped mesoporous graphene frameworks can significantly enhance OER activities with a low Tafel slope of 45 mV dec^{-1} and a decreased overpotential of 337 mV for 10 mA cm^{-2} and that the additional vulcanization of the NiFe LDHs to NiFe (oxy) sulfides by using thioacetamide can further improve OER activities, with a low overpotential of 286 mV for 10 mA cm^{-2}. Researchers have also reported that vdW heterostructures of graphene and LDH nanosheets can fully demonstrate the intrinsic activity of LDHs and the desirable properties of graphene [304–307]. For example, Jia et al. [307] studied a heterostructured NiFe LDH@defective graphene hybrid catalyst and reported extremely high OER activities and good HER activities in alkaline media (Fig. 15c) in which the overpotential for 10-mA cm^{-2} OER current density was as low as 210 mV and was superior to almost all non-noble metal catalysts.

Further theoretical calculations have revealed that the synergetic effect between highly exposed 3d transition metal

atoms and graphene defects is critical for high electrocatalytic activities. For example, Li et al. [417] developed a MoS_2 nanoparticle/rGO hybrid in 2011 through selective solvothermal synthesis for efficient HER in alkaline media in which the small size and high dispersion of MoS_2 on graphene nanosheets reportedly provided abundant and accessible edges; and the strong coupling between MoS_2 and the underlying graphene afforded rapid electron transport, resulting in the smallest Tafel slope (41 mV dec^{-1}) for MoS_2 catalysts reported in literature. Furthermore, various vdW heterostructures of graphene and MoS_2 and even 3D mesoporous structures have been explored as excellent HER catalysts [106, 418, 419] in which g-C_3N_4 has been reported to be an attractive candidate for hybridization or vdW heteroassembly with graphene nanosheets [308, 309, 420]. For example, Duan et al. [308] intentionally integrated 2D porous g-C_3N_4 nanosheets with nitrogen-doped GO nanolayers to synthesize a flexible 3D C_3N_4/N-graphene film with a vdW heterostructure and macroscopic architecture (Fig. 15d) and reported that this metal-free catalyst displayed an impressive HER performance with an onset overpotential (8 mV) close to that of Pt/C, a high exchange current density of 0.43 mA cm^{-2} and excellent durability over 500 cycles. Here, the researchers attributed the extraordinary performances to the unique structural characteristics of the 3D hpG material, including the highly exposed active sites from the in-plane pores and ultrathin nanosheets, the hierarchical porous scaffold, and the 3D conductive network.

4.2.3 Nitrogen Reduction Reaction

Recently, the electrocatalytic nitrogen reduction to ammonia has attracted great attention due to the critical role of ammonia in society [421–426]. This because ammonia is the second most produced chemical globally and is used in fertilizers, refrigerants, and the production of various chemicals. In addition, ammonia is an attractive energy carrier with high energy densities and technically ready operations [427]. However, the Haber–Bosch process for the industrial production of ammonia is expensive, energetically demanding and produces CO_2 pollutants; therefore, electrocatalytic nitrogen activation and ammonia production through the transformation of N_2 and H_2O to NH_3 powered by sustainable electric energy sources is appealing. And despite the significant challenges in activity and selectivity, various electrocatalysts have been reported with encouraging NRR performances including various 3D hpG materials.

Researchers have reported that 3D hpG materials possess NRR activity due to the presence of abundant defects and heteroatom dopants. For example, Li et al. [428] used thermal treatment to obtain nitrogen-free commercial carbon cloth with rich defects and reported a NH_3 yield of

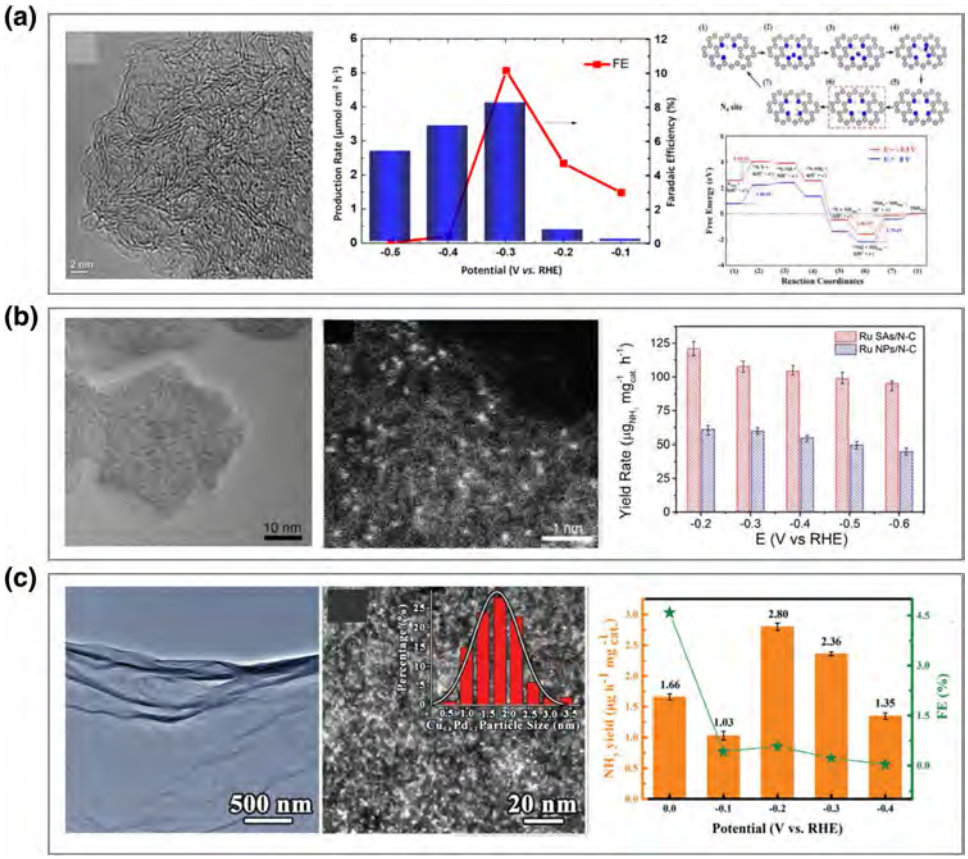

Fig. 16 Application in NRR electrocatalysis. **a** TEM image, NRR performance and reaction pathways of the nitrogen-doped highly disordered carbon electrocatalyst. Reprinted with permission from Ref. [434]. **b** TEM image, HAADF-STEM image and NRR performance of the nitrogen-doped carbon with Ru single atoms as a NRR electrocatalyst. Reprinted with permission from Ref. [436]. **c** TEM image, STEM image, and NRR performance of PdCu amorphous nanoclusters on rGO. Reprinted with permission from Ref. [440]

2.59×10^{-10} mol cm^{-2} s^{-1} and a Faradaic efficiency of 6.92% at −0.3 V (vs. RHE) in 0.1 M Na_2SO_4 + 0.02 M H_2SO_4. Furthermore, nitrogen or boron doping can further enhance activity and selectivity for NRR [429–435]. Wu et al. [434] reported that nitrogen-doped highly disordered carbons through the pyrolysis of MOF at 1100 °C were excellent NRR catalysts (Fig. 16a) in which the obtained porous carbon exhibited a high specific surface area of 780 m^2 g^{-1}, a pore volume of 0.93 cm^3 g^{-1} and a nitrogen content of 1.8%. More impressively, a high NH_3 yield of up to 3.4×10^{-6} mol cm^{-2} h^{-1} and a Faradaic efficiency of 10.2% were achieved at −0.3 V (vs RHE) in 0.1 M KOH. In addition, theoretical investigations revealed that the moiety consisting of three pyridinic nitrogen atoms adjacent to one carbon vacancy can strongly adsorb N_2 and promote the dissociation of N≡N triple bonds for subsequent protonation processes. Furthermore, Yu et al. [432] reported B-doped graphene as a metal-free electrocatalyst for NRR and achieved a NH_3 yield of 9.8 μg cm^{-2} h^{-1} and a Faradic efficiency of 10.8% at −0.5 V (vs RHE) in 0.05 M H_2SO_4 at a doping level of 6.2%. Here, the researchers suggested that the electron-deficient boron sites can enhance binding capability to N_2 molecules in which the BC_3 structure was revealed to be the activity origin with the lowest energy barrier for N_2 reduction.

The incorporation of active metal species into porous graphene matrixes in the form of single atoms or nanoclusters is an effective strategy to boost the electrocatalytic activity and selectivity of both carbon materials and metals. And through the routine ZIF-8 pyrolysis method, Geng et al. [436] fabricated a nitrogen-doped carbon with Ru single atoms as a NRR electrocatalyst (Fig. 16b) and reported that a Ru mass loading of 0.18%, a high Faradaic efficiency of up to 29.6% and a high NH_3 yield of 120.9 μg $mg_{cat.}^{-1}$ h^{-1} can be achieved at −0.2 V (vs RHE) in 0.05 M H_2SO_4. In addition, Sun et al. [437] found that the addition of ZrO_2 into nitrogen-doped porous carbon with Ru single atoms can significantly suppress competitive HER and further increase Faradic efficiency.

Au single atoms stabilized in N-doped porous carbon materials have also been reported to be promising for NRR electrocatalysis [438, 439] due to the strong π-π interaction between organic molecules and GO, allowing for the facile loading of metal nanoclusters onto GO nanosheets with facilitated mass transport and electron transfer. For example, Shi et al. [440] investigated the anchoring of PdCu amorphous nanoclusters on rGO through the coreduction of GO, Cu and Pd precursors using tannic acid and $NaBH_4$ mixed reductants (Fig. 16c) and reported that with an obtained metal mass loading of 2.92 wt% and a Pd/Cu atomic ratio of 0.24:0.76, a NH_3 yield of 2.80 μg h^{-1} $mg_{cat.}^{-1}$ can be achieved at −0.2 V (vs RHE) in 0.1 M KOH along with a Faradic efficiency lower than 1%. As a result of these promising studies, further efforts to optimize the composition and nanostructure of 3D hpG materials for highly active and selective NRR electrocatalysis are required.

5 Summary and Prospects

The construction of 3D hierarchical porous frameworks by using 2D graphene building units and the further functionalization or hybridization with guest components can provide an attractive family of energy materials with outstanding performances in electrochemical energy storage and conversion devices, such as LIBs, Li-S batteries, lithium metal anodes, ORR, OER, HER and NRR. In addition, various 3D hpG materials with controllable porosity, surface area and doping can be fabricated by using a series of strategies, including CVD growth on 3D porous templates, post-assembly/treatment of GO nanosheets, and templated polymerization. Here, mesoporous metal or metal oxide templates are favorable for the CVD of high-quality graphene with ultrathin thicknesses, high conductivities, large surface areas, and uniform micro-/mesopores, and GO-based strategies can efficiently alter the composition, surface doping, and hybridization of obtained 3D hpG materials. Furthermore, due to high surface areas and interconnected porosity it is versatile and facile to enrich the properties of 3D hpG materials through heteroatom doping, spatially confined decoration of active nanoparticles and surface hybridization with graphene-analogous components. And as a result, 3D hpG materials possessing the outstanding properties of graphene layers, porous scaffolds and guest components can be widely applied as energy materials.

However, despite the significant success of 3D hpG materials, several fundamental issues remain that need to be further investigated for more rational design, controllable fabrication, and enhanced performance. The first issue is that the growth mechanism and kinetics of CVD on metal oxide substrates and porous templates need to be systematically studied and are crucial for the controllable tailoring of the layer thickness, graphitic degree, defects and porosity of obtained 3D hpG materials. Secondly, more advanced and effective characterization techniques are needed to clearly probe the hierarchical porosity of 3D hpG materials and are crucial to elucidate the correlation between properties and performance. The third issue is that more efforts are needed to investigate the interface between adjacent 3D hpG units and between graphene and guest materials, which can greatly impact the apparent properties of 3D hpG materials in applications. And lastly, the performance of 3D hpG materials in devices needs to be evaluated based on practical requirements such as volumetric and specific capacitance and durability so as to guide further optimizations and promote practical applications. And overall, the information

from these future studies, especially the material design and synthetic strategies, can be applied in many fields of nanoscience and will deepen the understanding of nanostructured energy materials, providing feedback for various 2D materials and propelling the development of advanced nanomaterials even beyond energy applications.

Acknowledgements This work is supported by the National Key Research and Development Program (2016YFA0202500 and 2016YFA0200102) and the National Natural Science Foundation of China (21676160, 21825501, and U1801257).

References

1. Chu, S., Cui, Y., Liu, N.: The path towards sustainable energy. Nat. Mater. **16**, 16–22 (2017)
2. Goodenough, J.B., Park, K.S.: The Li-ion rechargeable battery: a perspective. J. Am. Chem. Soc. **135**, 1167–1176 (2013)
3. Peng, H.J., Huang, J.Q., Zhang, Q.: A review of flexible lithium-sulfur and analogous alkali metal-chalcogen rechargeable batteries. Chem. Soc. Rev. **46**, 5237–5288 (2017)
4. Lu, J., Chen, Z., Pan, F., et al.: High-performance anode materials for rechargeable lithium-ion batteries. Electrochem. Energy Rev. **1**, 35–53 (2018)
5. Jiao, Y., Zheng, Y., Jaroniec, M.T., et al.: Design of electrocatalysts for oxygen- and hydrogen-involving energy conversion reactions. Chem. Soc. Rev. **44**, 2060–2086 (2015)
6. Tang, C., Wang, H.F., Zhang, Q.: Multiscale principles to boost reactivity in gas-involving energy electrocatalysis. Acc. Chem. Res. **51**, 881–889 (2018)
7. Han, J., Wei, W., Zhang, C., et al.: Engineering graphenes from the nano- to the macroscale for electrochemical energy storage. Electrochem. Energy Rev. **1**, 139–168 (2018)
8. Hu, C., Xiao, Y., Zou, Y., et al.: Carbon-based metal-free electrocatalysis for energy conversion, energy storage, and environmental protection. Electrochem. Energy Rev. **1**, 84–112 (2018)
9. Mao, J.J., Iocozzia, J., Huang, J.Y., et al.: Graphene aerogels for efficient energy storage and conversion. Energy Environ. Sci. **11**, 772–799 (2018)
10. Zhang, C., Nicolosi, V.: Graphene and MXene-based transparent conductive electrodes and supercapacitors. Energy Storage Mater. **16**, 102–125 (2019)
11. Tang, C., Titirici, M.M., Zhang, Q.: A review of nanocarbons in energy electrocatalysis: multifunctional substrates and highly active sites. J. Energy Chem. **26**, 1077–1093 (2017)
12. Zhang, X.Q., Cheng, X.B., Zhang, Q.: Nanostructured energy materials for electrochemical energy conversion and storage: a review. J. Energy Chem. **25**, 967–984 (2016)
13. Wang, B., Cui, X., Huang, J.Q., et al.: Recent advances in energy chemistry of precious-metal-free catalysts for oxygen electrocatalysis. Chin. Chem. Lett. **29**, 1757–1767 (2018)
14. Kong, L., Yan, C., Huang, J.Q., et al.: A review of advanced energy materials for magnesium-sulfur batteries. Energy Environ. Mater. **1**, 100–112 (2018)
15. Li, B.Q., Xia, Z.J., Zhang, B.S., et al.: Regulating p-block metals in perovskite nanodots for efficient electrocatalytic water oxidation. Nat. Commun. **8**, 934 (2017)
16. Liu, X., Huang, J.Q., Zhang, Q., et al.: Nanostructured metal oxides and sulfides for lithium-sulfur batteries. Adv. Mater. **29**, 1601759 (2017)
17. Qiao, M., Tang, C., Tanase, L.C., et al.: Oxygenophilic ionic liquids promote the oxygen reduction reaction in pt-free carbon electrocatalysts. Mater. Horiz. **4**, 895–899 (2017)
18. Wang, H.F., Chen, R.X., Feng, J.Y., et al.: Freestanding non-precious metal electrocatalysts for oxygen evolution and reduction reactions. ChemElectroChem **5**, 1786–1804 (2018)
19. Ferrari, A.C., Bonaccorso, F., Fal'ko, V., et al.: Science and technology roadmap for graphene, related two-dimensional crystals, and hybrid systems. Nanoscale **7**, 4598–4810 (2015)
20. Novoselov, K.S., Fal'ko, V.I., Colombo, L., et al.: A roadmap for graphene. Nature **490**, 192–200 (2012)
21. Novoselov, K.S., Geim, A.K., Morozov, S.V., et al.: Electric field effect in atomically thin carbon films. Science **306**, 666–669 (2004)
22. Dong, Y.F., Wu, Z.S., Ren, W.C., et al.: Graphene: a promising 2D material for electrochemical energy storage. Sci. Bull. **62**, 724–740 (2017)
23. Zhang, J.T., Xia, Z.H., Dai, L.M.: Carbon-based electrocatalysts for advanced energy conversion and storage. Sci. Adv. **1**, e1500564 (2015)
24. Zhang, H., Chhowalla, M., Liu, Z.F.: 2D nanomaterials: graphene and transition metal dichalcogenides. Chem. Soc. Rev. **47**, 3015–3017 (2018)
25. Yusoff, A.B., Dai, L.M., Cheng, H.M., et al.: Graphene based energy devices. Nanoscale **7**, 6881–6882 (2015)
26. Su, D.S., Centi, G.: A perspective on carbon materials for future energy application. J. Energy Chem. **22**, 151–173 (2013)
27. Lang, J.W., Zhang, X., Liu, B., et al.: The roles of graphene in advanced Li-ion hybrid supercapacitors. J. Energy Chem. **27**, 43–56 (2018)
28. Hou, P.X., Du, J.H., Liu, C., et al.: Applications of carbon nanotubes and graphene produced by chemical vapor deposition. MRS Bull. **42**, 825–833 (2017)
29. Park, J., Cho, Y.S., Sung, S.J., et al.: Characteristics tuning of graphene-oxide-based-graphene to various end-uses. Energy Storage Mater. **14**, 8–21 (2018)
30. Yu, X.W., Cheng, H.H., Zhang, M., et al.: Graphene-based smart materials. Nat. Rev. Mater. **2**, 17046 (2017)
31. Raccichini, R., Varzi, A., Passerini, S., et al.: The role of graphene for electrochemical energy storage. Nat. Mater. **14**, 271–279 (2015)
32. El-Kady, M.F., Shao, Y.L., Kaner, R.B.: Graphene for batteries, supercapacitors and beyond. Nat. Rev. Mater. **1**, 16033 (2016)
33. Liu, X., Dai, L.: Carbon-based metal-free catalysts. Nat. Rev. Mater. **1**, 16064 (2016)
34. Morozov, S.V., Novoselov, K.S., Katsnelson, M.I., et al.: Giant intrinsic carrier mobilities in graphene and its bilayer. Phys. Rev. Lett. **100**, 016602 (2008)
35. Bolotin, K.I., Sikes, K.J., Jiang, Z., et al.: Ultrahigh electron mobility in suspended graphene. Solid State Commun. **146**, 351–355 (2008)
36. Balandin, A.A., Ghosh, S., Bao, W.Z., et al.: Superior thermal conductivity of single-layer graphene. Nano Lett. **8**, 902–907 (2008)
37. Liu, F., Ming, P.M., Li, J.: Ab initio calculation of ideal strength and phonon instability of graphene under tension. Phys. Rev. B **76**, 064120 (2007)
38. Han, S., Wu, D., Li, S., et al.: Porous graphene materials for advanced electrochemical energy storage and conversion devices. Adv. Mater. **26**, 849–864 (2014)
39. Li, Y., Fu, Z.-Y., Su, B.-L.: Hierarchically structured porous materials for energy conversion and storage. Adv. Funct. Mater. **22**, 4634–4667 (2012)
40. Lv, W., Li, Z.J., Deng, Y.Q., et al.: Graphene-based materials for electrochemical energy storage devices: opportunities and challenges. Energy Storage Mater. **2**, 107–138 (2016)

41. Yao, X., Zhao, Y.L.: Three-dimensional porous graphene networks and hybrids for lithium-ion batteries and supercapacitors. Chem **2**, 171–200 (2017)
42. Chen, K.N., Wang, Q.R., Niu, Z.Q., et al.: Graphene-based materials for flexible energy storage devices. J. Energy Chem. **27**, 12–24 (2018)
43. Huang, Y., Wang, Y., Tang, C., et al.: Atomic modulation and structure design of carbons for bifunctional electrocatalysis in metal-air batteries. Adv. Mater. **30**, 1803800 (2018)
44. Qiu, L., Li, D., Cheng, H.M.: Structural control of graphene-based materials for unprecedented performance. ACS Nano **12**, 5085–5092 (2018)
45. Kim, Y.A., Hayashi, T., Kim, J.H., et al.: Important roles of graphene edges in carbon-based energy storage devices. J. Energy Chem. **22**, 183–194 (2013)
46. Sheng, L.Z., Liang, S.C., Wei, T., et al.: Space-confinement of MnOnanosheets in densely stacked graphene: ultra-high volumetric capacity and rate performance for lithium-ion batteries. Energy Storage Mater. **12**, 94–102 (2018)
47. Su, Y.Z., Liu, Y.X., Liu, P., et al.: Compact coupled graphene and porous polyaryltriazine-derived frameworks as high performance cathodes for lithium-ion batteries. Angew. Chem. Int. Ed. **54**, 1812–1816 (2015)
48. Fan, X.L., Chen, X.L., Dai, L.M.: 3D graphene based materials for energy storage. Curr. Opin. Colloid Interface Sci. **20**, 429–438 (2015)
49. Chen, K., Sun, Z.H., Fang, R.P., et al.: Development of graphene-based materials for lithium-sulfur batteries. Acta Phys-Chim. Sin. **34**, 377–390 (2018)
50. Yu, M.P., Li, R., Wu, M.M., et al.: Graphene materials for lithium-sulfur batteries. Energy Storage Mater. **1**, 51–73 (2015)
51. Wu, R., Chen, S.G., Deng, J.H., et al.: Hierarchically porous nitrogen-doped carbon as cathode for lithium-sulfur batteries. J. Energy Chem. **27**, 1661–1667 (2018)
52. Fang, R.P., Zhao, S.Y., Pei, S.F., et al.: Toward more reliable lithium-sulfur batteries: an all-graphene cathode structure. ACS Nano **10**, 8676–8682 (2016)
53. Zheng, S.H., Wu, Z.S., Wang, S., et al.: Graphene-based materials for high-voltage and high-energy asymmetric supercapacitors. Energy Storage Mater. **6**, 70–97 (2017)
54. Zhang, W.L., Xu, C., Ma, C.Q., et al.: Nitrogen-superdoped 3D graphene networks for high-performance supercapacitors. Adv. Mater. **29**, 1701677 (2017)
55. Zhang, K., Yang, X.W., Li, D.: Engineering graphene for high-performance supercapacitors: enabling role of colloidal chemistry. J. Energy Chem. **27**, 1–5 (2018)
56. Yang, Q.Y., Xu, Z., Gao, C.: Graphene fiber based supercapacitors: strategies and perspective toward high performances. J. Energy Chem. **27**, 6–11 (2018)
57. Xu, B., Wang, H.R., Zhu, Q.Z., et al.: Reduced graphene oxide as a multi-functional conductive binder for supercapacitor electrodes. Energy Storage Mater. **12**, 128–136 (2018)
58. Wu, P.W., He, J., Chen, L.L., et al.: Few-layered graphene via gas-driven exfoliation for enhanced supercapacitive performance. J. Energy Chem. **27**, 1509–1515 (2018)
59. Wu, H., Zhang, Y.N., Cheng, L.F., et al.: Graphene based architectures for electrochemical capacitors. Energy Storage Mater. **5**, 8–32 (2016)
60. Wang, S., Wu, Z.S., Zheng, S.H., et al.: Scalable fabrication of photochemically reduced graphene-based monolithic micro-supercapacitors with superior energy and power densities. ACS Nano **11**, 4283–4291 (2017)
61. Shi, X.Y., Zheng, S.H., Wu, Z.S., et al.: Recent advances of graphene-based materials for high-performance and new-concept supercapacitors. J. Energy Chem. **27**, 25–42 (2018)
62. Wang, Q., Yan, J., Dong, Z.L., et al.: Densely stacked bubble-pillared graphene blocks for high volumetric performance supercapacitors. Energy Storage Mater. **1**, 42–50 (2015)
63. Yang, Z., Tian, J., Yin, Z., et al.: Carbon nanotube- and graphene-based nanomaterials and applications in high-voltage supercapacitor: a review. Carbon **141**, 467–480 (2019)
64. Tian, J., Yang, Z., Yin, Z., et al.: Perspective to the potential use of graphene in Li-ion battery and supercapacitor. Chem. Rec. (2018). https://doi.org/10.1002/tcr.201800090
65. Wang, H.F., Tang, C., Zhang, Q.: A review of precious-metal-free bifunctional oxygen electrocatalysts: rational design and applications in Zn–air batteries. Adv. Funct. Mater. **28**, 1803329 (2018)
66. Wang, H.F., Tang, C., Wang, B., et al.: Defect-rich carbon fiber electrocatalysts with porous graphene skin for flexible solid-state zinc-air batteries. Energy Storage Mater. **15**, 124–130 (2018)
67. Tu, Y.C., Deng, D.H., Bao, X.H.: Nanocarbons and their hybrids as catalysts for non-aqueous lithium-oxygen batteries. J. Energy Chem. **25**, 957–966 (2016)
68. Li, B.Q., Zhang, S.Y., Wang, B., et al.: A porphyrin covalent organic framework cathode for flexible Zn–air batteries. Energy Environ. Sci. **11**, 1723–1729 (2018)
69. Qin, L., Zhai, D.Y., Lv, W., et al.: Dense graphene monolith oxygen cathodes for ultrahigh volumetric energy densities. Energy Storage Mater. **9**, 134–139 (2017)
70. Wang, Y.J., Fang, B., Zhang, D., et al.: A review of carbon-composited materials as air-electrode bifunctional electrocatalysts for metal-air batteries. Electrochem. Energy Rev. **1**, 1–34 (2018)
71. Liu, L.Z., Zeng, G., Chen, J.X., et al.: N-doped porous carbon nanosheets as pH-universal ORR electrocatalyst in various fuel cell devices. Nano Energy **49**, 393–402 (2018)
72. Higgins, D., Zamani, P., Yu, A.P., et al.: The application of graphene and its composites in oxygen reduction electrocatalysis: a perspective and review of recent progress. Energy Environ. Sci. **9**, 357–390 (2016)
73. Dai, L.M., Xue, Y.H., Qu, L.T., et al.: Metal-free catalysts for oxygen reduction reaction. Chem. Rev. **115**, 4823–4892 (2015)
74. Dai, L.M.: Carbon-based catalysts for metal-free electrocatalysis. Curr. Opin. Electrochem. **4**, 18–25 (2017)
75. Duan, J.J., Chen, S., Jaroniec, M., et al.: Heteroatom-doped graphene-based materials for energy-relevant electrocatalytic processes. ACS Catal. **5**, 5207–5234 (2015)
76. Zhang, J.T., Dai, L.M.: Nitrogen, phosphorus, and fluorine tri-doped graphene as a multifunctional catalyst for self-powered electrochemical water splitting. Angew. Chem. Int. Ed. **55**, 13296–13300 (2016)
77. Wang, X., Vasileff, A., Jiao, Y., et al.: Electronic and structural engineering of carbon-based metal-free electrocatalysts for water splitting. Adv. Mater. **30**, 1803625 (2018)
78. Vasileff, A., Chen, S., Qiao, S.Z.: Three dimensional nitrogen-doped graphene hydrogels with in situ deposited cobalt phosphate nanoclusters for efficient oxygen evolution in a neutral electrolyte. Nanoscale Horiz. **1**, 41–44 (2016)
79. Hu, C.G., Dai, L.M.: Multifunctional carbon-based metal-free electrocatalysts for simultaneous oxygen reduction, oxygen evolution, and hydrogen evolution. Adv. Mater. **29**, 1604942 (2017)
80. Wang, B., Tang, C., Wang, H.F., et al.: Anion-regulated hydroxysulfide monoliths as oer/orr/her electrocatalysts and their applications in self-powered electrochemical water splitting. Small Methods **2**, 1800055 (2018)
81. Guo, X.T., Zheng, S.S., Zhang, G.X., et al.: Nanostructured graphene-based materials for flexible energy storage. Energy Storage Mater. **9**, 150–169 (2017)
82. Wen, L., Li, F., Cheng, H.M.: Carbon nanotubes and graphene for flexible electrochemical energy storage: from materials to devices. Adv. Mater. **28**, 4306–4337 (2016)

83. Shi, Y., Wen, L., Zhou, G.M., et al.: Graphene-based integrated electrodes for flexible lithium ion batteries. 2D Mater. **2**, 024004 (2015)
84. Lu, C., Li, Z.Z., Yu, L.H., et al.: Nanostructured Bi_2S_3 encapsulated within three-dimensional N-doped graphene as active and flexible anodes for sodium-ion batteries. Nano Res. **11**, 4614–4626 (2018)
85. Wang, K.L., Zheng, B.C., Shrestha, M., et al.: Magnetically enhanced plasma exfoliation of polyaniline-modified graphene for flexible solid-state supercapacitors. Energy Storage Mater. **14**, 230–237 (2018)
86. Liu, X.B., Zou, S.A., Liu, K.X., et al.: Highly compressible three-dimensional graphene hydrogel for foldable all-solid-state supercapacitor. J. Power Sources **384**, 214–222 (2018)
87. Song, W.L., Li, X.G., Fan, L.Z.: Biomass derivative/graphene aerogels for binder-free supercapacitors. Energy Storage Mater. **3**, 113–122 (2016)
88. Xu, Y., Shi, G., Duan, X.: Self-assembled three-dimensional graphene macrostructures: synthesis and applications in supercapacitors. Acc. Chem. Res. **48**, 1666–1675 (2015)
89. Cong, H.P., Chen, J.F., Yu, S.H.: Graphene-based macroscopic assemblies and architectures: an emerging material system. Chem. Soc. Rev. **43**, 7295–7325 (2014)
90. Ma, Y., Chen, Y.: Three-dimensional graphene networks: synthesis, properties and applications. Nat. Sci. Rev. **2**, 40–53 (2015)
91. Shao, Y.L., El-Kady, M.F., Wang, L.J., et al.: Graphene-based materials for flexible supercapacitors. Chem. Soc. Rev. **44**, 3639–3665 (2015)
92. Cao, X.H., Yin, Z.Y., Zhang, H.: Three-dimensional graphene materials: preparation, structures and application in supercapacitors. Energy Environ. Sci. **7**, 1850–1865 (2014)
93. Chabot, V., Higgins, D., Yu, A., et al.: A review of graphene and graphene oxide sponge: material synthesis and applications to energy and the environment. Energy Environ. Sci. **7**, 1564–1596 (2014)
94. Luo, B., Zhi, L.J.: Design and construction of three dimensional graphene-based composites for lithium ion battery applications. Energy Environ. Sci. **8**, 456–477 (2015)
95. Wu, Q., Yang, L.J., Wang, X.Z., et al.: From carbon-based nanotubes to nanocages for advanced energy conversion and storage. Acc. Chem. Res. **50**, 435–444 (2017)
96. Olszowska, K., Pang, J.B., Wrobel, P.S., et al.: Three-dimensional nanostructured graphene: synthesis and energy, environmental and biomedical applications. Synthetic. Met. **234**, 53–85 (2017)
97. Mao, S., Lu, G.H., Chen, J.H.: Three-dimensional graphene-based composites for energy applications. Nanoscale **7**, 6924–6943 (2015)
98. Xia, X.H., Chao, D.L., Zhang, Y.Q., et al.: Three-dimensional graphene and their integrated electrodes. Nano Today **9**, 785–807 (2014)
99. Wang, Z., Gao, H., Zhang, Q., et al.: Recent advances in 3D graphene architectures and their composites for energy storage applications. Small **15**, 1803858 (2019)
100. Chen, K.F., Song, S.Y., Liu, F., et al.: Structural design of graphene for use in electrochemical energy storage devices. Chem. Soc. Rev. **44**, 6230–6257 (2015)
101. Su, F.Y., Tang, R., He, Y.B., et al.: Graphene conductive additives for lithium ion batteries: origin, progress and prospect. Chin. Sci. Bull. **62**, 3743–3756 (2017)
102. Su, F.Y., He, Y.B., Li, B.H., et al.: Could graphene construct an effective conducting network in a high-power lithium ion battery? Nano Energy **1**, 429–439 (2012)
103. Zhang, L., Zhang, F., Yang, X., et al.: Porous 3D graphene-based bulk materials with exceptional high surface area and excellent conductivity for supercapacitors. Sci. Rep. **3**, 1408 (2013)
104. Jiao, Y., Zheng, Y., Davey, K., et al.: Activity origin and catalyst design principles for electrocatalytic hydrogen evolution on heteroatom-doped graphene. Nat. Energy **1**, 16130 (2016)
105. Tang, C., Wang, H.S., Wang, H.F., et al.: Spatially confined hybridization of nanometer-sized NiFe hydroxides into nitrogen-doped graphene frameworks leading to superior oxygen evolution reactivity. Adv. Mater. **27**, 4516–4522 (2015)
106. Tang, C., Zhong, L., Zhang, B.S., et al.: 3D mesoporous van der waals heterostructures for trifunctional energy electrocatalysis. Adv. Mater. **30**, 1705110 (2018)
107. Ren, W.C., Cheng, H.M.: The global growth of graphene. Nat. Nanotechnol. **9**, 726–730 (2014)
108. Zhu, Y.W., Murali, S., Cai, W.W., et al.: Graphene and graphene oxide: synthesis, properties, and applications. Adv. Mater. **22**, 3906–3924 (2010)
109. Lin, L., Deng, B., Sun, J.Y., et al.: Bridging the gap between reality and ideal in chemical vapor deposition growth of graphene. Chem. Rev. **118**, 9281–9343 (2018)
110. Cai, Z.Y., Liu, B.L., Zou, X.L., et al.: Chemical vapor deposition growth and applications of two-dimensional materials and their heterostructures. Chem. Rev. **118**, 6091–6133 (2018)
111. Li, X., Cai, W., An, J., et al.: Large-area synthesis of high-quality and uniform graphene films on copper foils. Science **324**, 1312–1314 (2009)
112. Zhang, Y., Zhang, L.Y., Zhou, C.W.: Review of chemical vapor deposition of graphene and related applications. Acc. Chem. Res. **46**, 2329–2339 (2013)
113. Deng, B., Liu, Z., Peng, H.: Toward mass production of CVD graphene films. Adv. Mater. **30**, 1800996 (2018)
114. Li, X., Cai, W., Colombo, L., et al.: Evolution of graphene growth on Ni and Cu by carbon isotope labeling. Nano Lett. **9**, 4268–4272 (2009)
115. Yan, K., Fu, L., Peng, H., et al.: Designed CVD growth of graphene via process engineering. Acc. Chem. Res. **46**, 2263–2274 (2013)
116. Chen, Z., Ren, W., Gao, L., et al.: Three-dimensional flexible and conductive interconnected graphene networks grown by chemical vapour deposition. Nat. Mater. **10**, 424–428 (2011)
117. Bi, H., Huang, F.Q., Liang, J., et al.: Large-scale preparation of highly conductive three dimensional graphene and its applications in cdte solar cells. J. Mater. Chem. **21**, 17366–17370 (2011)
118. Tang, B., Hu, G., Gao, H., et al.: Three-dimensional graphene network assisted high performance dye sensitized solar cells. J. Power Sources **234**, 60–68 (2013)
119. Tang, Y., Huang, F., Bi, H., et al.: Highly conductive three-dimensional graphene for enhancing the rate performance of $LiFePO_4$ cathode. J. Power Sources **203**, 130–134 (2012)
120. Van Hoa, N., Lamiel, C., Shim, J.-J.: Mesoporous 3D graphene@$NiCo_2O_4$ arrays on nickel foam as electrodes for high-performance supercapacitors. Mater. Lett. **170**, 105–109 (2016)
121. Li, N., Chen, Z.P., Ren, W.C., et al.: Flexible graphene-based lithium ion batteries with ultrafast charge and discharge rates. Proc. Natl. Acad. Sci. U.S.A. **109**, 17360–17365 (2012)
122. Xiehong, C., Yumeng, S., Wenhui, S., et al.: Preparation of novel 3D graphene networks for supercapacitor applications. Small **7**, 3163–3168 (2011)
123. Azimirad, R., Safa, S.: Preparation of three dimensional graphene foam-WO_3 nanocomposite with enhanced visible light photocatalytic activity. Mater. Chem. Phys. **162**, 686–691 (2015)
124. Xue, Y., Yu, D., Dai, L., et al.: Three-dimensional B, N-doped graphene foam as a metal-free catalyst for oxygen reduction reaction. Phys. Chem. Chem. Phys. **15**, 12220–12226 (2013)

125. Dong, X., Wang, X., Wang, L., et al.: 3D graphene foam as a monolithic and macroporous carbon electrode for electrochemical sensing. ACS Appl. Mater. Interfaces. **4**, 3129–3133 (2012)
126. Feng, X., Zhang, Y., Zhou, J., et al.: Three-dimensional nitrogen-doped graphene as an ultrasensitive electrochemical sensor for the detection of dopamine. Nanoscale **7**, 2427–2432 (2015)
127. Chen, Z.P., Xu, C., Ma, C.Q., et al.: Lightweight and flexible graphene foam composites for high-performance electromagnetic interference shielding. Adv. Mater. **25**, 1296–1300 (2013)
128. Shan, C.S., Tang, H., Wong, T.L., et al.: Facile synthesis of a large quantity of graphene by chemical vapor deposition: an advanced catalyst carrier. Adv. Mater. **24**, 2491–2495 (2012)
129. Chen, Z.P., Ren, W.C., Liu, B.L., et al.: Bulk growth of mono- to few-layer graphene on nickel particles by chemical vapor deposition from methane. Carbon **48**, 3543–3550 (2010)
130. Li, W., Gao, S., Wu, L., et al.: High-density three-dimension graphene macroscopic objects for high-capacity removal of heavy metal ions. Sci. Rep. **3**, 2125 (2013)
131. Zhang, Q.F., Wang, L.L., Wang, J., et al.: Low-temperature synthesis of edge-rich graphene paper for high-performance aluminum batteries. Energy Storage Mater. **15**, 361–367 (2018)
132. Sha, J., Gao, C., Lee, S.K., et al.: Preparation of three-dimensional graphene foams using powder metallurgy templates. ACS Nano **10**, 1411–1416 (2016)
133. Drieschner, S., Weber, M., Wohlketzetter, J., et al.: High surface area graphene foams by chemical vapor deposition. 2D Mater. **3**, 045013 (2016)
134. Zhang, L., DeArmond, D., Alvarez, N.T., et al.: Beyond graphene foam, a new form of three-dimensional graphene for supercapacitor electrodes. J. Mater. Chem. A **4**, 1876–1886 (2016)
135. Ito, Y., Tanabe, Y., Sugawara, K., et al.: Three-dimensional porous graphene networks expand graphene-based electronic device applications. Phys. Chem. Chem. Phys. **20**, 6024–6033 (2018)
136. Ito, Y., Qiu, H.J., Fujita, T., et al.: Bicontinuous nanoporous N-doped graphene for the oxygen reduction reaction. Adv. Mater. **26**, 4145–4150 (2014)
137. Ito, Y., Tanabe, Y., Qiu, H.J., et al.: High-quality three-dimensional nanoporous graphene. Angew. Chem. Int. Ed. **53**, 4822–4826 (2014)
138. Ito, Y., Cong, W., Fujita, T., et al.: High catalytic activity of nitrogen and sulfur co-doped nanoporous graphene in the hydrogen evolution reaction. Angew. Chem. Int. Ed. **54**, 2131–2136 (2015)
139. Tanabe, Y., Ito, Y., Sugawara, K., et al.: Electric properties of dirac fermions captured into 3D nanoporous graphene networks. Adv. Mater. **28**, 10304–10310 (2016)
140. Fujita, T., Qian, L.H., Inoke, K., et al.: Three-dimensional morphology of nanoporous gold. Appl. Phys. Lett. **92**, 251902 (2008)
141. Fujita, T., Okada, H., Koyama, K., et al.: Unusually small electrical resistance of three-dimensional nanoporous gold in external magnetic fields. Phys. Rev. Lett. **101**, 166601 (2008)
142. Di Bernardo, I., Avvisati, G., Mariani, C., et al.: Two-dimensional hallmark of highly interconnected three-dimensional nanoporous graphene. ACS Omega **2**, 3691–3697 (2017)
143. Qin, K.Q., Liu, E.Z., Li, J.J., et al.: Free-standing 3D nanoporous duct-like and hierarchical nanoporous graphene films for micron-level flexible solid-state asymmetric supercapacitors. Adv. Energy Mater. **6**, 1600755 (2016)
144. Qin, K., Kang, J., Li, J., et al.: Continuously hierarchical nanoporous graphene film for flexible solid-state supercapacitors with excellent performance. Nano Energy **24**, 158–164 (2016)
145. Rummeli, M.H., Kramberger, C., Gruneis, A., et al.: On the graphitization nature of oxides for the formation of carbon nanostructures. Chem. Mater. **19**, 4105–4107 (2007)
146. Rummeli, M.H., Schaffel, F., Bachmatiuk, A., et al.: Oxide catalysts for carbon nanotube and few layer graphene formation. Phys. Status Solidi B **246**, 2530–2533 (2009)
147. Rummeli, M.H., Bachmatiuk, A., Scott, A., et al.: Direct low-temperature nanographene CVD synthesis over a dielectric insulator. ACS Nano **4**, 4206–4210 (2010)
148. Scott, A., Dianat, A., Borrnert, F., et al.: The catalytic potential of high-κ dielectrics for graphene formation. Appl. Phys. Lett. **98**, 073110 (2011)
149. Ning, G.Q., Fan, Z.J., Wang, G., et al.: Gram-scale synthesis of nanomesh graphene with high surface area and its application in supercapacitor electrodes. Chem. Commun. **47**, 5976–5978 (2011)
150. Zhang, Q., Huang, J.Q., Zhao, M.Q., et al.: Carbon nanotube mass production: principles and processes. ChemSusChem **4**, 864–889 (2011)
151. Ma, X., Ning, G., Qi, C., et al.: Phosphorus and nitrogen dual-doped few-layered porous graphene: a high-performance anode material for lithium-ion batteries. ACS Appl. Mater. Interfaces. **6**, 14415–14422 (2014)
152. Fan, Z., Liu, Y., Yan, J., et al.: Template-directed synthesis of pillared-porous carbon nanosheet architectures: high-performance electrode materials for supercapacitors. Adv. Energy Mater. **2**, 419–424 (2012)
153. Jia, X., Zhang, G., Wang, T., et al.: Monolithic nitrogen-doped graphene frameworks as ultrahigh-rate anodes for lithium ion batteries. J. Mater. Chem. A **3**, 15738–15744 (2015)
154. Wang, H.F., Tang, C., Zhang, Q.: Template growth of nitrogen-doped mesoporous graphene on metal oxides and its use as a metal-free bifunctional electrocatalyst for oxygen reduction and evolution reactions. Catal. Today **301**, 25–31 (2018)
155. Xie, K., Qin, X., Wang, X., et al.: Carbon nanocages as supercapacitor electrode materials. Adv. Mater. **24**, 347–352 (2012)
156. Lyu, Z., Xu, D., Yang, L., et al.: Hierarchical carbon nanocages confining high-loading sulfur for high-rate lithium-sulfur batteries. Nano Energy **12**, 657–665 (2015)
157. Zhao, J., Lai, H., Lyu, Z., et al.: Hydrophilic hierarchical nitrogen-doped carbon nanocages for ultrahigh supercapacitive performance. Adv. Mater. **27**, 3541–3545 (2015)
158. Chen, S., Bi, J., Zhao, Y., et al.: Nitrogen-doped carbon nanocages as efficient metal-free electrocatalysts for oxygen reduction reaction. Adv. Mater. **24**, 5593–5597 (2012)
159. Cui, C., Qian, W., Yu, Y., et al.: Highly electroconductive mesoporous graphene nanofibers and their capacitance performance at 4 V. J. Am. Chem. Soc. **136**, 2256–2259 (2014)
160. Jia, X.L., Lu, Y.F., Wei, F.: Confined growth of $Li_4Ti_5O_{12}$ nanoparticles in nitrogen-doped mesoporous graphene fibers for high-performance lithium-ion battery anodes. Nano Res. **9**, 230–239 (2016)
161. Tian, J., Cui, C., Zheng, C., et al.: Mesoporous tubular graphene electrode for high performance supercapacitor. Chinese Chem. Lett. **29**, 599–602 (2018)
162. Tian, J., Cui, C., Xie, Q., et al.: EMIMBF4–GBL binary electrolyte working at − 70 °C and 3.7 V for a high performance graphene-based capacitor. J. Mater. Chem. A **6**, 3593–3601 (2018)
163. Zheng, Z.M., Guo, H.C., Pei, F., et al.: High sulfur loading in hierarchical porous carbon rods constructed by vertically oriented porous graphene-like nanosheets for Li–S batteries. Adv. Funct. Mater. **26**, 8952–8959 (2016)
164. Tang, C., Li, B.Q., Zhang, Q., et al.: CaO-templated growth of hierarchical porous graphene for high-power lithium-sulfur battery applications. Adv. Funct. Mater. **26**, 577–585 (2016)
165. Xu, B., Peng, L., Wang, G., et al.: Easy synthesis of mesoporous carbon using nano-$CaCO_3$ as template. Carbon **48**, 2377–2380 (2010)

166. Zhao, C., Wang, W., Yu, Z., et al.: Nano-$CaCO_3$ as template for preparation of disordered large mesoporous carbon with hierarchical porosities. J. Mater. Chem. **20**, 976–980 (2010)
167. Shi, L., Chen, K., Du, R., et al.: Scalable seashell-based chemical vapor deposition growth of three-dimensional graphene foams for oil-water separation. J. Am. Chem. Soc. **138**, 6360–6363 (2016)
168. Chen, K., Li, C., Chen, Z., et al.: Bioinspired synthesis of CVD graphene flakes and graphene-supported molybdenum sulfide catalysts for hydrogen evolution reaction. Nano Res. **9**, 249–259 (2016)
169. Shlyakhova, E.V., Bulusheva, L.G., Kanygin, M.A., et al.: Synthesis of nitrogen-containing porous carbon using calcium oxide nanoparticles. Phys. Status Solidi B **251**, 2607–2612 (2014)
170. Xu, B., Zheng, D., Jia, M., et al.: Nano-CaO templated carbon by CVD: from nanosheets to nanocages. Mater. Lett. **143**, 159–162 (2015)
171. Zhou, M., Lin, T., Huang, F., et al.: Highly conductive porous graphene/ceramic composites for heat transfer and thermal energy storage. Adv. Funct. Mater. **23**, 2263–2269 (2013)
172. Tian, M., Wang, W., Liu, Y., et al.: A three-dimensional carbon nano-network for high performance lithium ion batteries. Nano Energy **11**, 500–509 (2015)
173. Xue, Y.H., Ding, Y., Niu, J.B., et al.: Rationally designed graphene-nanotube 3D architectures with a seamless nodal junction for efficient energy conversion and storage. Sci. Adv. **1**, e1400198 (2015)
174. Bi, H., Chen, I.W., Lin, T., et al.: A new tubular graphene form of a tetrahedrally connected cellular structure. Adv. Mater. **27**, 5943–5949 (2015)
175. Strubel, P., Thieme, S., Biemelt, T., et al.: ZnOhard templating for synthesis of hierarchical porous carbons with tailored porosity and high performance in lithium-sulfur battery. Adv. Funct. Mater. **25**, 287–297 (2015)
176. Chen, K., Zhang, F., Sun, J.Y., et al.: Growth of defect-engineered graphene on manganese oxides for Li-ion storage. Energy Storage Mater. **12**, 110–118 (2018)
177. Min, K.A., Park, J., Ryou, J., et al.: Polar oxide substrates for graphene growth: a first-principles investigation of graphene on MgO(111). Curr. Appl. Phys. **13**, 803–807 (2013)
178. Kelber, J.A., Gaddam, S., Vamala, C., et al.: Direct graphene growth on MgO(111) by physical vapor deposition: interfacial chemistry and band gap formation. Spintronics Iv **8100**, 81000Y (2011)
179. Zhao, M.Q., Zhang, Q., Huang, J.Q., et al.: Hierarchical nanocomposites derived from nanocarbons and layered double hydroxides - properties, synthesis, and applications. Adv. Funct. Mater. **22**, 675–694 (2012)
180. Tian, G.L., Zhao, M.Q., Zhang, B.S., et al.: Monodisperse embedded nanoparticles derived from an atomic metal-dispersed precursor of layered double hydroxide for architectured carbon nanotube formation. J. Mater. Chem. A **2**, 1686–1696 (2014)
181. Zhao, M.Q., Zhang, Q., Zhang, W., et al.: Embedded high density metal nanoparticles with extraordinary thermal stability derived from guest-host mediated layered double hydroxides. J. Am. Chem. Soc. **132**, 14739–14741 (2010)
182. Zhao, M.Q., Zhang, Q., Huang, J.Q., et al.: Unstacked double-layer templated graphene for high-rate lithium-sulphur batteries. Nat. Commun. **5**, 3410 (2014)
183. Tian, G.L., Zhang, Q., Zhao, M.Q., et al.: Fluidized-bed CVD of unstacked double-layer templated graphene and its application in supercapacitors. AIChE J. **61**, 747–755 (2015)
184. Shi, J.L., Wang, H.F., Zhu, X.L., et al.: The nanostructure preservation of 3D porous graphene: new insights into the graphitization and surface chemistry of non-stacked double-layer templated graphene after high-temperature treatment. Carbon **103**, 36–44 (2016)
185. Shi, J.L., Peng, H.J., Zhu, L., et al.: Template growth of porous graphene microspheres on layered double oxide catalysts and their applications in lithium-sulfur batteries. Carbon **92**, 96–105 (2015)
186. Shi, J.L., Tian, G.L., Zhang, Q., et al.: Customized casting of unstacked graphene with high surface area ($> 1300\ m^2\ g^{-1}$) and its application in oxygen reduction reaction. Carbon **93**, 702–712 (2015)
187. Shi, J.L., Tang, C., Peng, H.J., et al.: 3D mesoporous graphene: cVD self-assembly on porous oxide templates and applications in high-stable Li–S batteries. Small **11**, 5243–5252 (2015)
188. Wang, H., Zhi, L., Liu, K., et al.: Thin-sheet carbon nanomesh with an excellent electrocapacitive performance. Adv. Funct. Mater. **25**, 5420–5427 (2015)
189. Zhang, H., Zhang, X., Sun, X., et al.: Shape-controlled synthesis of nanocarbons through direct conversion of carbon dioxide. Sci. Rep. **3**, 3534 (2013)
190. Zhang, H.T., Zhang, X., Sun, X.Z., et al.: Large-scale production of nanographene sheets with a controlled mesoporous architecture as high-performance electrochemical electrode materials. ChemSusChem **6**, 1084–1090 (2013)
191. Chakrabarti, A., Lu, J., Skrabutenas, J.C., et al.: Conversion of carbon dioxide to few-layer graphene. J. Mater. Chem. **21**, 9491–9493 (2011)
192. Wang, H., Sun, K., Tao, F., et al.: 3D honeycomb-like structured graphene and its high efficiency as a counter-electrode catalyst for dye-sensitized solar cells. Angew. Chem. Int. Ed. **52**, 9210–9214 (2013)
193. Chen, X., Wu, B., Liu, Y.Q.: Direct preparation of high quality graphene on dielectric substrates. Chem. Soc. Rev. **45**, 2057–2074 (2016)
194. Chen, J.Y., Guo, Y.L., Jiang, L.L., et al.: Near-equilibrium chemical vapor deposition of high-quality single-crystal graphene directly on various dielectric substrates. Adv. Mater. **26**, 1348–1353 (2014)
195. Lin, T.Q., Chen, I.W., Liu, F.X., et al.: Nitrogen-doped mesoporous carbon of extraordinary capacitance for electrochemical energy storage. Science **350**, 1508–1513 (2015)
196. Bi, H., Lin, T., Xu, F., et al.: New graphene form of nanoporous monolith for excellent energy storage. Nano Lett. **16**, 349–354 (2016)
197. Chen, K., Chai, Z.G., Li, C., et al.: Catalyst-free growth of three-dimensional graphene flakes and graphene/g-C_3N_4 composite for hydrocarbon oxidation. ACS Nano **10**, 3665–3673 (2016)
198. Yingying, L., Yin, F., Zhangxiong, W., et al.: In-situ confined growth of monodisperse pt nanoparticle@graphene nanobox composites as electrocatalytic nanoreactors. Small **11**, 1003–1010 (2015)
199. Zhong, L., Tang, C., Wang, B., et al.: SAPO-34 templated growth of hierarchical porous graphene cages as electrocatalysts for both oxygen reduction and evolution. New Carbon Mater. **32**, 509–516 (2017)
200. Ning, G.Q., Xu, C.G., Cao, Y.M., et al.: Chemical vapor deposition derived flexible graphene paper and its application as high performance anodes for lithium rechargeable batteries. J. Mater. Chem. A **1**, 408–414 (2013)
201. Xu, C.G., Ning, G.Q., Zhu, X., et al.: Synthesis of graphene from asphaltene molecules adsorbed on vermiculite layers. Carbon **62**, 213–221 (2013)
202. Tang, C., Zhang, Q., Zhao, M.Q., et al.: Nitrogen-doped aligned carbon nanotube/graphene sandwiches: facile catalytic growth on bifunctional natural catalysts and their applications as scaffolds for high-rate lithium-sulfur batteries. Adv. Mater. **26**, 6100–6105 (2014)

203. Tang, C., Zhang, Q., Zhao, M.Q., et al.: Resilient aligned carbon nanotube/graphene sandwiches for robust mechanical energy storage. Nano Energy **7**, 161–169 (2014)
204. Chen, K., Li, C., Shi, L., et al.: Growing three-dimensional biomorphic graphene powders using naturally abundant diatomite templates towards high solution processability. Nat. Commun. **7**, 13440 (2016)
205. Qin, J., He, C.N., Zhao, N.Q., et al.: Graphene networks anchored with Sn@graphene as lithium ion battery anode. ACS Nano **8**, 1728–1738 (2014)
206. Shi, L., Chen, K., Du, R., et al.: Direct synthesis of few-layer graphene on NaCl crystals. Small **11**, 6302–6308 (2015)
207. Li, N., Yang, G., Sun, Y., et al.: Free-standing and transparent graphene membrane of polyhedron box-shaped basic building units directly grown using a nacl template for flexible transparent and stretchable solid-state supercapacitors. Nano Lett. **15**, 3195–3203 (2015)
208. Zhu, Y.W., Ji, H.X., Cheng, H.M., et al.: Mass production and industrial applications of graphene materials. Nat. Sci. Rev. **5**, 90–101 (2018)
209. Jin, H.L., Bu, Y.F., Li, J., et al.: Strong graphene 3D assemblies with high elastic recovery and hardness. Adv. Mater. **30**, 1707424 (2018)
210. Lim, J., Lee, G.Y., Lee, H.J., et al.: Open porous graphene nanoribbon hydrogel via additive-free interfacial self-assembly: fast mass transport electrodes for high-performance biosensing and energy storage. Energy Storage Mater. **16**, 251–258 (2019)
211. Zhang, L., Shi, G.Q.: Preparation of highly conductive graphene hydrogels for fabricating supercapacitors with high rate capability. J. Phys. Chem. C **115**, 17206–17212 (2011)
212. Cong, H.P., Ren, X.C., Wang, P., et al.: Macroscopic multifunctional graphene-based hydrogels and aerogels by a metal ion induced self-assembly process. ACS Nano **6**, 2693–2703 (2012)
213. Xu, Y.X., Sheng, K.X., Li, C., et al.: Self-assembled graphene hydrogel via a one-step hydrothermal process. ACS Nano **4**, 4324–4330 (2010)
214. Hu, H., Zhao, Z., Wan, W., et al.: Ultralight and highly compressible graphene aerogels. Adv. Mater. **25**, 2219–2223 (2013)
215. Zhao, Y., Hu, C., Hu, Y., et al.: A versatile, ultralight, nitrogen-doped graphene framework. Angew. Chem. Int. Ed. **51**, 11371–11375 (2012)
216. Sudeep, P.M., Narayanan, T.N., Ganesan, A., et al.: Covalently interconnected three-dimensional graphene oxide solids. ACS Nano **7**, 7034–7040 (2013)
217. Xie, X., Zhou, Y.L., Bi, H.C., et al.: Large-range control of the microstructures and properties of three-dimensional porous graphene. Sci. Rep. **3**, 2117 (2013)
218. Tao, Y., Xie, X., Lv, W., et al.: Towards ultrahigh volumetric capacitance: graphene derived highly dense but porous carbons for supercapacitors. Sci. Rep. **3**, 2975 (2013)
219. Shao, J.J., Wu, S.D., Zhang, S.B., et al.: Graphene oxide hydrogel at solid/liquid interface. Chem. Commun. **47**, 5771–5773 (2011)
220. Liu, L., Niu, Z., Zhang, L., et al.: Nanostructured graphene composite papers for highly flexible and foldable supercapacitors. Adv. Mater. **26**, 4855–4862 (2014)
221. Choi, B.G., Yang, M., Hong, W.H., et al.: 3D macroporous graphene frameworks for supercapacitors with high energy and power densities. ACS Nano **6**, 4020–4028 (2012)
222. Huang, X.D., Sun, B., Li, K.F., et al.: Mesoporous graphene paper immobilised sulfur as a flexible electrode for lithium-sulfur batteries. J. Mater. Chem. A **1**, 13484–13489 (2013)
223. Huang, X., Qian, K., Yang, J., et al.: Functional nanoporous graphene foams with controlled pore sizes. Adv. Mater. **24**, 4419–4423 (2012)
224. Wang, J., Wang, H.S., Wang, K., et al.: Ice crystals growth driving assembly of porous nitrogen-doped graphene for catalyzing oxygen reduction probed by in situ fluorescence electrochemistry. Sci. Rep. **4**, 6723 (2014)
225. Li, Y., Chen, J., Huang, L., et al.: Highly compressible macroporous graphene monoliths via an improved hydrothermal process. Adv. Mater. **26**, 4789–4793 (2014)
226. Zou, J.L., Kim, F.: Diffusion driven layer-by-layer assembly of graphene oxide nanosheets into porous three-dimensional macrostructures. Nat. Commun. **5**, 5254 (2014)
227. Huang, X.D., Sun, B., Su, D.W., et al.: Soft-template synthesis of 3D porous graphene foams with tunable architectures for lithium-O_2 batteries and oil adsorption applications. J. Mater. Chem. A **2**, 7973–7979 (2014)
228. Gao, Y.D., Zhang, Y.Y., Zhang, Y., et al.: Three-dimensional paper-like graphene framework with highly orientated laminar structure as binder-free supercapacitor electrode. J. Energy Chem. **25**, 49–54 (2016)
229. Chen, X., Xiao, Z.B., Ning, X.T., et al.: Sulfur-impregnated, sandwich-type, hybrid carbon nanosheets with hierarchical porous structure for high-performance lithium-sulfur batteries. Adv. Energy Mater. **4**, 1301988 (2014)
230. Sun, W.W., Peng, T., Liu, Y.M., et al.: Ordered mesoporous carbon-decorated reduced graphene oxide as efficient counter electrode for dye-sensitized solar cells. Carbon **77**, 18–24 (2014)
231. Song, Y.F., Yang, J., Wang, K., et al.: In-situ synthesis of graphene/nitrogen-doped ordered mesoporous carbon nanosheet for supercapacitor application. Carbon **96**, 955–964 (2016)
232. Cong, H.P., Wang, P., Gong, M., et al.: Facile synthesis of mesoporous nitrogen-doped graphene: an efficient methanol-tolerant cathodic catalyst for oxygen reduction reaction. Nano Energy **3**, 55–63 (2014)
233. Niu, W.H., Li, L.G., Liu, J., et al.: Graphene-supported mesoporous carbons prepared with thermally removable templates as efficient catalysts for oxygen electroreduction. Small **12**, 1900–1908 (2016)
234. Zhu, Y.W., Murali, S., Stoller, M.D., et al.: Carbon-based supercapacitors produced by activation of graphene. Science **332**, 1537–1541 (2011)
235. Huang, J., Wang, J., Wang, C., et al.: Hierarchical porous graphene carbon-based supercapacitors. Chem. Mater. **27**, 2107–2113 (2015)
236. Su, H., Zhang, H.T., Liu, F.Y., et al.: High power supercapacitors based on hierarchically porous sheet-like nanocarbons with ionic liquid electrolytes. Chem. Eng. J. **322**, 73–81 (2017)
237. You, Y., Zeng, W.C., Yin, Y.X., et al.: Hierarchically micro/mesoporous activated graphene with a large surface area for high sulfur loading in Li–S batteries. J. Mater. Chem. A **3**, 4799–4802 (2015)
238. Kim, T.H., Bae, J., Lee, T.H., et al.: Room-temperature hydrogen storage via two-dimensional potential well in mesoporous graphene oxide. Nano Energy **27**, 402–411 (2016)
239. Xu, X.T., Liu, Y., Wang, M., et al.: Design and fabrication of mesoporous graphene via carbothermal reaction for highly efficient capacitive deionization. Electrochim. Acta **188**, 406–413 (2016)
240. Palaniselvam, T., Kashyap, V., Bhange, S.N., et al.: Nanoporous graphene enriched with Fe/Co-N active sites as a promising oxygen reduction electrocatalyst for anion exchange membrane fuel cells. Adv. Funct. Mater. **26**, 2150–2162 (2016)
241. Sun, H.T., Mei, L., Liang, J.F., et al.: Three-dimensional holey-graphene/niobia composite architectures for ultrahigh-rate energy storage. Science **356**, 599–604 (2017)
242. Gu, X.Y., Hu, M., Du, Z.S., et al.: Fabrication of mesoporous graphene electrodes with enhanced capacitive deionization. Electrochim. Acta **182**, 183–191 (2015)

243. Melinte, G., Florea, I., Moldovan, S., et al.: A 3D insight on the catalytic nanostructuration of few-layer graphene. Nat. Commun. **5**, 4109 (2014)
244. Zhao, Y., Hu, C.G., Song, L., et al.: Functional graphene nanomesh foam. Energy Environ. Sci. **7**, 1913–1918 (2014)
245. Lacey, S.D., Kirsch, D.J., Li, Y.J., et al.: Extrusion-based 3D printing of hierarchically porous advanced battery electrodes. Adv. Mater. **30**, 1705651 (2018)
246. Yang, X., Zhang, L., Zhang, F., et al.: Sulfur-infiltrated graphene-based layered porous carbon cathodes for high-performance lithium-sulfur batteries. ACS Nano **8**, 5208–5215 (2014)
247. Wang, D.W., Li, F., Liu, M., et al.: 3D aperiodic hierarchical porous graphitic carbon material for high-rate electrochemical capacitive energy storage. Angew. Chem. Int. Ed. **47**, 373–376 (2008)
248. Niu, W.H., Li, L.G., Liu, X.J., et al.: Mesoporous N-doped carbons prepared with thermally removable nanoparticle templates: an efficient electrocatalyst for oxygen reduction reaction. J. Am. Chem. Soc. **137**, 5555–5562 (2015)
249. Pan, F.P., Duan, Y.X., Zhang, X.K., et al.: A facile synthesis of nitrogen/sulfur co-doped graphene for the oxygen reduction reaction. ChemCatChem **8**, 163–170 (2016)
250. Li, J., Wang, N., Tian, J., et al.: Cross-coupled macro-mesoporous carbon network toward record high energy-power density supercapacitor at 4 V. Adv. Funct. Mater. **28**, 1806153 (2018)
251. Wang, J.W., Jia, X.L., Atinafu, D.G., et al.: Synthesis of "graphene-like" mesoporous carbons for shape-stabilized phase change materials with high loading capacity and improved latent heat. J. Mater. Chem. A **5**, 24321–24328 (2017)
252. Xu, G.Y., Ding, B., Nie, P., et al.: Hierarchically porous carbon encapsulating sulfur as a superior cathode material for high performance lithium-sulfur batteries. ACS Appl. Mater. Interfaces **6**, 194–199 (2014)
253. Tang, C., Wang, H.F., Chen, X., et al.: Topological defects in metal-free nanocarbon for oxygen electrocatalysis. Adv. Mater. **28**, 6845–6851 (2016)
254. Peng, H.J., Liang, J.Y., Zhu, L., et al.: Catalytic self-limited assembly at hard templates: a mesoscale approach to graphene nanoshells for lithium-sulfur batteries. ACS Nano **8**, 11280–11289 (2014)
255. Yoon, J.C., Lee, J.S., Kim, S.I., et al.: Three-dimensional graphene nano-networks with high quality and mass production capability via precursor-assisted chemical vapor deposition. Sci. Rep. **3**, 1788 (2013)
256. Jiao, Y.C., Han, D.D., Liu, L.M., et al.: Highly ordered mesoporous few-layer graphene frameworks enabled by Fe_3O_4 nanocrystal superlattices. Angew. Chem. Int. Ed. **54**, 5727–5731 (2015)
257. Jiao, Y., Han, D., Ding, Y., et al.: Fabrication of three-dimensionally interconnected nanoparticle superlattices and their lithium-ion storage properties. Nat. Commun. **6**, 6420 (2015)
258. Han, D.D., Yan, Y.C., Wei, J.S., et al.: Fine-tuning the wall thickness of ordered mesoporous graphene by exploiting ligand exchange of colloidal nanocrystals. Front. Chem. **5**, 117 (2017)
259. Ji, L., Guo, G.N., Sheng, H.Y., et al.: Free-standing, ordered mesoporous few-layer graphene framework films derived from nanocrystal superlattices self-assembled at the solid- or liquid-air interface. Chem. Mater. **28**, 3823–3830 (2016)
260. Yu, H.J., Guo, G.N., Ji, L., et al.: Designed synthesis of ordered mesoporous graphene spheres from colloidal nanocrystals and their application as a platform for high-performance lithium-ion battery composite electrodes. Nano Res. **9**, 3757–3771 (2016)
261. Dai, L.M.: Functionalization of graphene for efficient energy conversion and storage. Acc. Chem. Res. **46**, 31–42 (2013)
262. Yuan, H., Kong, L., Li, T., et al.: A review of transition metal chalcogenide/graphene nanocomposites for energy storage and conversion. Chin. Chem. Lett. **28**, 2180–2194 (2017)
263. Hu, C.G., Liu, D., Xiao, Y., et al.: Functionalization of graphene materials by heteroatom-doping for energy conversion and storage. Prog. Nat. Sci. **28**, 121–132 (2018)
264. Jiao, Y., Zheng, Y., Jaroniec, M., et al.: Origin of the electrocatalytic oxygen reduction activity of graphene-based catalysts: a roadnnap to achieve the best performance. J. Am. Chem. Soc. **136**, 4394–4403 (2014)
265. Hu, C.G., Dai, L.M.: Carbon-based metal-free catalysts for electrocatalysis beyond the ORR. Angew. Chem. Int. Ed. **55**, 11736–11758 (2016)
266. Ma, Y.F., Guo, Q.B., Yang, M., et al.: Highly doped graphene with multi-dopants for high-capacity and ultrastable sodium-ion batteries. Energy Storage Mater. **13**, 134–141 (2018)
267. Ma, Z.L., Dou, S., Shen, A.L., et al.: Sulfur-doped graphene derived from cycled lithium-sulfur batteries as a metal-free electrocatalyst for the oxygen reduction reaction. Angew. Chem. Int. Ed. **54**, 1888–1892 (2015)
268. Xu, H.F., Ma, L.B., Jin, Z.: Nitrogen-doped graphene: synthesis, characterizations and energy applications. J. Energy Chem. **27**, 146–160 (2018)
269. Lee, W.J., Lim, J., Kim, S.O.: Nitrogen dopants in carbon nanomaterials: defects or a new opportunity? Small Methods **1**, 1600014 (2017)
270. Li, M.T., Zhang, L.P., Xu, Q., et al.: N-doped graphene as catalysts for oxygen reduction and oxygen evolution reactions: theoretical considerations. J. Catal. **314**, 66–72 (2014)
271. Hou, T.Z., Chen, X., Peng, H.J., et al.: Design principles for heteroatom-doped nanocarbon to achieve strong anchoring of polysulfides for lithium-sulfur batteries. Small **12**, 3283–3291 (2016)
272. Li, J.C., Hou, P.X., Zhao, S.Y., et al.: A 3D bi-functional porous N-doped carbon microtube sponge electrocatalyst for oxygen reduction and oxygen evolution reactions. Energy Environ. Sci. **9**, 3079–3084 (2016)
273. Zhang, J.A., Song, Y., Kopec, M., et al.: Facile aqueous route to nitrogen-doped mesoporous carbons. J. Am. Chem. Soc. **139**, 12931–12934 (2017)
274. Qin, L., Ding, R.M., Wang, H.X., et al.: Facile synthesis of porous nitrogen-doped holey graphene as an efficient metal-free catalyst for the oxygen reduction reaction. Nano Res. **10**, 305–319 (2017)
275. Liu, X.B., Amiinu, I.S., Liu, S.J., et al.: Transition metal/nitrogen dual-doped mesoporous graphene-like carbon nanosheets for the oxygen reduction and evolution reactions. Nanoscale **8**, 13311–13320 (2016)
276. Zhang, J., Zhao, Z., Xia, Z., et al.: A metal-free bifunctional electrocatalyst for oxygen reduction and oxygen evolution reactions. Nat. Nanotechnol. **10**, 444–452 (2015)
277. Yang, H.B., Miao, J.W., Hung, S.F., et al.: Identification of catalytic sites for oxygen reduction and oxygen evolution in N-doped graphene materials: development of highly efficient metal-free bifunctional electrocatalyst. Sci. Adv. **2**, e1501122 (2016)
278. Chen, S., Duan, J.J., Jaroniec, M., et al.: Nitrogen and oxygen dual-doped carbon hydrogel film as a substrate-free electrode for highly efficient oxygen evolution reaction. Adv. Mater. **26**, 2925–2930 (2014)
279. Chen, S., Duan, J., Zheng, Y., et al.: Ionic liquid-assisted synthesis of N/S-double doped graphene microwires for oxygen evolution and Zn–air batteries. Energy Storage Mater. **1**, 17–24 (2015)
280. Kim, J.H., Kannan, A.G., Woo, H.S., et al.: A bi-functional metal-free catalyst composed of dual-doped graphene and mesoporous carbon for rechargeable lithium-oxygen batteries. J. Mater. Chem. A **3**, 18456–18465 (2015)

281. Jia, Y., Zhang, L.Z., Du, A.J., et al.: Defect graphene as a trifunctional catalyst for electrochemical reactions. Adv. Mater. **28**, 9532–9538 (2016)
282. Shi, J.L., Tang, C., Huang, J.Q., et al.: Effective exposure of nitrogen heteroatoms in 3D porous graphene framework for oxygen reduction reaction and lithium-sulfur batteries. J. Energy Chem. **27**, 167–175 (2018)
283. Qiao, M., Tang, C., He, G., et al.: Graphene/nitrogen-doped porous carbon sandwiches for the metal-free oxygen reduction reaction: conductivity versus active sites. J. Mater. Chem. A **4**, 12658–12666 (2016)
284. Li, R., Wei, Z., Gou, X.: Nitrogen and phosphorus dual-doped graphene/carbon nanosheets as bifunctional electrocatalysts for oxygen reduction and evolution. ACS Catal. **5**, 4133–4142 (2015)
285. Qu, K.G., Zheng, Y., Dai, S., et al.: Polydopamine-graphene oxide derived mesoporous carbon nanosheets for enhanced oxygen reduction. Nanoscale **7**, 12598–12605 (2015)
286. Zhu, C., Fu, S., Shi, Q., et al.: Single-atom electrocatalysts. Angew. Chem. Int. Ed. **56**, 13944–13960 (2017)
287. Bayatsarmadi, B., Zheng, Y., Vasileff, A., et al.: Recent advances in atomic metal doping of carbon-based nanomaterials for energy conversion. Small **13**, 1700191 (2017)
288. Li, Z., Wang, D., Wu, Y., et al.: Recent advances in the precise control of isolated single-site catalysts by chemical methods. Nat. Sci. Rev. **5**, 673–689 (2018)
289. Tang, C., Zhang, Q.: Can metal-nitrogen-carbon catalysts satisfy oxygen electrochemistry? J. Mater. Chem. A **4**, 4998–5001 (2016)
290. Qiu, H.J., Ito, Y., Cong, W.T., et al.: Nanoporous graphene with single-atom nickel dopants: an efficient and stable catalyst for electrochemical hydrogen production. Angew. Chem. Int. Ed. **54**, 14031–14035 (2015)
291. Chen, Y.J., Ji, S.F., Wang, Y.G., et al.: Isolated single iron atoms anchored on N-doped porous carbon as an efficient electrocatalyst for the oxygen reduction reaction. Angew. Chem. Int. Ed. **56**, 6937–6941 (2017)
292. Li, J., Chen, M., Cullen, D.A., et al.: Atomically dispersed manganese catalysts for oxygen reduction in proton-exchange membrane fuel cells. Nat. Cat. **1**, 935–945 (2018)
293. Yang, W., Li, X., Li, Y., et al.: Applications of metal–organic-framework-derived carbon materials. Adv. Mater. **30**, 1804740 (2018)
294. Zhang, L., Jia, Y., Gao, G., et al.: Graphene defects trap atomic Ni species for hydrogen and oxygen evolution reactions. Chem **4**, 285–297 (2018)
295. Tang, C., Wang, B., Wang, H.F., et al.: Defect engineering toward atomic Co-N_x-C in hierarchical graphene for rechargeable flexible solid Zn–air batteries. Adv. Mater. **29**, 1703185 (2017)
296. Wang, J., Huang, Z., Liu, W., et al.: Design of N-coordinated dual-metal sites: a stable and active Pt-free catalyst for acidic oxygen reduction reaction. J. Am. Chem. Soc. **139**, 17281–17284 (2017)
297. Chen, S., Duan, J., Ran, J., et al.: N-doped graphene film-confined nickel nanoparticles as a highly efficient three-dimensional oxygen evolution electrocatalyst. Energy Environ. Sci. **6**, 3693–3699 (2013)
298. Peng, H.J., Zhang, Z.W., Huang, J.Q., et al.: A cooperative interface for highly efficient lithium-sulfur batteries. Adv. Mater. **28**, 9551–9558 (2016)
299. Wang, H.F., Tang, C., Wang, B., et al.: Bifunctional transition metal hydroxysulfides: room-temperature sulfurization and their applications in Zn–air batteries. Adv. Mater. **29**, 1702327 (2017)
300. Li, B.Q., Zhang, S.Y., Tang, C., et al.: Anionic regulated NiFe (oxy)sulfide electrocatalysts for water oxidation. Small **13**, 1700610 (2017)
301. Tang, C., Wang, H.F., Wang, H.S., et al.: Guest-host modulation of multi-metallic (oxy) hydroxides for superb water oxidation. J. Mater. Chem. A **4**, 3210–3216 (2016)
302. Geim, A.K., Grigorieva, I.V.: Van der waals heterostructures. Nature **499**, 419–425 (2013)
303. Novoselov, K.S., Mishchenko, A., Carvalho, A., et al.: 2D materials and van der waals heterostructures. Science **353**, aac9439 (2016)
304. Long, X., Li, J., Xiao, S., et al.: A strongly coupled graphene and FeNi double hydroxide hybrid as an excellent electrocatalyst for the oxygen evolution reaction. Angew. Chem. Int. Ed. **53**, 7584–7588 (2014)
305. Ma, W., Ma, R., Wang, C., et al.: A superlattice of alternately stacked Ni-Fe hydroxide nanosheets and graphene for efficient splitting of water. ACS Nano **9**, 1977–1984 (2015)
306. Ma, R.Z., Liu, X.H., Liang, J.B., et al.: Molecular-scale heteroassembly of redoxable hydroxide nanosheets and conductive graphene into superlattice composites for high-performance supercapacitors. Adv. Mater. **26**, 4173–4178 (2014)
307. Jia, Y., Zhang, L.Z., Gao, G.P., et al.: A heterostructure coupling of exfoliated Ni-Fe hydroxide nanosheet and defective graphene as a bifunctional electrocatalyst for overall water splitting. Adv. Mater. **29**, 1700017 (2017)
308. Duan, J.J., Chen, S., Jaroniec, M., et al.: Porous C_3N_4 nanolayers@N-graphene films as catalyst electrodes for highly efficient hydrogen evolution. ACS Nano **9**, 931–940 (2015)
309. Han, Q., Cheng, Z.H., Gao, J., et al.: Mesh-on-mesh graphitic-C_3N_4@graphene for highly efficient hydrogen evolution. Adv. Funct. Mater. **27**, 1606352 (2017)
310. Tang, C., Zhang, Q.: Nanocarbon for oxygen reduction electrocatalysis: dopants, edges, and defects. Adv. Mater. **29**, 1604103 (2017)
311. Winter, M., Barnett, B., Xu, K.: Before Li ion batteries. Chem. Rev. **118**, 11433–11456 (2018)
312. Zhu, J., Wang, T., Fan, F.R., et al.: Atomic-scale control of silicon expansion space as ultrastable battery anodes. ACS Nano **10**, 8243–8251 (2016)
313. Su, F.Y., You, C.H., He, Y.B., et al.: Flexible and planar graphene conductive additives for lithium-ion batteries. J. Mater. Chem. **20**, 9644–9650 (2010)
314. Wu, G., Ran, R., Zhao, B.T., et al.: 3D amorphous carbon and graphene co-modified $LiFePO_4$ composite derived from polyol process as electrode for high power lithium-ion batteries. J. Energy Chem. **23**, 363–375 (2014)
315. Xu, Y.X., Lin, Z.Y., Zhong, X., et al.: Solvated graphene frameworks as high-performance anodes for lithium-ion batteries. Angew. Chem. Int. Ed. **54**, 5345–5350 (2015)
316. Yan, X.J., Wang, Y.Y., Liu, C.C., et al.: Engineering two-dimensional pores in freestanding TiO_2/graphene gel film for high performance lithium ion battery. J. Energy Chem. **27**, 176–182 (2018)
317. Dong, C.F., Guo, L.J., He, Y.Y., et al.: Sandwich-like Ni_2P nanoarray/nitrogen-doped graphene nanoarchitecture as a high-performance anode for sodium and lithium ion batteries. Energy Storage Mater. **15**, 234–241 (2018)
318. Gao, X., Wang, B.Y., Zhang, Y., et al.: Graphene-scroll-sheathed α-MnS coaxial nanocables embedded in N, S co-doped graphene foam as 3D hierarchically ordered electrodes for enhanced lithium storage. Energy Storage Mater. **16**, 46–55 (2019)
319. Gerber, O., Begin-Colin, S., Pichon, B.P., et al.: Design of $Fe_{3-x}O_4$ raspberry decorated graphene nanocomposites with high performances in lithium-ion battery. J. Energy Chem. **25**, 272–277 (2016)

320. Wang, L., Wei, Z.X., Mao, M.L., et al.: Metal oxide/graphene composite anode materials for sodium-ion batteries. Energy Storage Mater. **16**, 434–454 (2019)
321. Li, Z.J., Kong, D.B., Zhou, G.M., et al.: Twin-functional graphene oxide: compacting with Fe_2O_3 into a high volumetric capacity anode for lithium ion battery. Energy Storage Mater. **6**, 98–103 (2017)
322. Zhang, D., Wang, S., Ma, Y., et al.: Two-dimensional nanosheets as building blocks to construct three-dimensional structures for lithium storage. J. Energy Chem. **27**, 128–145 (2018)
323. Odkhuu, D., Jung, D.H., Lee, H., et al.: Negatively curved carbon as the anode for lithium ion batteries. Carbon **66**, 39–47 (2014)
324. Zheng, Z.M., Zhang, X., Pei, F., et al.: Hierarchical porous carbon microrods composed of vertically aligned graphene-like nanosheets for Li-ion batteries. J. Mater. Chem. A **3**, 19800–19806 (2015)
325. Chen, X.C., Wei, W., Lv, W., et al.: A graphene-based nanostructure with expanded ion transport channels for high rate Li-ion batteries. Chem. Commun. **48**, 5904–5906 (2012)
326. Choi, S.H., Lee, J.K., Kang, Y.C.: Three-dimensional porous graphene-metal oxide composite microspheres: preparation and application in Li-ion batteries. Nano Res. **8**, 1584–1594 (2015)
327. Zhou, G.M., Li, F., Cheng, H.M.: Progress in flexible lithium batteries and future prospects. Energy Environ. Sci. **7**, 1307–1338 (2014)
328. Peng, H.J., Huang, J.Q., Cheng, X.B., et al.: Review on high-loading and high-energy lithium-sulfur batteries. Adv. Energy Mater. **7**, 1700260 (2017)
329. Zhang, G., Zhang, Z.W., Peng, H.J., et al.: A toolbox for lithium-sulfur battery research: methods and protocols. Small Methods **1**, 1700134 (2017)
330. Huang, J.Q., Zhai, P.Y., Peng, H.J., et al.: Metal/nanocarbon layer current collectors enhanced energy efficiency in lithium-sulfur batteries. Sci. Bull. **62**, 1267–1274 (2017)
331. Peng, H.J., Huang, J.Q., Liu, X.Y., et al.: Healing high-loading sulfur electrodes with unprecedented long cycling life: spatial heterogeneity control. J. Am. Chem. Soc. **139**, 8458–8466 (2017)
332. Yang, X., Li, X., Adair, K., et al.: Structural design of lithium–sulfur batteries: from fundamental research to practical application. Electrochem. Energy Rev. **1**, 239–293 (2018)
333. Ji, X., Lee, K.T., Nazar, L.F.: A highly ordered nanostructured carbon-sulphur cathode for lithium-sulphur batteries. Nat. Mater. **8**, 500–506 (2009)
334. Zhou, G.M., Li, L., Ma, C.Q., et al.: A graphene foam electrode with high sulfur loading for flexible and high energy Li–S batteries. Nano Energy **11**, 356–365 (2015)
335. Zhou, X.Y., Chen, F., Yang, J.: Core@shell sulfur@polypyrrole nanoparticles sandwiched in graphene sheets as cathode for lithium-sulfur batteries. J. Energy Chem. **24**, 448–455 (2015)
336. Zhang, H., Zhao, Z.B., Liu, Y., et al.: Nitrogen-doped hierarchical porous carbon derived from metal-organic aerogel for high performance lithium-sulfur batteries. J. Energy Chem. **26**, 1282–1290 (2017)
337. Kim, J.W., Ocon, J.D., Park, D.W., et al.: Enhanced reversible capacity of Li–S battery cathode based on graphene oxide. J. Energy Chem. **22**, 336–340 (2013)
338. Huang, J., Sun, Y., Wang, Y., et al.: Review on advanced functional separators for lithium-sulfur batteries. Acta Chim. Sinica **75**, 173–188 (2017)
339. Li, H., Yang, X., Wang, X., et al.: Dense integration of graphene and sulfur through the soft approach for compact lithium/sulfur battery cathode. Nano Energy **12**, 468–475 (2015)
340. Zhou, G., Yin, L.-C., Wang, D.-W., et al.: Fibrous hybrid of graphene and sulfur nanocrystals for high-performance lithium-sulfur batteries. ACS Nano **7**, 5367–5375 (2013)
341. Zheng, J.H., Guo, G.N., Li, H.W., et al.: Elaborately designed micro-mesoporous graphitic carbon spheres as efficient polysulfide reservoir for lithium-sulfur batteries. ACS Energy Lett. **2**, 1105–1114 (2017)
342. Oschatz, M., Borchardt, L., Pinkert, K., et al.: Hierarchical carbide-derived carbon foams with advanced mesostructure as a versatile electrochemical energy-storage material. Adv. Energy Mater. **4**, 1300645 (2014)
343. Peng, H.J., Zhang, Q.: Designing host materials for sulfur cathodes: from physical confinement to surface chemistry. Angew. Chem. Int. Ed. **54**, 11018–11020 (2015)
344. Peng, H.J., Zhang, G., Chen, X., et al.: Enhanced electrochemical kinetics on conductive polar mediators for lithium-sulfur batteries. Angew. Chem. Int. Ed. **55**, 12990–12995 (2016)
345. Chen, C.Y., Peng, H.J., Hou, T.Z., et al.: A quinonoid-imine-enriched nanostructured polymer mediator for lithium-sulfur batteries. Adv. Mater. **29**, 1606802 (2017)
346. Yin, L.C., Liang, J., Zhou, G.M., et al.: Understanding the interactions between lithium polysulfides and n-doped graphene using density functional theory calculations. Nano Energy **25**, 203–210 (2016)
347. Kong, L., Li, B.Q., Peng, H.J., et al.: Porphyrin-derived graphene-based nanosheets enabling strong polysulfide chemisorption and rapid kinetics in lithium-sulfur batteries. Adv. Energy Mater. **8**, 1800849 (2018)
348. Hou, T.Z., Xu, W.T., Chen, X., et al.: Lithium bond chemistry in lithium-sulfur batteries. Angew. Chem. Int. Ed. **56**, 8178–8182 (2017)
349. Li, L., Zhou, G.M., Yin, L.C., et al.: Stabilizing sulfur cathodes using nitrogen-doped graphene as a chemical immobilizer for Li–S batteries. Carbon **108**, 120–126 (2016)
350. Li, B.Q., Zhang, S.Y., Kong, L., et al.: Porphyrin organic framework hollow spheres and their applications in lithium-sulfur batteries. Adv. Mater. **30**, 1707483 (2018)
351. Li, S.Y., Wang, W.P., Duan, H., et al.: Recent progress on confinement of polysulfides through physical and chemical methods. J. Energy Chem. **27**, 1555–1565 (2018)
352. Sun, Z.H., Zhang, J.Q., Yin, L.C., et al.: Conductive porous vanadium nitride/graphene composite as chemical anchor of polysulfides for lithium-sulfur batteries. Nat. Commun. **8**, 14627 (2017)
353. Liang, J., Yin, L.C., Tang, X.N., et al.: Kinetically enhanced electrochemical redox of polysulfides on polymeric carbon nitrides for improved lithium-sulfur batteries. ACS Appl. Mater. Interfaces. **8**, 25193–25201 (2016)
354. Yuan, Z., Peng, H.J., Hou, T.Z., et al.: Powering lithium-sulfur battery performance by propelling polysulfide redox at sulfiphilic hosts. Nano Lett. **16**, 519–527 (2016)
355. Li, H.P., Sun, L.C., Zhang, Y.G., et al.: Enhanced cycle performance of Li/S battery with the reduced graphene oxide/activated carbon functional interlayer. J. Energy Chem. **26**, 1276–1281 (2017)
356. Qin, J.L., Peng, H.J., Huang, J.Q., et al.: Solvent-engineered scalable production of polysulfide-blocking shields to enhance practical lithium-sulfur batteries. Small Methods **2**, 1800100 (2018)
357. Zhuang, T.Z., Huang, J.Q., Peng, H.J., et al.: Rational integration of polypropylene/graphene oxide/Nafion as ternary-layered separator to retard the shuttle of polysulfides for lithium-sulfur batteries. Small **12**, 381–389 (2016)
358. Peng, H.J., Wang, D.W., Huang, J.Q., et al.: Janus separator of polypropylene-supported cellular graphene framework for sulfur cathodes with high utilization in lithium-sulfur batteries. Adv. Sci. **3**, 1500268 (2016)
359. Zhai, P.Y., Peng, H.J., Cheng, X.B., et al.: Scaled-up fabrication of porous-graphene-modified separators for high-capacity lithium-sulfur batteries. Energy Storage Mater. **7**, 56–63 (2017)

360. Zhang, X.Q., Zhao, C.Z., Huang, J.Q., et al.: Recent advances in energy chemical engineering of next-generation lithium batteries. Engineering **4**, 831–847 (2018)
361. Chen, X.R., Zhang, R., Cheng, X.B., et al.: Dendrite-free carbon/lithium metal anodes for use in flexible lithium metal batteries. New Carbon Mater. **32**, 600–604 (2017)
362. Cheng, X.B., Yan, C., Huang, J.Q., et al.: The gap between long lifespan Li–S coin and pouch cells: the importance of lithium metal anode protection. Energy Storage Mater. **6**, 18–25 (2017)
363. Cheng, X.B., Zhang, R., Zhao, C.Z., et al.: Toward safe lithium metal anode in rechargeable batteries: a review. Chem. Rev. **117**, 10403–10473 (2017)
364. Zhang, R., Li, N.W., Cheng, X.B., et al.: Advanced micro/nanostructures for lithium metal anodes. Adv. Sci. **4**, 1600445 (2017)
365. Zhang, X.Q., Cheng, X.B., Zhang, Q.: Advances in interfaces between Li metal anode and electrolyte. Adv. Mater. Interfaces **5**, 1701097 (2018)
366. Zhang, C., Huang, Z.J., Lv, W., et al.: Carbon enables the practical use of lithium metal in a battery. Carbon **123**, 744–755 (2017)
367. Zhang, R., Chen, X., Shen, X., et al.: Coralloid carbon fiber-based composite lithium anode for robust lithium metal batteries. Joule **2**, 764–777 (2018)
368. Deng, W., Zhu, W.H., Zhou, X.F., et al.: Graphene nested porous carbon current collector for lithium metal anode with ultrahigh areal capacity. Energy Storage Mater. **15**, 266–273 (2018)
369. Meng, Q.Q., Deng, B., Zhang, H.M., et al.: Heterogeneous nucleation and growth of electrodeposited lithium metal on the basal plane of single-layer graphene. Energy Storage Mater. **16**, 419–425 (2019)
370. Cheng, X.B., Peng, H.J., Huang, J.Q., et al.: Dual-phase lithium metal anode containing a polysulfide-induced solid electrolyte interphase and nanostructured graphene framework for lithium-sulfur batteries. ACS Nano **9**, 6373–6382 (2015)
371. Zhang, R., Cheng, X.B., Zhao, C.Z., et al.: Conductive nanostructured scaffolds render low local current density to inhibit lithium dendrite growth. Adv. Mater. **28**, 2155–2162 (2016)
372. Deng, W., Zhou, X.F., Fang, Q.L., et al.: Microscale lithium metal stored inside cellular graphene scaffold toward advanced metallic lithium anodes. Adv. Energy Mater. **8**, 1703152 (2018)
373. Lin, D.C., Liu, Y.Y., Liang, Z., et al.: Layered reduced graphene oxide with nanoscale interlayer gaps as a stable host for lithium metal anodes. Nat. Nanotechnol. **11**, 626–632 (2016)
374. Zhang, R., Chen, X.R., Chen, X., et al.: Lithiophilic sites in doped graphene guide uniform lithium nucleation for dendrite-free lithium metal anodes. Angew. Chem. Int. Ed. **56**, 7764–7768 (2017)
375. Liu, H., Chen, X., Cheng, X.B., et al.: Uniform lithium nucleation guided by atomically dispersed lithiophilic conx sites for safe lithium metal batteries. Small Methods **2**, 1800354 (2018)
376. Li, Y.G., Dai, H.J.: Recent advances in zinc-air batteries. Chem. Soc. Rev. **43**, 5257–5275 (2014)
377. Debe, M.K.: Electrocatalyst approaches and challenges for automotive fuel cells. Nature **486**, 43–51 (2012)
378. Gong, K., Du, F., Xia, Z., et al.: Nitrogen-doped carbon nanotube arrays with high electrocatalytic activity for oxygen reduction. Science **323**, 760–764 (2009)
379. Jeon, I.Y., Zhang, S., Zhang, L., et al.: Edge-selectively sulfurized graphene nanoplatelets as efficient metal-free electrocatalysts for oxygen reduction reaction: the electron spin effect. Adv. Mater. **25**, 6138–6145 (2013)
380. Zhang, L., Xia, Z.: Mechanisms of oxygen reduction reaction on nitrogen-doped graphene for fuel cells. J. Phys. Chem. C **115**, 11170–11176 (2011)
381. Yan, D.F., Li, Y.X., Huo, J., et al.: Defect chemistry of nonprecious-metal electrocatalysts for oxygen reactions. Adv. Mater. **29**, 1606459 (2017)
382. Liang, J., Du, X., Gibson, C., et al.: N-doped graphene natively grown on hierarchical ordered porous carbon for enhanced oxygen reduction. Adv. Mater. **25**, 6226–6231 (2013)
383. Liang, J., Zheng, Y., Chen, J., et al.: Facile oxygen reduction on a three-dimensionally ordered macroporous graphitic C_3N_4/carbon composite electrocatalyst. Angew. Chem. Int. Ed. **51**, 3892–3896 (2012)
384. Liang, J., Jiao, Y., Jaroniec, M., et al.: Sulfur and nitrogen dual-doped mesoporous graphene electrocatalyst for oxygen reduction with synergistically enhanced performance. Angew. Chem. Int. Ed. **51**, 11496–11500 (2012)
385. Zhang, L., Xu, Q., Niu, J., et al.: Role of lattice defects in catalytic activities of graphene clusters for fuel cells. Phys. Chem. Chem. Phys. **17**, 16733–16743 (2015)
386. Tao, L., Wang, Q., Dou, S., et al.: Edge-rich and dopant-free graphene as a highly efficient metal-free electrocatalyst for the oxygen reduction reaction. Chem. Commun. **52**, 2764–2767 (2016)
387. Jiang, Y., Yang, L., Sun, T., et al.: Significant contribution of intrinsic carbon defects to oxygen reduction activity. ACS Catal. **5**, 6707–6712 (2015)
388. Ito, Y., Shen, Y., Hojo, D., et al.: Correlation between chemical dopants and topological defects in catalytically active nanoporous graphene. Adv. Mater. **28**, 1604318 (2016)
389. Zhang, Z.P., Sun, J.T., Wang, F., et al.: Efficient oxygen reduction reaction (ORR) catalysts based on single iron atoms dispersed on a hierarchically structured porous carbon framework. Angew. Chem. Int. Ed. **57**, 9038–9043 (2018)
390. Wang, J.Y., Zhang, H.N., Wang, C.W., et al.: Co-synthesis of atomic Fe and few-layer graphene towards superior ORR electrocatalyst. Energy Storage Mater. **12**, 1–7 (2018)
391. Chen, X.Q., Yu, L., Wang, S.H., et al.: Highly active and stable single iron site confined in graphene nanosheets for oxygen reduction reaction. Nano Energy **32**, 353–358 (2017)
392. Yin, P.Q., Yao, T., Wu, Y., et al.: Single cobalt atoms with precise N-coordination as superior oxygen reduction reaction catalysts. Angew. Chem. Int. Ed. **55**, 10800–10805 (2016)
393. Song, P., Luo, M., Liu, X.Z., et al.: Zn single atom catalyst for highly efficient oxygen reduction reaction. Adv. Funct. Mater. **27**, 1700802 (2017)
394. Han, Y.H., Wang, Y.G., Chen, W.X., et al.: Hollow N-doped carbon spheres with isolated cobalt single atomic sites: superior electrocatalysts for oxygen reduction. J. Am. Chem. Soc. **139**, 17269–17272 (2017)
395. Wang, X.X., Cullen, D.A., Pan, Y.T., et al.: Nitrogen-coordinated single cobalt atom catalysts for oxygen reduction in proton exchange membrane fuel cells. Adv. Mater. **30**, 1706758 (2018)
396. Zhang, Z.P., Dou, M.L., Liu, H.J., et al.: A facile route to bimetal and nitrogen-codoped 3D porous graphitic carbon networks for efficient oxygen reduction. Small **12**, 4193–4199 (2016)
397. Li, Q.H., Chen, W.X., Xiao, H., et al.: Fe isolated single atoms on S, N codoped carbon by copolymer pyrolysis strategy for highly efficient oxygen reduction reaction. Adv. Mater. **30**, 1800588 (2018)
398. Fei, H.L., Dong, J.C., Feng, Y.X., et al.: General synthesis and definitive structural identification of MN_4C_4 single-atom catalysts with tunable electrocatalytic activities. Nat. Cat. **1**, 63–72 (2018)
399. Wang, X.Q., Chen, Z., Zhao, X.Y., et al.: Regulation of coordination number over single Co sites: triggering the efficient electroreduction of CO_2. Angew. Chem. Int. Ed. **57**, 1944–1948 (2018)
400. Jiang, K., Siahrostami, S., Akey, A.J., et al.: Transition-metal single atoms in a graphene shell as active centers for highly efficient artificial photosynthesis. Chem **3**, 950–960 (2017)

401. Jiang, K., Siahrostami, S., Zheng, T.T., et al.: Isolated Ni single atoms in graphene nanosheets for high-performance CO_2 reduction. Energy Environ. Sci. **11**, 893–903 (2018)
402. Su, X., Yang, X.F., Huang, Y., et al.: Single-atom catalysis toward efficient CO_2 conversion to CO and formate products. Acc. Chem. Res. (2018). https://doi.org/10.1021/acs.accounts.8b00478
403. Sun, T., Zhao, S., Chen, W., et al.: Single-atomic cobalt sites embedded in hierarchically ordered porous nitrogen-doped carbon as a superior bifunctional electrocatalyst. Proc. Natl. Acad. Sci. U.S.A. **115**, 12692–12697 (2018)
404. Zhao, Y., Nakamura, R., Kamiya, K., et al.: Nitrogen-doped carbon nanomaterials as non-metal electrocatalysts for water oxidation. Nat. Commun. **4**, 2390 (2013)
405. Zheng, Y., Jiao, Y., Zhu, Y.H., et al.: Hydrogen evolution by a metal-free electrocatalyst. Nat. Commun. **5**, 3783 (2014)
406. Zhu, Y.P., Ran, J.R., Qiao, S.Z.: Scalable self-supported graphene foam for high-performance electrocatalytic oxygen evolution. ACS Appl. Mater. Interfaces. **9**, 41980–41987 (2017)
407. Zhao, Z.H., Xia, Z.H.: Design principles for dual-element-doped carbon nanomaterials as efficient bifunctional catalysts for oxygen reduction and evolution reactions. ACS Catal. **6**, 1553–1558 (2016)
408. Zheng, Y., Jiao, Y., Li, L.H., et al.: Toward design of synergistically active carbon-based catalysts for electrocatalytic hydrogen evolution. ACS Nano **8**, 5290–5296 (2014)
409. Qu, K., Zheng, Y., Dai, S., et al.: Graphene oxide-polydopamine derived N, S-codoped carbon nanosheets as superior bifunctional electrocatalysts for oxygen reduction and evolution. Nano Energy **19**, 373–381 (2016)
410. Chen, P.Z., Xu, K., Zhou, T.P., et al.: Strong-coupled cobalt borate nanosheets/graphene hybrid as electrocatalyst for water oxidation under both alkaline and neutral conditions. Angew. Chem. Int. Ed. **55**, 2488–2492 (2016)
411. Chen, S., Duan, J.J., Tang, Y.H., et al.: Molybdenum sulfide clusters-nitrogen-doped graphene hybrid hydrogel film as an efficient three-dimensional hydrogen evolution electrocatalyst. Nano Energy **11**, 11–18 (2015)
412. Xue, S., Chen, L., Liu, Z.B., et al.: $NiPS_3$ nanosheet-graphene composites as highly efficient electrocatalysts for oxygen evolution reaction. ACS Nano **12**, 5297–5305 (2018)
413. Wang, H.F., Tang, C., Zhang, Q.: Towards superior oxygen evolution through graphene barriers between metal substrates and hydroxide catalysts. J. Mater. Chem. A **3**, 16183–16189 (2015)
414. Wang, H.L., Dai, H.J.: Strongly coupled inorganic-nano-carbon hybrid materials for energy storage. Chem. Soc. Rev. **42**, 3088–3113 (2013)
415. Tang, C., Wang, H.F., Zhu, X.L., et al.: Advances in hybrid electrocatalysts for oxygen evolution reactions: rational integration of NiFe layered double hydroxides and nanocarbon. Part. Part. Syst. Char. **33**, 473–486 (2016)
416. Zhang, Q.F., Xu, Z., Lu, B.A.: Strongly coupled MoS_2-3D graphene materials for ultrafast charge slow discharge libs and water splitting applications. Energy Storage Mater. **4**, 84–91 (2016)
417. Li, Y.G., Wang, H.L., Xie, L.M., et al.: MoS_2 nanoparticles grown on graphene: an advanced catalyst for the hydrogen evolution reaction. J. Am. Chem. Soc. **133**, 7296–7299 (2011)
418. Biroju, R.K., Das, D., Sharma, R., et al.: Hydrogen evolution reaction activity of graphene-MoS_2 van der waals heterostructures. ACS Energy Letters **2**, 1355–1361 (2017)
419. Zheng, X.L., Xu, J.B., Yan, K.Y., et al.: Space-confined growth of MoS_2 nanosheets within graphite: the layered hybrid of MoS_2 and graphene as an active catalyst for hydrogen evolution reaction. Chem. Mater. **26**, 2344–2353 (2014)
420. Duan, J., Chen, S., Chambers, B.A., et al.: 3D WS_2 nanolayers@heteroatom-doped graphene films as hydrogen evolution catalyst electrodes. Adv. Mater. **27**, 4234–4241 (2015)
421. Cui, X.Y., Tang, C., Zhang, Q.: A review of electrocatalytic reduction of dinitrogen to ammonia under ambient conditions. Adv. Energy Mater. **8**, 1800369 (2018)
422. Guo, C., Ran, J., Vasileff, A., et al.: Rational design of electrocatalysts and photo(electro) catalysts for nitrogen reduction to ammonia (NH_3) under ambient conditions. Energy Environ. Sci. **11**, 45–56 (2018)
423. Chen, J.G., Crooks, R.M., Seefeldt, L.C., et al.: Beyond fossil fuel–driven nitrogen transformations. Science **360**, eaar6611 (2018)
424. Chen, G.F., Ren, S., Zhang, L., et al.: Advances in electrocatalytic N_2 reduction—strategies to tackle the selectivity challenge. Small Methods **2**, 1800337 (2018)
425. Yan, D., Li, H., Chen, C., et al.: Defect engineering strategies for nitrogen reduction reactions under ambient conditions. Small Methods **2**, 1800331 (2018)
426. Cui, X., Tang, C., Liu, X.M., et al.: Highly selective electrochemical reduction of dinitrogen to ammonia at ambient temperature and pressure over iron oxide catalysts. Chem. Eur. J. **24**, 18494 (2018)
427. Guo, J., Chen, P.: Catalyst: NH_3 as an energy carrier. Chem **3**, 709–712 (2017)
428. Li, W., Wu, T., Zhang, S., et al.: Nitrogen-free commercial carbon cloth with rich defects for electrocatalytic ammonia synthesis under ambient conditions. Chem. Commun. **54**, 11188–11191 (2018)
429. Liu, Y., Su, Y., Quan, X., et al.: Facile ammonia synthesis from electrocatalytic N_2 reduction under ambient conditions on N-doped porous carbon. ACS Catal. **8**, 1186–1191 (2018)
430. Lv, C., Qian, Y., Yan, C., et al.: Defect engineering metal-free polymeric carbon nitride electrocatalyst for effective nitrogen fixation under ambient conditions. Angew. Chem. Int. Ed. **57**, 10246–10250 (2018)
431. Wang, H., Wang, L., Wang, Q., et al.: Ambient electrosynthesis of ammonia: electrode porosity and composition engineering. Angew. Chem. Int. Ed. **57**, 12360–12364 (2018)
432. Yu, X., Han, P., Wei, Z., et al.: Boron-doped graphene for electrocatalytic N_2 reduction. Joule **2**, 1610–1622 (2018)
433. Chen, G.F., Cao, X.R., Wu, S.Q., et al.: Ammonia electrosynthesis with high selectivity under ambient conditions via a Li^+ incorporation strategy. J. Am. Chem. Soc. **139**, 9771–9774 (2017)
434. Mukherjee, S., Cullen, D.A., Karakalos, S., et al.: Metal-organic framework-derived nitrogen-doped highly disordered carbon for electrochemical ammonia synthesis using N_2 and H_2O in alkaline electrolytes. Nano Energy **48**, 217–226 (2018)
435. Song, Y., Johnson, D., Peng, R., et al.: A physical catalyst for the electrolysis of nitrogen to ammonia. Sci. Adv. **4**, e1700336 (2018)
436. Geng, Z., Liu, Y., Kong, X., et al.: Achieving a record-high yield rate of 120.9 $\mu g NH_3\ mg_{cat}^{-1}\ h^{-1}$ for N_2 electrochemical reduction over Ru single-atom catalysts. Adv. Mater. **30**, 1803498 (2018)
437. Tao, H., Choi, C., Ding, L.X., et al.: Nitrogen fixation by Ru single-atom electrocatalytic reduction. Chem. **5**, 204–214 (2019)
438. Wang, X., Wang, W., Qiao, M., et al.: Atomically dispersed Au catalyst towards efficient electrochemical synthesis of ammonia. Sci. Bull. **63**, 1246–1253 (2018)
439. Qin, Q., Heil, T., Antonietti, M., et al.: Single-site gold catalysts on hierarchical N-doped porous noble carbon for enhanced electrochemical reduction of nitrogen. Small Methods **2**, 1800202 (2018)
440. Shi, M.M., Bao, D., Li, S.J., et al.: Anchoring PdCu amorphous nanocluster on graphene for electrochemical reduction of N_2 to NH_3 under ambient conditions in aqueous solution. Adv. Energy Mater. **8**, 1800124 (2018)

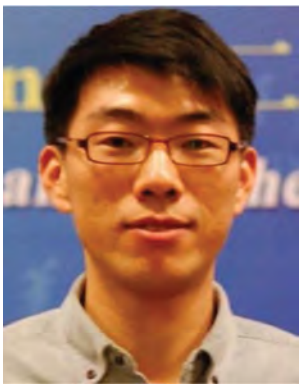

Cheng Tang received his B.Eng. and Ph.D. from the Department of Chemical Engineering, Tsinghua University, in 2013 and 2018 under the supervision of Prof. Qiang Zhang and Prof. Fei Wei. Currently, Dr. Tang is a postdoctoral researcher at The University of Adelaide working with Prof. Shi-Zhang Qiao, and his research focuses on nanomaterials and energy electrocatalysis, including 3D graphene, hierarchical nanomaterials, oxygen reduction/evolution, hydrogen evolution, nitrogen reduction, etc.

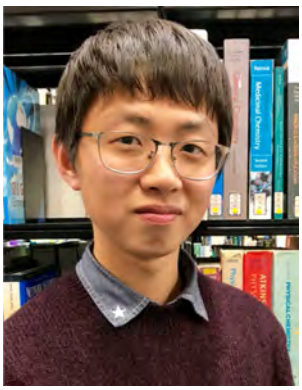

Hao-Fan Wang received his B.Eng. and Ph.D. in 2013 and 2018 from the Department of Chemical Engineering, Tsinghua University under the supervision of Prof. Qiang Zhang. His research focuses on advanced energy materials for application in bifunctional oxygen electrocatalysis, metal–air batteries, etc.

Jia-Qi Huang received his B.Eng. (2007) and Ph.D. (2012) in chemical engineering from Tsinghua University, China. Currently, Dr. Huang is a professor at the Advanced Research Institute of Multidisciplinary Science (ARIMS) in Beijing Institute of Technology and his research focuses on synthetic approaches and applications of nanomaterials for rechargeable batteries, including Li-S batteries, Li metal anodes, etc.

Weizhong Qian obtained his Ph.D. in chemical engineering from Tsinghua University (PR China) in 2002 and is currently a professor of chemical engineering at Tsinghua University. His scientific interests include nanomaterials, advanced catalysis, and chemical engineering.

Fei Wei obtained his Ph.D. in chemical engineering from the China University of Petroleum in 1990 and after a postdoctoral fellowship at Tsinghua University (China), Dr. Wei was appointed as an associate professor in 1992 and professor of chemical engineering at Tsinghua University (China) in 1996. Dr. Wei's scientific interests include technological applications of chemical reaction engineering, multiphase flow, carbon nanomaterials and sustainable energy. In addition, Dr. Wei has designed and successfully runs over 30 industrial fluidized bed reactors.

Shi-Zhang Qiao is currently a Chair Professor and Australian Laureate Fellow at the School of Chemical Engineering of The University of Adelaide, Australia. Dr. Qiao received his Ph.D. in chemical engineering from the Hong Kong University of Science and Technology in 2000 and his research expertise is in nanomaterials for electrocatalysis, photocatalysis and energy storage and conversion technologies. Dr. Qiao is also a Thomson Reuters/Clarivate Analytics Highly Cited Researcher (Chemistry, Materials Science), and in recognition of his achievements in research, he was honored with the prestigious ARC Discovery Outstanding Researcher Award (2013), the Emerging Researcher Award (2013, ENFL Division of the American Chemical Society) and the ARC, ARF and APD Fellowships.

Qiang Zhang received his B.Sc. and Ph.D. from Tsinghua University in 2004 and 2009 and after stays at the Case Western Reserve University, USA, and the Fritz Haber Institute of the Max Planck Society, Germany, was appointed as a faculty member at Tsinghua University in 2011. Dr. Zhang's research focuses on energy materials such as Li-S batteries, Li metal anode, 3D graphene and electrocatalysts and he has been awarded the National Science Fund for Distinguished Young Scholars, the Young Top-Notch Talent from China and the Newton Advanced Fellowship from the Royal Society, UK. Currently, Dr. Zhang is also an associate editor for the Journal of Energy Chemistry and sits on the advisory board of Matter, Advanced Functional Materials, EnergyChem, Advanced Materials Interfaces, Philosophical Transactions A, Science China Materials, Science China Chemistry, Chinese Chemical Letters, and so on.